The Paleogene continental basins from SE France: new geographic and climatic insights from an integrated approach

Nazim Semmani, François Fournier, Jean-Pierre Suc, Séverine Fauquette, Nicolas Godeau, Abel Guihou, Speranța-Maria Popescu, Mihaela Carmen Melinte-Dobrinescu, Christophe Thomazo, Lionel Marié, et al.

The Paleogene continental basins from SE France: new geographic and climatic insights from an integrated approach

Nazim Semmani[1,], François Fournier[1,*], Jean-Pierre Suc[2], Séverine Fauquette[3], Nicolas Godeau[1,2], Abel Guihou[1], Speranța-Maria Popescu[4], Mihaela Carmen Melinte-Dobrinescu[5], Christophe Thomazo[6], Lionel Marié[1], Pierre Deschamps[1], Jean Borgomano[1]

[1]: Aix Marseille Université, CNRS, IRD, Cerege, Um 34, 3 Place Victor Hugo (Case 67), 13331, Marseille Cedex 03, France.

[2]: Sorbonne Université, CNRS-INSU, Institut des Sciences de la Terre Paris, ISTeP, UMR 7193, 75005 Paris, France

[3]: ISEM, Université de Montpellier, CNRS, IRD, EPHE, Montpellier, France

[4]: GeoBioStratData.Consulting, 385 Route du Mas Rillier, 69140 Rillieux-la-Pape

[5]: National Institute of Marine Geology and Geo-Ecology, 23–25 Dimitrie Onciul Street, 70318 Bucharest, Romania

6: Université de Bourgogne Franche-Comté, UMR CNRS/uB6282 Biogéosciences, 6 Bd Gabriel, 21000 Dijon, France

[*]Corresponding author: fournier@cerege.fr

Abstract

New insights into the geodynamic evolution, the paleogeographic framework and the paleoclimatic setting of the Upper Eocene-Oligocene lacustrine basins from South-East France have been provided by an integrative approach combining geochronology, micropaleontology

and stable isotope analyses. U-Pb dating on calcite, pollen-based climatostratigraphy and strontium and sulfur isotope signatures of sulfates provided a robust chronostratigraphic framework for the Upper Eocene and Oligocene succession from the Vistrenque, Alès and Roussillon basins. The thick Priabonian- lower Rupelian lacustrine succession from the Vistrenque Basin is interpreted to be deposited in a strike-slip basin associated with the latest stages of pyrenean shortening. Floral assemblages are used to reconstruct the vegetation cover in the lacustrine systems and their neighbouring lowlands and highlands. Composition of saltwater inferred from strontium and sulfur isotope signatures of sulfates, the occurrence of calcareous nannofossils, dinoflagellate cysts and pollen grains of mangrove-related plants provided strong evidence for marine intrusions into the Alès Basin during the Priabonian and the Vistrenque Basin during the Rupelian and Chattian. Paleogeographic reconstructions of Southeast France during the Priabonian and late Rupelian strongly suggest marine incursions from the Alpine Sea via two potential pathways: upper Rhône Valley via the Crest Sill and lower Rhône Valley via the Haut-Var Pyrenean synclines. On the other hand, Upper Oligocene evaporite basins in the Camargue area have been subjected to marine intrusions from the Western Mediterranean Sea following the collapse of the eastern pyrenean relief during the Liguro-Provençal rifting stage. Finally, pollen analysis and Climate Amplitude Method revealed a brief but significant stage of cooling and aridification at the very base of the Rupelian which could represent the regional and terrestrial expression of the global climate cooling following the Eocene-Oligocene Transition.

Keywords: Priabonian, Rupelian, Eocene-Oligocene Transition, U/Pb dating, pollens, strontium and sulfur isotopes, climatostratigraphy, marine intrusion.

1. Introduction

In Southeast France, several continental basins were formed during the Paleogene and are located in Languedoc (e.g. Alès, Saint-Chaptes and Issirac (ASCI) basins, Sanchis and Séranne, 2000; Lettéron et al., 2022; Séranne et al., 2021), Rhone Valley (Mormoiron Basin, Triat and Truc, 1974), Provence (e.g. Apt-Manosque-Forcalquier Basin, Lesueur, 1991; Marseille Basin, Nury, 1990), and Camargue (e.g. Vistrenque Basin, Benedicto et al., 1996). These basins are characterized by thick siliciclastic, carbonate and evaporite sedimentation (e.g. Rouchy, 1997). The formation and the filling of these basins initiated during the Late Eocene (Priabonian) and lasted until the Late Oligocene (Chattian). These basins were interpreted as branches of the European Cenozoic Rift System (ECRIS, **Fig 1A**) (Ziegler, 1992) or resulting exclusively from the Oligocene to Aquitanian extension linked to the Liguria-Provence rifting (e.g., Vistrenque Basin, Benedicto et al., 1996), and a few cases as polyphased extensional structures (e.g. Sanchis and Séranne, 2000) (**Fig. 1B, 1C**). In their recent work, Séranne et al. (2021) reassessed the origin of Priabonian continental basins located in Languedoc, between the Northeast trending Cévennes and Nîmes major regional faults and found that those basins resulted from left-lateral strike-slip movements of these faults which accommodated both the Western European rift system extension (ECRIS) and the still active N-S shortening of the Central and Western Pyrenees.

The origin of evaporites in the saline paleolakes within the Paleogene basins of Southeast France is poorly understood and is still a matter of controversy that has lasted for decades particularly on the origin of the salt water that may result from marine incursions and/or the recycling of Triassic evaporites (Giraud, 1902; Fontes et al., 1996; Bodergat et al., 1999; Sissingh, 2001, 2006; Dèzes et al., 2004; Ziegler and Dèzes, 2007; Briot, 2008; Lettéron et al., 2017). Questions also remain on the patterns of saline water masses connections and diachronism of the evaporite intervals between the different basins but also on the role of

changing climate on evaporite deposition and continental depositional system evolution at the key Eocene-Oligocene transition (e.g., Sissingh, 2001; Lettéron et al., 2022) which represents a crucial period for the Cenozoic global climate evolution. Until recently, assumptions have been made about the role of the Camargue area as a saline water corridor into the Languedoc and Rhône Valley continental basins (e.g., Lettéron et al., 2018).

Since the Camargue area is located in a pivotal position among these France south-eastern basins, between the Languedoc basins to the west, the Provence basins to the east, and the Valence and Bresse grabens to the north (see location in **Fig. 1A**), the Paleogene Vistrenque Basin occupies a key geographic position for constraining the geodynamic and structural evolution of southeast France and Gulf of Lion areas during the Late Eocene and Oligocene times and provides new insights into these hitherto unresolved paleogeographic issues.

The Vistrenque Basin is considered as the deepest (~ 5 km) Cenozoic basin in southeast France and in the Gulf of Lion margin (Benedicto et al., 1996). The Paleogene sequence, up to 3200 m-thick, is entirely buried beneath the Rhône Delta sediments (Valette and Benedicto, 1995) (**Fig 2**). The drill cores have yielded very scarce and poorly preserved biota thus preventing the definition of a detailed and well-constrained chronostratigraphic framework. The correlation of thick halite and anhydrite deposits (Valette and Benedicto, 1995) with the Priabonian and Oligocene evaporites from the neighbouring Rhone and Languedoc basins is not yet established, thus preventing the reconstruction of a well-constrained paleogeographic map of these basins during the Paleogene and the elucidation of the question of their potential connection with the marine realm.

Comprehensive and detailed analyses of subsurface data from the Paleogene sedimentary record of the Vistrenque Basin (cores, cuttings, well logs) as well as from the neighbouring Alès Basin were undertaken to resolve these tectonic and paleogeographic issues (**Fig. 3**, **Fig. 4**). Based on the integration of different dating methods such as U-Pb absolute dating on

carbonates, pollen-based climatostratigraphy, the interpretation of strontium and sulfur isotopes measurements, and additional micropaleontological analyses (dinoflagellate cysts, calcareous nannofossils), the present work aims at: (1) constraining the lithostratigraphic and chronostratigraphic framework of the Paleogene sedimentary succession from the Vistrenque Basin; (2) bringing new insights into the pending issue of of the origin of salts in the Paleogene saline lakes of Southeast France and the occurrence of marine incursions, and (3) refining the paleogeographic and paleoclimatic reconstructions of Southeast France during the Late Eocene and Oligocene times. In order to complement the overview in time and space of the regional vegetation and climate evolution during the Oligocene, pollen data from the Canet 1 borehole from the Roussillon Basin (Eastern Pyrenees) (location in **Fig. 1B**) have been integrated in this study.

2. Geological setting

2.1 Regional tectonic setting and stratigraphy

Following the development of Upper Cretaceous carbonate platforms in Southeast France, the Mesozoic to Eocene cover has been folded and thrusted during the Pyrenean shortening which resulted from the convergence and collision of the Iberia-Corsica-Sardinia block with the European plate (e.g. Arthaud and Laurent, 1995; Séranne et al., 1995; Bestani et al., 2015). In Languedoc, the Nîmes and Cévennes faults have been shown to accommodate sinistral strike-slip movements as early as the Priabonian in response to both the Pyrenean shortening and Western European Rift extension (Séranne et al., 2021). As a consequence, within a 50 km wide wrenching zone located between the Cévennes and Nîmes faults, fluvial and lacustrine sedimentation occurred during Priabonian times, in releasing bends and oversteps of left-lateral strike-slip faults, (Séranne et al., 2021). The pyrenean orogen and associated syn- and tardi-

orogenic basins have been It was later dismantled from the late Rupelian to the Aquitanian to form the Gulf of Lion rifted margin (Arthaud et al., 1981; Arthaud and Séguret, 1981; Gorini et al.,1994; Séranne et al., 1995; Mauffret and Gorini, 1996; Mascle and Vially, 1999; Séranne, 1999; Guennoc et al., 2000; Lacombe and Jolivet, 2005). The Oligocene-Aquitanian Gulf of Lion rifting phase accompanied the retreat of slab and is followed by the Burdigalian break-up. Paleogeographic reconstructions made by Benedicto et al., 1996 suggest a high relief, more than 1 km of elevation, at the southern margin while the total extension across the Vistrenque Basin is estimated to range from 9 to 9.5 km. The break-up event was dated to the early to middle Burdigalian (Oudet *et al*., 2010a) and corresponds to the onset of the spreading of the Liguro-Provençal Basin which led to the south-eastward drift of the Corsica-Sardinia Block (Gorini et al., 1993; Séranne et al., 1995). During the Burdigalian, a marine transgression followed the break-up and Burdigalian to Tortonian post-rift marine sediments were deposited (**Fig. 2B-C-D**). By the end of the Miocene, the Messinian Salinity Crisis resulted in valley incision into the Miocene deposits and affected the Oligocene deposits in places. The resulting canyons are overlain by Pliocene and Quaternary sediments (Beaufort, 1954; Benedicto et al., 1996; Leroux et al., 2017).

2.2 The Paleogene Vistrenque Basin

The Camargue region is constituted of two main Cenozoic basins separated by the Mesozoic Albaron High (**Fig. 2A-C**): the Vistrenque Basin to the West and the Vaccarès Basin (=Petit-Rhône Basin) to the East. The Vistrenque Basin is oriented NE-SW and extends over 50*30 Km²s This basin is linked to the northeast with the Pujaut Through (**Fig. 2A**) along the bounding NNE-SSW trending major Nîmes Fault that separates the basin from the Mesozoic hills of the Garrigues region (**Fig. 2C**; Semmani et al., 2022). The Vistrenque Basin is bounded to the south by the Highs of Grau-du-Roi and Saintes-Maries-de-la-Mer (**Fig. 2A**). The basin is structured

by a set of syn-rift faults mostly parallel to the Nîmes Fault (**Fig. 1C**, **Fig. 2B-C**) that determine tilted blocks within the basin but also by transfer faults that separate different sectors with specific structural styles (e.g., **Fig. 2B**; Benedicto et al., 1996 and their figures).

The maximum thickness of the Cenozoic sedimentary succession of the Vistrenque Basin is known from the Pierrefeu 1 well (4920 m) where it rests on a Lower Cretaceous marine carbonate basement (**Fig. 2B**). The Cenozoic infill of the Vistrenque Basin is subdivided into poorly defined pre-rift series, syn-rift series attributed to the Oligocene-Aquitanian extension, and post-rift series of Burdigalian to Pliocene and Quaternary age (**Fig. 2B-C-D**; Valette and Benedicto, 1995; Benedicto et al., 1996). Below the Aquitanian deposits, the Paleogene strata have been subdivided classically into three main lithological units of hundreds to thousands of metres thick: from top to bottom: *Série Calcaréo-salifère* Formation, *Série Rouge* Formation and *Série Grise* Formation (**Fig. 2D**). These subdivisions have been adopted by Cavelier et al. (1984) in their synthesis on the Paleogene of Southeast France and these authors suggested an Eocene age for the lowermost parts of the *Série Grise* Formation based on the observed similarities in the sedimentary trends with the neighbouring basins.

The compartmentalization of the Vistrenque Basin by transfer faults results in different stratigraphic successions between the northern Pierrefeu sector and the southern Gallician sector (**Fig. 3A-C**). The depositional setting and stratigraphic architecture of the Vistrenque Basin has been recently reassessed by Semmani (2022). The Paleogene lithological succession at the reference well (Gallician 9) from the Gallician sector is composed of five distinct formations (**Fig. 3A**). 1) The lowermost *Série Grise* Formation is several hundred metres thick (the base of the Paleogene is not reached in this sector) and is made of a monotonous succession of sandstones (calcarenites), conglomerates, marlstones and less frequent evaporites deposited in lacustrine settings. 2) The overlying *Série Calcaire* Formation is around 250 m thick and is made essentially of sandstones (calcarenites) and calcisiltites (siltstones), and a few monomictic

conglomerates at the base. These lithologies become scarce upward while variegated calcareous claystones and vacuolar limestones become more frequent, and the unit is capped by a major subaerial exposure surface. 3) The *Série Mixte* Formation is 42 m thick and characterized by alternation of dominantly polymictic conglomerates, siliciclastic sandstones, variegated calcareous claystones and limestones. 4) The *Série Rouge* Formation is made of alternations of siliciclastic-dominated sandstones and marlstones with frequent conglomerates at the base. 5) The *Série Calcaréo-salifère* Formation is around 300 m thick in the Gallician sector and constituted mainly of limestones and papyraceous marlstones at the base. The upper part of the unit is made of two sequences made of alternations of sandstones, marlstones, limestones, anhydrite and halite.

In Pierrefeu 1 well (**Fig. 3A**), the nomenclature is slightly different and the *Série Calcaire* and *Série Mixte* formations have not been recognized probably because of lateral variations of facies. The top of the Série Grise from the Pierrefeu 1 well likely corresponds to the *Série Calcaire* defined in the Gallician sector. Compared to the Gallician sector, the considerable thickness of the evaporite-rich *Série Calcaréo-salifère* Formation (~900 m) from the Pierrefeu sector results from the abnormal overlay of evaporite intervals caused by halotectonic gravity slides on top of the NW-dipping roll-over of the Nimes Fault, linked to the Oligocene-Aquitanian extension (Valette and Benedicto, 1995).

2.3 The Paleogene Alès and Saint-Chaptes basins

Located between the Nîmes and Cévennes faults, the Alès and Saint-Chaptes basins are characterized by a thick Priabonian fluvial and lacustrine succession (up to 900m) deposited during the latest stages of pyrenean compression (Séranne et al., 2021). The Priabonian succession is unconformably overlain by Chattian continental deposits accumulated in extensional setting related to the Gulf of Lion rifting (Sanchis and Séranne,

2000). The Alès Basin is located along the Cévennes fault with a NE-SW direction (25 km long, 5 km large), while the Saint-Chaptes Basin occupied by a saline lake (ASCI lake system) whose mixed carbonate, siliciclastic and evaporitic sedimentation has been exhaustively studied by Letteron et al. (2018; 2022). These authors subdivided the Priabonian deposits in six unconformity-bounded parasequences from SPr1 to SPr6 defined as transgressive-regressive (T-R) cycles (**Fig. 4**). The chronostratigraphy of the Priabonian deposits is well-constrained and based on mammalian (Rémy, 1985, 1994; Rémy and Fournier, 2003; Rémy and Lesage, 2005) and charophyte biostratigraphy (Feist-Castel, 1971; Lettéron et al., 2017) coupled with magnetostratigraphic analyses (Lettéron et al., 2022).

2.4 The Roussillon Basin: Canet 1 borehole

The Canet 1 well, located in the Roussillon Basin (location: **Fig. 1B**, **Table S1**), cuts through a 1785 m thick sequence of Quaternary to Permo-Triassic deposits overlying the Hercynian basement (Gottis, 1958). The lithostratigraphic succession and chronstratigraphic framework of well Canet 1 are summarized in **Figure S1**. This section displays around 700 m of sandy-clayey-lignitic deposits (1015–1716 m depth) which may correlate the Late Oligocene to the Early Miocene interval (Gottis, 1958) and thus has been ascribed to the rifting episode of the Gulf of Lion evolution (Mauffret et al., 2001; Séranne, 1999; Romagny et al., 2020).

3. Material and methods

This work is based on the analysis of cores, well cuttings and well logs from boreholes drilled in the Gallician and Parrapon sectors of the Vistrenque Basin, boreholes and exposed sections from the ASCI system and cuttings from Canet 1 well located in the Roussillon Basin (see locations in **Fig. 1B**, **Fig. 3** and **Fig. 4**; **Supplementary data, Table S1**).

3.1 Chronostratigraphic framework construction

The chronostratigraphic framework of the studied basins (Vistrenque, Alès, Saint-Chaptes and Roussillon basins) has been defined or improved by using U-Pb dating on carbonates, pollen-based climatostratigraphy and calcareous nannofossil biostratigraphy.

3.1.1 U-Pb geochronology

Sampling

The *Série Grise* Formation being almost entirely detrital, the U-Pb method has been used exclusively for calcite veins. In contrast, the overlying formations are carbonate-rich and display various carbonate mineral phases (cements, pedogenic carbonates, root calcifications, molluscan shells -*neomorphs*) making the dating method possible. The dating of these calcite phases, and therefore the corresponding geological events (e.g. subaerial exposure) helps to approximate the depositional age of the sedimentary intervals. Events post-dating the deposition give younger ages whereas events pre-dating the following depositional unit give maximum ages.

Analytical method

In order to carry out U-Pb dating on calcite, 30 samples containing a calcite mineral phase were selected for the confection of thin sections. For each sample, a 30 µm-thick and a 100 µm-thick thin section have been prepared respectively for petrographic observations and for the sampling by laser ablation for spectrometric analyses.

Prior to the analyses, sedimentological and diagenetic observations were carried thoroughly in order to identify the relevant mineral phases that should be dated and to avoid sampling from two different mineral phases, since sampling from different calcite generations would result in misinterpretations of ages. Diagenetic analysis and carbonate phase selection were performed by coupling cathodoluminescence and fluorescence microscopy. Confocal microscopy observations have been performed at the PRATIM (Aix-Marseille University) using an Axio-observer Z1 inverted confocal microscope with single or two-photon laser scanning comprising 04 visible lasers (Argon multi-ray laser: 458, 488 and 514 nm, DPSS 561 nm, He-Ne 594 nm, and He-Ne 633 nm) and a Chaméléon Vision II IR laser with pre-compensation system coupled with a ZEN 2010 software. Cathodoluminescence observations have been made at the CEREGE (Marseille, France) using a Cathodyne cold-cathodoluminescence from NewTec ® operating at 16 to 18 Kv and 160 to 200 µA coupled to an Olympus BH-2 microscope and Olympus-UPMTVC camera.

Once a carbonate phase has been individualized, the next step consists of the screening on this area for U and Pb content on thin section in order to estimate the variability of U/Pb ratios. For this purpose, elemental mapping of U, Pb, Fe and Sr was performed on the area of interest of the thin section. U-Pb dating on calcite used *in situ* Laser Ablation Inductively Coupled Plasma Mass Spectrometry (LA-ICP-MS) method which requires scattered U/Pb ratios in order to make robust statistical calculations thus allowing a reliable age, with the least uncertainty, to be obtained. Analyses were performed at the DatCarb A*midex platform (CEREGE, Aix-Marseille university).

Where the screening shows suitable U and Pb concentrations variability, about 30 circular spots of 100 µm diameter are picked within the mineral phase to perform the Laser Ablation. Calcite ablation on thick sections was performed using an ESI (Electro Scientific Industries) laser (193nm ArF Excimer laser) the resolution of which is 100 µm. Reference standards were used to correct the inter-elemental fractionation. The raw data were processed with the Lolite ® software designed for laser ablation analyses. An Excel macro, inhouse to the CEREGE, is used to handle the U-Pb data. Finally, the U-Pb age is calculated by using the Tera-Wasserburg diagram with add-on isoplot 4.15 (Excel). The obtained absolute ages have been calibrated on the Geological Time Scale of Gradstein *et al*. (2012). Further details on the methodology and the analytic parameters are given in Godeau *et al*. (2018) and their online supporting data section.

3.1.2 Pollen-based climatostratigraphy

Pollen grains have been extracted at the GeoBioStratData.Consulting laboratory (Rillieux-la-Pape, France) and the results have been integrated within a regional climatostratigraphic chart (e.g., Suc, 1984; Suc *et al*., 2018, 2020). 52 samples of about 20-30 grams weight have been processed in order to obtain pollen floras using the classical method (acid digestions with hydrochloric acid (HCl) and hydrofluoric acid (HF), concentration in $ZnCl_2$ at density 2, and sieving at 10 µm). Only 18 samples yielded pollen grains in enough quantities (their geographic distribution is shown in **Figure 1B** and specified in **Supplementary data**, **Table S3**). The residues are mounted within glycerol between the slide and coverslip that allows to slightly move each pollen grain for observation purposes under various sides. Some pollen records, from the wells (Gallician 1, 4 and 9, Maruéjols 1) and the exposed Monteils section (Saint-Chaptes Basin, ASCI system), display a number of taxa that is lower than 25 (= systematic entities equivalent to families or genera). This value is the diversity threshold to assess the

representativeness of a pollen flora sample. These non-representative samples should be interpreted with caution.

The main advantage of this new pollen analysis approach based on a detailed taxonomic investigation is that it aims to reconstruct the botanical flora and is therefore a peculiar approach for the Paleogene times. The accurate examination of the morphological characters of fossil pollen grains and their comparison with modern pollen grains of rich and varied collections (ISEM mainly, GeoBioStratData.Consulting) and iconographic databases allow to confidently identify fossil pollen grains at least at the family level and very often at the genus level. A powerful ecological interpretation of pollen floras results from such botanical identifications. These botanical identifications are robust as it has been demonstrated that almost all the modern genera of plants already existed since the Early Paleogene and were altitudinally-latitudinally distributed similarly to the present time (Suan et al., 2017; Salpin et al., 2019; Suc et al., 2020). The significance of our pollen records in terms of ecological-climatological changes are also enhanced thanks to pollen countings. To date, pollen counting approach has been a routine investigation for the Pliocene and Quaternary and less used for ancient series.

High-quality in botanical pollen identification and pollen countings have allowed to successfully apply on these pollen floras the 'Climatic Amplitude Method' (Fauquette et al., 1998) in order to quantify the Paleogene paleoclimatic conditions (Suan et al., 2017; Salpin et al., 2019; Suc et al., 2020). The analyses have been performed on a AX10 Zeiss light microscope at X250 magnification, each pollen grain being observed at X1000 magnification for its identification.

A minimum of 150 pollen grains were counted per sample extra those of *Pinus* (a cosmopolitan genus), those of meso-microthermal trees, inhabiting mid-altitudes (*Cathaya*, *Podocarpus*, *Fagus*, *Cedrus*, *Tsuga*), and those of microthermal trees, inhabiting higher altitudes (*Abies* and *Picea*). The detailed pollen analyses are provided in **Supplementary data**

(**Table S3**). Taxa are grouped according to the climatic and/or ecological significance of their modern representatives (**Table S3**), resulting in two types of synthetic pollen diagrams. The first type includes all the pollen grains excepted those of *Pinus* and provides a local and regional image of the vegetation (including that growing on reliefs); the second type excludes the mid- and high-altitude plants and provides a perception of the local vegetation (i.e., that of low altitudes). In such diagrams, plants are grouped mainly according to the classification of Nix (1982) based on the mean annual temperature (MAT), the concerned taxa usually requiring relatively elevated to high precipitation: megatherms (MAT > 24 °C), mega-mesotherms (20 °C < MAT < 24 °C), mesotherms (14 °C < MAT < 20 °C), meso-microtherms (12 °C < MAT <14 °C), and microtherms (MAT < 12 °C). The other groups have various significations: environmental for the herbaceous plants (more often not-identifiable at the infra-family level), ecological for the water plants, indicative of some dryness (Mediterranean sclerophyllous plants, steppe plants and subdesertic plants), insignificant (for example, the Cupressaceae with a *Cupressus-Juniperus* like pollen unidentifiable at the genus level). Details about taxa composing the groups are provided in **Table S3**. Reworked palynomorphs from older periods are not very abundant except in few samples (Canet 1 1100 and 1701 m; Gallician 1 1648 m; Gallician 9 2530 m; **Table S3**). They are easily recognizable by their morphology and/or their darker colour and/or their altered preservation.

The varying content of successive pollen locations is mostly considered as markedly driven by global climate changes which was affected by major and secondary fluctuations during the time interval 38–23 Ma as illustrated by the global oxygen reference isotope curve (Westerhold et al., 2020). Accordingly, pollen floras are hypothesized to correlate with the global climatic evolution, which constitutes the principle of climatostratigraphy (Suc, 1984; Suc et al., 1995, 2018, 2020; Popescu et al., 2010). Factually, we propose to correlate each pollen assemblage with the oxygen isotope stage that corresponds the best to its climatic significance, still within

the established stratigraphic succession and/or within the chronologic range separately indicated by mammal fauna or calcareous nannofossils when available.

This approach contrasts with the traditional palynostratigraphy based on the direct attribution of a chronological value to some pollen grains (Sittler *et al.*, 1975; Châteauneuf, 1980; Châteauneuf et al., 2019) that may lead to serious misinterpretations (see the **Supplementary Data**).

3.1.3 Calcareous nannofossils

The analysis of calcareous nannofossils has been performed for refining the chronostratigraphic framework and evidencing potential marine incursions. Calcareous nannofossils have been studied in the fraction of 2–30 µm and separated by decantation method using a 7% solution of H_2O_2. Smear-slides were mounted with Canada balsam and analyzed with an Olympus transmitting light microscope at x 1200 magnification. Nannofossil identifications follows the taxonomic classification of Perch-Nielsen (1985) and Raffi et al. (2006). Nannofossil zones are after Martini (1971). Further calibration follows Raffi et al. (2006) and Gradstein et al. (2012).

3.2 Climatic Amplitude Method

The endeavour in pollen identification and counting implies the possibility to use the Climatic Amplitude Method to reconstruct climate conditions during the deposition of the sediments. This method allows estimating past climate variables by transposing the climatic requirements of the maximum of modern taxa to the fossil records. This approach relies on the relationship between the relative pollen abundance of each individual taxa and climate, defined after comparison with more than 6,000 present-day pollen records distributed worldwide. This

363 method accounts not only for the presence/absence criterion but also pollen percentages to
364 provide more reliable reconstructions (Fauquette et al., 1998). The estimated mean annual
365 temperatures (MAT), mean temperatures of the coldest (MTC) and warmest (MTW) months
366 and mean annual precipitation (MAP) concern low-elevation vegetation because meso-
367 microthermal and microthermal taxa (*Cedrus*, *Fagus*, *Tsuga*, *Cathaya*, *Podocarpus Abies* and
368 *Picea* which live today at higher elevations in tropical-subtropical regions) were excluded from
369 the process (but not from the percentages) to avoid a cold bias linked to transport from higher
370 elevations. *Pinus*, which may inhabit different vegetation belts, is also excluded from the
371 calculation. The excluded taxa were defined based on the distribution of vegetation today.
372 Indeed, the types of vegetation deduced from our pollen data are found in South-eastern China
373 today at around 25°N and 110 to 120°E (Hou, 1983). In this region, the vertical distribution of
374 the vegetation is characterized, from the base to the top of the massifs by evergreen broad-
375 leaved forest, mixed evergreen and deciduous (*Betula*, *Acer*) broad-leaved forest,
376 *Cathaya*/*Tsuga* forest, *Picea*/*Abies* forest and high mountain meadows (Hou, 1983). In the
377 Climatic Amplitude Method, the estimates for each climatic parameter are given as an interval
378 (minimum and maximum values of the parameter). A most likely value (MLV) is calculated,
379 which corresponds to a weighted mean. The MLV has been statistically tested on modern pollen
380 data and has provided reliable results (Fauquette et al., 1998).

381

382 **3.3 Geochemical modelling of strontium and sulfur isotopes on sulfates**

383 Strontium and sulfur isotope compositions of gypsum and anhydrite have been proved to be
384 reliable markers of the origin of the waters from which they precipitated and geochemical
385 modelling approaches make it possible to quantify the proportions of different salt waters within
386 a mixture (Denison et al., 1998).

387 **3.3.1 Sampling and measurements**

Five anhydrite samples from Pierrefeu-1 well (Vistrenque Basin, see position in **Fig. 5**) and three anhydrite samples from Les Fumades wells (SC-1 and SC-2, Alès Basin, see position in **Fig. 4**) have been selected for $\delta^{34}S$ and $^{87}Sr/^{86}Sr$ laboratory measurements.

Strontium isotope measurements were carried by the SARM-CRPG laboratory (Vandoeuvre-les-Nancy, France). Samples have been powdered (<50 µm), weighted and mixed with HNO_3 and HF and after evaporation, mixed with concentrated HCl. After complete digestion of the sample and Sr separation, $^{87}Sr/^{86}Sr$ was measured by using a TIMS Triton Plus (Thermo electron) in static mode. The standard NBS987 has been used as a reference. All measurements have 2σ error are lower than 0.000012.

S isotopic composition of sulfates from anhydrite and gypsum samples and elemental (native) sulfur was measured by combustion using an Elementar vario PYRO cube elemental analyzer (Elementar GmbH) in-line with an Isoprime 100 mass spectrometer (Manchester, UK) in continuous flow mode at the University of Burgundy in Dijon, France. Isotope data are expressed in delta notation and reported in units per mil (‰). The $\delta^{34}S$ data are reported with respect to the international standard Vienna Cañon Diablo Troilite (VCDT). Analytical errors are ± 0.3 ‰ (2σ) based on replicates for standard materials.

3.3.2 Modelling of strontium and sulfur isotope composition of mixed waters

The Sr isotope composition of two-component mixtures/endmembers has been described in detail by Faure (1986) and applied to Sr and S isotopes (Andersson et al., 1992; Denison et al., 1998). The isotopic ratio ($^{87}Sr/^{86}Sr$ and $^{34}S/^{32}S$) Im is computed as follows:

$$\mathbf{Im=[f1.C_1.I_1+(1-f_1).C_2.I_2] / [f_1.C_1 + (1-f_1).C_2]} \quad \mathbf{(1)}$$

Where I_1 and I_2 represent the isotopic ratios of the first and second end member, respectively. C_1 and C_1 are the Sr or SO_4^{2-} concentration in the first and second end members, respectively and f1 is the volume fraction of the first end member water in the mixture.

Various endmembers have been selected for the modelling: 1) seawater, 2) continental water whose Sr and S content is controlled by the leaching of Triassic evaporites, 3) continental water whose composition derived from the leaching of metamorphic rocks.

The Sr concentration of Paleogene seawater (15 ppm) is derived from the estimations by Vollstaedt et al. (2014); such a value is close to modern concentrations (~8 ppm). Sulfur concentration was assumed to be similar to that of modern seawater (2800 ppm). The $^{87}Sr/^{86}Sr$ values for Priabonian to Chattian seawater range from 0.7077 to 0.7083 (Mc Arthur et al., 2012) while $\delta^{34}S$ is assumed to be close to modern values (+20‰).

Riverine waters influenced by the leaching of Triassic evaporites have been considered to have retained the $^{87}Sr/^{86}Sr$ and $\delta^{34}S$ of the original gypsum or anhydrite. $^{87}Sr/^{86}Sr$ values ranging from 0.7076 to 0.7080 have been reported for Triassic (Keuper) evaporites from the French Pyrenees (Albarède and Michard, 1987), Italy (Dinelli et al., 1999), Spain (Alonso-Azcarate et al. 2006; Ortí et al., 2014), while $\delta^{34}S$ values range from +10 ‰ to +17 ‰ (Utrilla et al., 1992; Dinelli et al., 1999; Boschetti et al., 2011).

Riverine waters draining metamorphic or igneous bedrocks should have higher $^{87}Sr/^{86}Sr$ ratios as shown in present time in the Cevennes Massif, with values ranging from 0.712 to 0.714 for waters draining granites and from 0.714 to 0.717 for waters draining schists (Petelet-Giraud et al., 2006). Regarding sulfur isotope composition, magmatic and metamorphic rocks are known to be characterized by $\delta^{34}S$ ranging from -12 ‰ to +12‰ (Chaussidon et al., 1989; Giacometti et al., 2014).

4. Results and interpretation

4.1 U-Pb dating

Among the examined 12 samples, only three samples meet the conditions of the U-Pb dating method: (a) G9 13D, (b) G9 7, and (c) G9 K35. Relevant samples and associated ages are summarized in **Table 1**.

4.1.1 G9 13D Sample: *subaerial exposure on top of the Série Calcaire*

In this sample, microstalactitic calcite (A1) lines the walls of a dissolution vug. It is post-dated by an anisopachous calcite cement (A2) which is in turn post-dated by an isopachous equant sparry calcite cement (I1) (**Fig. 6A**). Only cement A1 displays dull luminescence while the following cements are non-luminescent and thus cannot be distinguished under cathodoluminescence. However, observations under confocal microscope made it possible to distinguish the cement generations (**Fig. 6C**). Uranium concentrations are very low in the A2 and I1 cements thus precluded dating analyses (**Fig. 6B**). However, the cement stage A1 displays enough U and Pb thus allowing the dating method to be applied (**Fig. 6D**). The calculated age of the early diagenetic microstalactitic cement A1 is 31.27 +/- 1.90 Ma which gives a early to middle Rupelian age after GTS2012 (Gradstein et al., 2012).

4.1.2 G9 7 sample: *vadose cement within the lowermost interval of the Série Rouge*

This sample displays anisopachous pendant microsparite cements, up to 600 µm thick around clasts in a polymictic conglomerate (**Fig. 7A**). In this sample, carbone and oxygen isotope analyses on the calcite yielded very negative values ($\delta^{18}O$ = -5.11 ‰ V-PDB & $\delta^{13}C$ =

-5.59 ‰ V-PDB) thus indicating meteoric origin of the precipitation water. In addition, the anisopachous nature of the cement suggests precipitation under vadose meteoric conditions. Such cements represent the earliest phase of cementation and formed prior to burial and mechanical compaction. The cement therefore likely formed shortly after deposition and infill of the fluvial channel, in a vadose environment within an alluvial plain. U and Pb concentrations are favourable thus making it possible to test the dating method. 74 spots have been used and the concentrations show sufficient dispersal of the U/Pb ratio thus enhancing the accuracy of the method (**Fig. 7B**). The U-Pb age found for this carbonate phase using the Tera-Wasserburg diagram is 27.88 +/- 1.71 Ma which indicates a late Rupelian to early Chattian age according to the GTS (Gradstein et al., 2012). The initial composition ratio of $^{207}Pb/^{206}Pb$ is 0.8321 +/- 0.034.

4.1.3 G9 K35 sample: *calcite veins within the lower Série Grise*

The K35 sample is from the terrigenous-rich *Série Grise* Formation. In this sample, the calcite analysed for U-Pb dating consists of the filling of fractures (veins) within the silty marlstones host rock (**Fig. 7C**). The vein is about 1 mm wide and it is filled with equant to fibrous calcite, the crystals sizes average 200 µm.

Under cathodoluminescence, the calcite vein is non-luminescent (**Fig. 7D**). In the calcite vein, U and Pb concentrations are favourable to the dating method (**Fig. 7E**). The calculated Tera-Wasserburg U-Pb age for the calcite vein infill is 21.46 +/- 2.19 Ma.

4.2 Calcareous nannofossils

Calcareous nannofossils are recorded in seven samples (**Supplementary data: Table S2**), supporting some marine water incursions into the Alès Basin during the Priabonian (crossroad

D716/D981 sample), in agreement with the occurrence of dinoflagellate cysts and mangrove pollen grains. Some other marine water incursions are indicated in the Gallician 1 borehole at depths 1810 m (from the lowermost *Série Calcaréo-salifère* Formation ascribed to late Chattian) and 1594 m (ascribed to earliest Aquitanian), consistently with the occurrence of marine dinoflagellate cysts in the studied samples from the Canet 1 borehole. The calcareous nannofossil assemblages identified from the Alès and Vistrenque basins (Crossroad D716/D981, Maruéjols 1 433 m, Gallician 1 1810 m and 1594 m) are poor in species with a short biostratigraphic range: only *Reticulofenestra bisecta* and *R. lockeri* point out a chronological interval from ca. 38 Ma to ca. 23 Ma (Anthonissen and Ogg, 2012 in Gradstein et al., 2012) i.e., covering the time interval investigated in this study including the Priabonian and the entire Oligocene. More accuracy is provided by the calcareous nannofossil assemblages from the Canet 1 borehole (**Table S2**): sample at 1701 m can be referred to biozones NP23–NP24 (32–26.8 Ma), sample at 1470 m to biozones NP24–NP25 (29.7–23.2 Ma), sample at 1100 m to biozones NP25–NN1 (26.8–22.8 Ma) (Martini, 1971; Raffi et al., 2006; Anthonissen and Ogg, 2012).

4.3 Pollen-based reconstructed paleoclimates and climatostratigraphy

4.3.1 Results

A total of 122 taxa have been identified in the 18 pollen records (**Table S3**). These pollen floras show prevalent mega-mesothermal plants and, secondarily, mesothermal plants and the conifers *Cathaya* and *Podocarpus*. Megathermal elements are mostly present in the Priabonian samples where they show relevant variations. Steppe elements mainly occur in the Rupelian samples. The other plant groups are intermittently represented.

Pollen record of five samples from wells in the Vistrenque Basin (Gallician 1 1648m, Gallician 1 1775m, Gallician 4 1580m, Gallician 9 2530m, and Vauvert 1 3200m; **Fig. 8**, see location in **Fig. 5**) was relatively poorly diversified and poorly preserved. Indeed, these pollen grains have been partially vitrified and therefore some of their morphological characters (ornamentation, structure) are severely altered. A certain amount of pollen can still be identified even though a great percentage of undeterminable pollen grains may lead to lessen the significance of some of these microflora (percentage of unidentifiable pollen grains: Gallician 1 1648 m: 8.19%; Gallician 4 1580 m: 37.36%; Vauvert 1 3200 m: 10.81%).

In addition, some of these pollen floras are characterized by a low number of taxa (Gallician 1: 24 taxa at 1648 m, 19 taxa at 1775 m; Gallician 4 1580 m: 13 taxa; Gallician 9 2530 m: 20 taxa). Among the possible hypotheses to explain such biases in preservation and plant diversity (oxidation, transport, diagenesis), the usual occurrence of oil traces during the sample processing points to a thermal diagenesis in relation with sediment maturation within the oil window. In the Gallician samples, the dominant pollen grains are those of Gymnosperms which remain often identifiable despite their poor preservation, especially of meso-microthermal (*Cathaya*, *Podocarpus*, and some *Tsuga*) and microthermal (*Abies*) trees which may reflect the relief of the Pyrenees and subsidiarily of the Alps.

The pollen record of the Gallician 9 2530m sample shows the dominance of mega-mesothermal (Cupressaceae papillate pollen representative of the former ‘Taxodiaceae’ family) and both *Cathaya* and *Podocarpus* but a significant feature of this sample is the occurrence of some mesothermal plants, Cupressaceae *(Cupressaceae-Juniperus*-type*)* and *Ephedra* (steppe plants).

In **Figure 8**, the vertical arrangement of samples first follows the stratigraphic knowledge of the studied basins (Gottis, 1958; Clauzon, 1990; Séranne, 1999; Lettéron et al., 2017, 2018, 2022) and chronology is specified thanks to informations provided by (1) mammal faunas

(Depéret, 1917; Rémy, 1985; Rémy, 1994; Rémy and Fournier, 2003; Rémy and Lesage, 2005) and (2) calcareous nannofossils that have been searched in the samples containing frequent to abundant marine dinoflagellate cysts: they are specified below and in the **Supplementary data (Table S2)**.

The climate has been quantified for all the pollen spectra except for Gallician1 1775 m, Gallician 4 1580 m and Saint-Jean de Maruéjols – Pit hill because of the low taxa diversity. The results are given, for each climatic parameter, as an interval and a Most Likely Value for each site (**Table 2**).

4.3.2 Interpretation

The analysed pollen records allow to reconstruct the local and regional vegetation, from low altitude to elevated reliefs (**Fig. 8**). Lower places were sporadically occupied by *Avicennia* mangrove with probably Rhizophoraceae, suggesting nearby marine environments, which are also supported by the record of marine dinoflagellate cysts. Occurrence of lakes is revealed by frequent freshwater plants (*Aglaoreidia*, *Myriophyllum*, Oenotheraceae, Restionaceae, etc.) and the *Botryococcus* microalga. The coastal environments and lake banks were also inhabited by riparian swamps with *Taxodium-Glyptostrobus* (i.e., illustrated by the *Taxodium*-type pollen grains). Lowlands were occupied by an evergreen subtropical forest rich in mega-mesothermal plants (*Alangium*, *Engelhardia*, *Embolanthera*, *Distylium*, *Nyssa*, *Mussaenda*-type, *Rhoiptelea*, Sapotaceae, *Symplocos*, *Uncaria*-type, Cupressaceae former 'Taxodiaceae', etc.) including some megathermal plants (*Amanoa*, *Bombax*-type, *Afzelia-Peltophorum*-type, *Canthium*-type, *Croton-Jatropha*, *Peltophorum*-type, *Mappianthus*, *Phyllanthus*, *Peltogyne*-type, *Sapindaceae*, *Thumbergia*, etc.). Vicinity of higher lands is attested by abundant mesothermal plants (*Acer*, Araliaceae, *Carpinus*, *Carya*, *Eucommia*, *Liquidambar*, *Parrotia*, *Pterocarya*, *Quercus*, *Ulmus*, *Zelkova*, etc.), which constituted a mesophilous deciduous forest. The development of

555 altitudinal forest vegetation (*Cathaya*, *Podocarpus*, *Cedrus*, *Tsuga*, *Abies*, *Picea*) suggests the
556 occurrence of reliefs, especially of high reliefs to the south as evidenced by Canet 1 well and
557 Gallician wells pollen floras.

558 Cupressaceae trees (*Cupressus*-*Juniperus*-type) may contribute to the lowland and higher
559 vegetation as they can be represented by diverse taxa growing today in subtropical to high
560 altitude forests, because of our inability to distinguish their pollen. Sclerophyllous
561 Mediterranean elements (*Olea* mainly, *Phillyrea*, *Quercus ilex*-type) episodically developed,
562 simultaneously with decrease in taxa requiring great humidity and increase in herbaceous taxa.
563 It is possible to conceive that these plants already grew on drier soils and tolerated less humid
564 periods. Drier conditions are revealed by development of steppe assemblages (mainly
565 constituted of *Ephedra*), in parallel with reducing of taxa requiring humid climate.

566 Variability observed in the Priabonian pollen assemblages appears to be referred to climate
567 fluctuations during a warmer phase. All these pollen records come from exposed sections and
568 are not concerned by biases in preservation which often affect deep sediments from boreholes.
569 They mainly consist in opposed amounts of thermophilous forest elements (megatherms and
570 mega-mesotherms) and herbaceous and steppe elements (*Ephedra*) pointing to more open and
571 drier environments. Variability observed in the Oligocene pollen assemblages could refer to
572 climate fluctuations during a cooler phase resulting in alternations of drier and more humid
573 episodes.

574 All the Oligocene pollen records come from drilled sediments in which pollen preservation
575 may be poor, that makes uncertain their paleoenvironmental interpretation. However, these
576 major (Priabonian–Rupelian transition) and minor (intra-Priabonian and intra-Rupelian–
577 Chattian) changes displayed by pollen assemblages are consistent with the reference oxygen
578 isotope curve (**Fig. 8**; Westerhold et al., 2020). For example, the sample Gallician 9 (2530 m)
579 is understood as illustrating the major change in climate marking the Eocene–Oligocene

transition because of scarcity in megathermal plants in opposition to the abundance of *Ephedra*. Finally, the two samples Gallician 1 (1775 and 1648 m) are correlated with two successive warmer episodes during the late Chattian because of high amount of mega-mesothermal plants and the persistence of *Ephedra* in low percentage.

Paleogeographic reconstructions indicate the existence of elevated topography southwards to the Camargue and Languedoc basins (Benedicto et al., 1996). These reliefs supplied detrital sediments and pollen grains of high-altitude plants that have undergone low to moderate transport to the depositional areas of the Vistrenque and of the Alès basins. The abundance of *Podocarpus* in the Gallician samples, a marker of the Pyrenean flora during the Paleogene, indicates that the pollen of these samples is sourced from these highlands.

In the Alès Basin, the climatic deterioration at the Eocene-Oligocene transition is expected to follow the Montchamp pollen flora, indicating persistent warm conditions. The reconstructed MAT and MTC are very high for this location (**Table 2**). Because of their low percentage in megathermal plants in contrast to the occurrence of *Ephedra*, the pollen records of Monteils and of the Pit hill of Saint-Jean de Maruéjols attest less warm and weakly drier conditions than the Crossroads D716/D981, Célas, and Montchamp microfloras. The estimated MAT at Monteils is the lowest for this time period (Most Likely value around 18.7°C instead of 20 to 21°C, **Table 2**). Some cooling is also evidenced by the Serre de Cauvel pollen assemblage with respect to decreased megathermal plants and increased Mediterranean sclerophyllous elements. However, this cooling should be less important as it is not observed in the estimated climate. The Monchamp microflora contains *Avicennia* and Rhizophoraceae pollen grains. The latter are also recorded at Serre de Cauvel while *Avicennia* is also recorded at Saint-Jean de Maruéjols Pit hill, Célas Tunnel and Crossroads D716/D981. Mean temperature of the warmest month (MTW) is stable all along the period (**Table 2**). Euzet Hill, Serre de Cauvel, Crossroads D716/D981, Maruéjols 1 798 m, and Saint-Jean de Maruéjols Pit hill samples contain high

605 proportions of conifers (*Podocarpus*, *Cathaya*) that do not result from preservation bias because
606 of their high floristic diversity (>30 taxa) but from high pollen supply from mid-altitude.

607 In the Vauvert 1 3200 m sample, the presence of relatively frequent pollen of Mediterranean
608 sclerophyllous plants may point to the climatic cooling at earliest Oligocene, supported by few
609 megathermal plants, reduced mega-mesothermal plants and increasing herbaceous open
610 environments in a context of shortening freshwater bodies. This cooling and lower humidity
611 are also well marked in the estimated mean annual temperature (MAT), mean temperature of
612 the coldest month (MTC) and mean annual precipitation (MAP) (**Table 2**). The estimated MAT
613 at Vauvert is in agreement with the value obtained at Saint-Lions, located 150 km northeastward
614 of the Camargue, presently in the Digne thrust, for the same period (Fauquette et al., 2015). In
615 the Gallician 9 2530 m sample, some aridification of the climate is suggested by the local
616 expansion of *Ephedra* that leads to a low estimate of mean annual precipitation (**Table 2**).
617 Pollen assemblages of Gallician 4 1580 m and Gallician 1 1648 m are consistent with a Late
618 Oligocene age.

619 Our ascription of the studied interval of Canet 1 well (1701–1100 m) to Oligocene is based
620 on the occurrence of above-mentioned calcareous nannofossils (**Table S2**) and corresponds to
621 the presence-abundance of *Podocarpus* pollen, never recorded in Southern France since the
622 earliest Aquitanian (Bessedik, 1984). Considering the calcareous nannofossil range, the sample
623 Canet 1 (1701 m) is ascribed to a warmer and still dry episode during the late Rupelian because
624 of increased percentage in megathermal plants and a significant occurrence of *Ephedra*.
625 Similarly, the sample Canet 1 (1470 m) is referred to a cooler episode of the early Chattian as
626 supported by the absence of megathermal plants and a relative high presence of *Ephedra*
627 associated to *Calligonum*. The sample Canet 1 (1186 m) is located in an intermediate cooler
628 episode of the mid-Chattian because of the absence of megathermal plants, a relatively weak
629 occurrence of mega-mesothermal plants and the persistence of *Ephedra* in a low proportion.

Finally, the uppermost Canet 1 (1100 m) sample is ascribed to a lesser warm episode just before the Chattian–Aquitanian transition because of its lower amount of mega-mesothermal plants and greater percentage of mesothermal plants. Climate reconstruction of Canet 1 well show that MAT are 1 to 2°C and MTC are 1 to 5°C lower than during the Priabonian. MAP are also slightly lower than during the Priabonian (**Table 2**).

4.4 Geochemical modelling of the strontium and sulfur isotopes of sulfates

4.4.1 Pierrefeu-1 well (Vistrenque Basin)

Anhydrite samples from Pierrefeu 1 well display $^{87}Sr/^{86}Sr$ values ranging from 0.70777 to 0.708201 and $\delta^{34}S$ values comprised between +10.92 ‰ and +17.10 ‰ **(Table 3)**. Anhydrites from core K2 fall within the domain of Triassic evaporites while samples from cores K5 and K6 display significantly higher $^{87}Sr/^{86}Sr$ values (**Fig. 9A**).

Mixing fluid models revealed that Sr and S isotope composition of anhydrites from Pierrefeu-1 is consistent with a formation from a mixed water composed of a riverine end-member whose Sr and S content is controlled by the leaching of Triassic evaporites and a marine end-member. The Sr and S concentrations and isotope composition of the volume fraction of each end-member for the best-case scenario, are given in Supplementary Materials (**Table S4)**. Matching between mixed-water models and isotope measurements on anhydrites integrates the effect of fractional precipitation which may lead to a difference of up to +2 ‰ in $\delta^{34}S$ between sulfates and precipitating water (Raab and Spiro, 1991).

4.4.2 SC-1 and SC-2 wells (Alès Basin)

Anhydrite from the Alès Basin (SC-1 and SC-2 wells) display a narrow range of $^{87}Sr/^{86}Sr$ values (0.70768-0.70790) while $\delta^{34}S$ is comprised between +12.11 ‰ and +26.98 ‰ **(Table 3)**. The sample from SC-1 well fall within the domain of Triassic evaporites while samples from SC-2 exhibit $\delta^{34}S$ values which are significantly higher than those of Priabonian sea-water (**Figure 9B**).

The high $\delta^{34}S$ values of gypsum minerals from SC-2 most likely arise from isotope fractionation during microbially mediated reduction of sulfates. If sulfate reduction takes place in a closed basin, the $\delta^{34}S$ of residual dissolved sulfates will be higher compared to the original fluid (Utrilla et al., 1992; Palmer et al., 2004). Additionally, measurements on native sulfur formed within anhydrite-bearing horizons in SC-2 well yielded negative $\delta^{34}S$ values ranging from -5.99 ‰ to -6.43 ‰. These negative $\delta^{34}S$ values strongly suggest that the elemental sulfur from SPr3 evaporitic interval is a byproduct of sulfate-reducing bacterial activity (Lindtke et al., 2011).

As a consequence, although the SC-1 sample unequivocally indicates precipitation from a water influenced by the dissolution of Triassic sulfates, the bacterial sulfate-reduction processes affecting the anhydrites from SC-2 prevent to draw any conclusion regarding a possible mixing with marine water.

5. Discussion

5.1 Chronostratigraphic framework of the Paleogene of the Vistrenque Basin

Sedimentological and diagenetic studies, and petrographical observations on core from the Paleogene succession in the Gallician 9 well revealed than the top of the *Série Calcaire* and the

whole overlying *Série Mixte* are affected by repeated subaerial exposition (Semmani, 2022) as suggested by the occurrence of pedogenic limestones and karst features. The development of dissolution vugs and the subsequent formation of anisopachous calcite cements (meteoric vadose environment) in the sample G9 13D (Gallician 9: 1960 m depth) are linked to these repeated stages of subaerial exposition affecting the top of the *Série Calcaire* Formation and the whole overlying *Série Mixte* Formation. The 31.2 Ma age obtained for the subaerial exposures towards the top of the *Série Calcaire* (G9 13D) represents the oldest possible age for the deposition of the overlying *Série Mixte* Formation (**Fig. 10**).

The 27.88 Ma age obtained within an early vadose cement from a fluvial conglomerate, in Gallician 9 well at 1984 m, suggests a late Rupelian to early Chattian age for the lower part of the *Série Rouge* Formation. The difference between the two absolute ages (~ 3.4 Ma) corresponds therefore to the time deposition of the *Série Mixte* and lower part of *Série Rouge*. Such a long duration, compared to the preserved thickness (~ 45 m) is consistent with low sedimentary rates and the occurrence of hiatuses punctuating the sedimentation as suggested by subaerial exposures affecting the interval (Semmani, 2022).

In addition, pollen-based climatostratigraphic approach suggests that the sample from Vauvert 1 at 3200m deposited very close to the Priabonian to Rupelian transition, thus indicating likely a Late Eocene (Priabonian) age for the lowermost part of the *Série Grise* Formation (**Fig. 10**). In Gallician-9, the 31.2 Ma age obtained at 1960 m and the early Rupelian age at 2530 m suggest sedimentation rates greater than 200 m/Myr in the upper *Série Grise* and *Série Calcaire* interval. Correlations with Vauvert-1 (**Fig. 5**) suggest sedimentation rates ranging from 300 to 500 m/Myr. The base of the *Série Grise* being not reached at 3630 m in Vauvert-1, extrapolating such sedimentation rates below 3200 m would suggest that the formation covers large parts of the Priabonian – if not the entire stage.

The late Priabonian oolithic lacustrine carbonates evidenced north of the Vistrenque Basin (Semmani *et al.*, 2022) would therefore represent a marginal lake, lateral equivalent of the *Série Grise* Formation from the basin depocenter. The *Série Grise* Formation may also have deposited coevally with part or all of the Priabonian fluvial and lacustrine succession from the neighbouring Alès, Saint-Chaptes and Issirac basins (Lettéron *et al.*, 2022).

Pollen records from Gallician 4 1580m and Gallician 1 1648m suggest a Late Oligocene (early Chattian) age for the lowermost part of the *Série Calcaréo-salifère* Formation. These findings agree with Chattian to Aquitanian ages derived from the Sr and S isotope signatures of sulfates from this interval in Pierrefeu 1 well (**Fig. 9**). Based on these age constraints, the *Série Rouge* Formation is late Rupelian to early Chattian in age (**Fig. 10**). Finally, the Aquitanian absolute age (21.46 +/- 2.19 Ma) of the calcite vein affecting the *Série Grise* in sample G9-K35 from Gallician 9 well is consistent with the infill of a fracture formed during the Oligocene-Aquitanian rifting of the Gulf of Lion margin (Séranne et al., 1995).

5.2 Tectonic and geodynamic implications

The here-defined chronostratigraphic framework of the Vistrenque Basin evidences the occurrence of a thick Priabonian to lower Rupelian sedimentary succession, thus being coeval with the fluvial-lacustrine sedimentation occurring west of the Nîmes fault in the Alès, Saint-Chaptes and North Montpellier basins (Séranne et al., 2021; Lettéron et al., 2022). The regional mapping of syn-depositional structures within these basins evidenced a left-lateral shearing of the area comprised between the NE-trending Cévennes and Nîmes faults during the Priabonian (Séranne et al., 2021). The elevated sedimentation rates, greater than 200 m/Myr, revealed in the Vistrenque Basin are consistent with a basin subsidence controlled by the major Nîmes strike-slip fault. In contrast with Languedoc basins where early to middle Rupelian are lacking, the sedimentation in the Vistrenque Basin suggests that the strike-slip movement of the Nîmes

fault was still active during the Rupelian. In addition, the sharp decrease in sedimentation rates between the upper part of the *Série Grise* (31.2 Ma in Gallician-9) and the *Série Rouge* (27.88 Ma in Gallician-9) suggest that the strike-slip movement of the Nîmes fault, associated to the ongoing shortening in the Spanish Pyrénées, ceased in the middle to late Rupelian times. The *Série Grise* Formation from the Vistrenque Basin records therefore the latest stages of Pyrenean compression until the Rupelian together with the earliest stages of the dismantling of the Languedoc-Provence segment of Pyrénées. Finally, the Chattian evaporitic succession (*Série Calcareo-salifère* Formation) and the overlying Aquitanian terrigenous sequence were deposited during the Liguro-Provençal Rifting stage (Benedicto, 1996; Séranne et al., 2021).

5.3 Evidence of marine incursions into Priabonian to Chattian continental basins from Southeast France

Saline lake sedimentation associated with the deposition of sulfates (gypsum and anhydrite) occurred during the Priabonian and/or Rupelian in various basins from SE France: Alès, Saint-Chaptes and Issirac basins (Lettéron et al., 2017, 2018, 2022) as well as in the Mormoiron–Carpentras and Apt–Manosque–Forcalquier basins (e.g. Triat and Truc, 1974; Cavelier et al., 1984). The present work documents saline lake conditions and deposition of evaporites in the Vistrenque Basin as early as the early Rupelian (within the *Série Grise*) and during the Chattian (*Série Calcaréo-salifère*).

The origin of dissolved ions (Briot, 2008) in the Paleogene saline lake waters, and the possibilities and pathways of salinization of these lacustrine systems of Southeast France and Western-European rift system are still discussed (e.g., Lettéron et al., 2017, 2018, 2022; Semmani et al., 2022). Lettéron et al. (2017) considered the relevance of the occurrence of benthic foraminifera and halophile molluscs in the lacustrine deposits from the Issirac Basin to demonstrate marine connections and discarded evidence of marine connections based on these

750 faunal contents. Moreover, these organisms have been shown to be tolerant to salinity variations
751 and can thrive in athalassic lakes (Plaziat and Younis, 2005). Nevertheless, strong evidence of
752 incursions of marine-influenced waters within the ASCI lake system during the Priabonian and
753 the Vistrenque Basin from the Late Eocene to Late Oligocene can be provided by the occurrence
754 of calcareous nannofossils, dinoflagellate cysts and halophilous plant pollen grains, and by the
755 contribution of geochemical modelling.

756 In the ASCI system, the occurrence of marine dinoflagellate cysts in Serre-de-Cauvel and at
757 the crossroad D716/D981 (Saint-Chaptes Basin: **Fig. 4**) is indicative of marine connections as
758 early as the early-to-middle Priabonian. Additionally, the presence of *Avicennia* pollen grains
759 in the Saint-Chaptes (Crossroads D716/D981) and Alès basins (Célas Tunnel, Saint-Jean de
760 Maruéjols Pit hill and Montchamp) suggests the persistent influence of marine water from the
761 middle to the latest Priabonian. The occurrence of Rhizophoraceae pollen grains from Serre de
762 Cauvel and Montchamp is consistent with such an interpretation. Finally, the Sr and S isotope
763 signatures of evaporites from the Ales Basin, although altered by sulfate-reduction processes
764 likely derive from a mixture between a continental water influenced by Triassic evaporites and
765 seawater.

766 In the Vistrenque Basin, the presence of the dinoflagellate *Deflandrea phosphoritica*
767 (chronological range: 54.6-21.2 Ma; Powell et al., 1996) in the *Série Grise* (Gallician 9 well at
768 2530 m depth) provides evidence of marine incursion into the Vistrenque Basin during the early
769 Rupelian times. The presence of pollen grains of *Ephedra* is a characteristic feature of this
770 pollen record. The present-day species of *Ephedra* are all living in arid and semi-arid regions
771 (González-Juárez et al., 2020). The few species growing on coastal sands are not salt adapted
772 and thus are not considered as halophytes (Halophytes Database). For example, *Ephedra*, which
773 is currently frequent along the Mediterranean coastline (*E. distachya* L.: Coste, 1937), is
774 represented by very scarce pollen grains in present-day pollen assemblages from the Camargue

and Roussillon coastal areas (Cambon et al., 1997; Beaudouin et al., 2005a; Suc and Fauquette, 2012). It is also very scarce in the pollen records of warm phases (Holocene and older interglacials) although it is frequent to abundant during the drier episodes corresponding to cold phases (Beaudouin et al., 2005b; Tesson et al., 2011; Arnaud-Fassetta and Suc, 2015). This comparison with modern to recent pollen records supports the interpretation of *Ephedra* as marker of both cooling and aridification phases rather than of marine incursion. On the other hand, the Sr and S isotope signatures of sulfate evaporites from the *Série Calcaréo-salifère* Formation and mixing-water modelling strongly suggest an intrusion of marine water into the Vistrenque Basin during the late Chattian.

5.4 Paleogeographic reconstructions of Southeast France during the Late Eocene and Oligocene

The potential pathways of the marine incursions into the Southeast France continental basin are displayed in the palaeogeographic reconstructions of **Figures 11**, **12**, and **13**. During the Priabonian and Rupelian, the Southeast France lake basins as well as the West Alpine Sea were bounded to the south by the EW-trending Pyrenean-Corsica-Sardinia Massif (Joseph and Lomas, 2004; Séranne et al., 2021). This relief likely yielded most of the terrigenous supply of the ASCI and Vistrenque lake basins (Lettéron et al., 2022; Semmani et al., 2022) and deep-marine West Alpine foreland Basin (Joseph and Lomas, 2004). Moreover, it was likely sufficiently continuous and elevated to prevent from connections with the Western Neotethys to the south (**Fig. 11** and **Fig. 12**). In addition, the Atlantic shoreline was located at more than 300 km west of the Alès Basin during the Priabonian and Rupelian times (Gely and Sztrákos, 2000; Sztrákos and Steurbaut, 2017), and fluvial sedimentation dominates in south-western Languedoc basins (Calvet et al., 2021; Séranne et al., 2021) thus making unlikely marine intrusion from the Atlantic Ocean into Languedoc, Rhône Valley and Camargue areas. Finally,

800 the demise of lacustrine sedimentation in the ASCI basins during the latest Priabonian or earliest
801 Rupelian and the depositional hiatus of most of the Rupelian interval (Lettéron et al., 2022) do
802 not support connections with the marine realm west of the Nîmes fault during the Rupelian
803 (**Fig. 12**).

804 In contrast, the proximity of the West Alpine foreland (<30 km from the Manosque-
805 Forcalquier Basin, and <50 km from the Valence Basin), and the probable interconnection
806 between the different SE France saline lake basins, as suggested by previous studies (Lettéron
807 et al., 2022; Semmani et al., 2022) makes marine intrusions more plausible from the West
808 Alpine Sea during the Priabonian and Rupelian (**Fig. 11** and **Fig. 12**).

809 The reconstruction of Pyrenean structures and their differentiation from later Alpine
810 deformation (Balansa et al., 2022) provides a structural framework allowing a realistic
811 reconstruction of continental paleo-reliefs during the Priabonian and Rupelian and the
812 identification of two potential marine incursion pathways, from the West Alpine Sea to the
813 Southeast France lake basins (**Fig. 11** and **Fig. 12**). A northern potential pathway would connect
814 the West Alpine Sea with the Valence Graben, north of the Diois-Barronies High. This
815 corresponds with the "Crest Sill" identified by Sissingh (2001) as a possible marine corridor
816 supplying seawater into the Western European rift basins. A connection of the Valence lake
817 Basin with the Mormoiron and Vistrenque to the south and finally with the ASCI system during
818 periods of maximum lake expansion would therefore explain the occurrence of calcareous
819 nannofossils, dinoflagellate cysts and mangrove pollen grains within the Alès Basin during the
820 Priabonian and in the Vistrenque Basin during the Rupelian.

821 A southern potential pathway of marine incursion would connect the West Alpine Sea with
822 the Manosque-Forcalquier, Mormoiron and Vistrenque-ASCI basins through a set of Pyrenean
823 synclines in the Haut-Var region (Bauduen, Montmeyan, Salernes and Rians basins). The
824 hypothesis of such a marine corridor is corroborated by the presence of Paleogene marine

825 markers such as calcareous nannofossils and dinoflagellate cysts in the “Sables Bleutés du Var”
826 Formation in the Montmeyan Basin (Châteauneuf et al., 2019) even though the age of these
827 deposits remains very much debated (e.g., Philip et al., 2017). Such a southern sea-water
828 pathway may also explain the occurrence of dinoflagellate cysts in the Rupelian from the
829 Marseilles Basin (Châteuneuf and Nury, 1995).

830 The Chattian paleography of SE France (**Fig. 13**) differs significantly from that of
831 Priabonian-Rupelian times, since the West Alpine Sea closed as a result of sedimentary infill
832 and westward accretion of the Alpine orogenic wedge (Joseph and Lomas, 2004) during the
833 late Rupelian. In addition, the Chattian is regionally characterized by widespread active rifting
834 that formed NE-SW oriented rift-basins, onshore and offshore in the Gulf of Lion. This rifting
835 led to the collapse of the Pyrenean-Corsica-Sardinia. This resulted in marine intrusions from
836 the southern Western Neotethys, into Provence as evidenced by the occurrence of late Chattian,
837 strictly marine, shallow-water carbonate sediments west of Marseilles (‘*Côte Bleue*’ shoreline:
838 Oudet *et al*., 2010a) and marine biological markers including dinoflagellate cysts, coelenterates
839 and marine fishes in brackish-water lacustrine/lagoonal deposits from the Aix-en-Provence
840 Basin (Nury and Thomassin, 1994). The marine influence revealed by strontium and sulfur
841 isotope signatures of Chattian evaporites from the Vistrenque Basin could therefore results from
842 a marine connection to the south probably through the offshore Vistrenque Basin, the Central
843 Graben and the Catalan fault zone domain (**Fig. 13**). Such a marine water pathway, suggested
844 by Oudet *et al.* (2010b) is supported by the presence of Chattian to Aquitanian planktonic
845 foraminifera in well Tramontane 1 in the Central Graben (Cravatte *et al*., 1974). The Vistrenque
846 Basin may also have been connected with the Sardinian Graben (via Offshore Vistrenque and
847 Grand Faraman Graben) where the earliest marine ingression occurred during the latest
848 Chattian-early Aquitanian (e.g. Casula *et al*., 2001). The Chattian carbonate and evaporite
849 sediments from the *Série Calcaréo-salifère* Formation in the Vistrenque Basin could therefore

have deposited in a saline lake with transient connections with seawater during sea-level or lake-level highstands, or within a coastal sabkha with periodic marine intrusions.

5.5 Paleoclimatic implications

This present study, based on both botanical pollen identification and counting, robustly documents for the first time the climate evolution of the 38–23 Ma interval in South of France, which encompasses the Eocene–Oligocene transition. The four pollen floras from the Canet 1 borehole complete those from the Alès and Vistrenque basins for documenting the climate knowledge during the late Rupelian and early Chattian.

According to our pollen data, we demonstrate that the Eocene–Oligocene transition is marked by the suddenness and the great amplitude of the climate deterioration with lowering temperature and increasing dryness at low elevations while high humidity continued in higher altitude. The climate parameters estimated from analyses of pollen from the Vistrenque samples do not show a drastic climate deterioration. This may be due to the large climatic tolerance intervals attributed to the plants, some of them may live under large temperature and/or precipitation amplitudes at the genus or family level. However, the cooling between the Priabonian and the Rupelian is indicated by a decrease in mean annual temperature, mean temperature of the coldest month and in mean annual precipitation at Vauvert but more particularly at Gallician 9 2530 m. Following that event, temperature and precipitation increase, although they remain lower than during the Priabonian. Vegetation and climate changes, deduced from the relative abundance of megathermal and mega-mesothermal vs. herbaceous and steppic plants in the pollen diagrams, seem to indicate that the cooling in Southeast France was brief and took place at the very early Rupelian. From a vegetation and climatic point of view, the Mediterranean region is considered as a very particular region since the Paleogene as

it was certainly sheltered from cold air masses (Popescu et al., 2021). The cooling phases were thus certainly less pronounced than elsewhere in Europe.

Finally, the upper Chattian succession shows a climate evolution towards the Aquitanian conditions with very scarce megathermal plants as described by Bessedik (1984), Zheng (1990) and Suc et al. (2018), despite persistence of *Podocarpus* in the mountains up to the latest Chattian.

6. Conclusion

The definition of a robust chronostratigraphic framework for the Vistrenque Basin and the neighboring Paleogene basins, combined with the analysis of a set of micropaleontological and geochemical data, has led to significant improvements in knowledge of the geodynamic evolution, the paleogeographic framework and the paleoclimatic setting of the Upper Eocene-Oligocene lacustrine basins from South-East France:

1) The *Série Grise* Formation (Priabonian to early Rupelian) from the Vistrenque Basin was deposited in a highly subsident basin associated with the strike-slip movement of the Nîmes fault and records the latest stages of the Pyrenean shortening. Drastic decrease in sedimentation rates above the *Série Grise* suggests that the strike-slip movement of the Nîmes fault ceased around the middle-to late Rupelian. The evaporitic sedimentation of the *Série Calcareo-salifère* Formation (Chattian) is related to the stage of Liguro-Provençal rifting.
2) The pollen data recorded during this study allow climatostratigraphic correlations with the reference oxygen isotope curve and thus help to specify the age of the studied sections. The floral assemblages from the Priabonian and Rupelian of the neighbouring

Languedoc and Camargue areas constitute a powerful tool to document the climatic deterioration at the Eocene-Oligocene transition. In addition, pollen analyses made it possible to reconstruct a mangrove and freshwater lake vegetation in the Alès Basin, and a dominant evergreen subtropical forest in the surroundings of the lake which also record fluctuations with a high-altitude vegetation in the southern paleo-Pyrenean relief during the Priabonian. Vegetation cover has been shown to be rather dominated by mesothermal and herbaceous plants. During the early Rupelian and Chattian times, a clear influence of altitude vegetation is referred to the inherited Pyrenean relief, south of the study area. Simultaneously, cooler and drier climate conditions affected the surroundings of the Camargue area.

3) The use of the Climate Amplitude Method allowed evidencing a short but significant stage of climate cooling and aridification in the early Rupelian which could result from the global climate cooling following the Eocene-Oligocene Transition.

4) Strong evidence for successive intrusions of marine-influenced saltwater into the Languedoc and Camargue areas during the Priabonian, early Rupelian and Chattian intervals is provided by the occurrence of calcareous nannofossils, dinoflagellate cysts and the halophilous *Avicennia* and Rhizophoracea plants documented by their pollen. Strontium and sulfur isotope signatures of sulfates from the Série Calcaréo-salifère Formation strongly suggest incursions of marine water into the Vistrenque lacustrine system during the Chattian.

5) During the Priabonian and Rupelian, marine water likely derived from the Western Alpine Sea. Two possible pathways of seawater intrusion are suggested from paleogeographic reconstructions: the Crest Sill north to the Diois-Barronies High and/or the Pyrenean synclines in the Haut-Var area south of the Diois-Barronies High. The paleogeographic setting of south-east France significantly changed as a result of the

closure of the Alpine Sea and the formation of rift basins in the Gulf of Lion during the Chattian have made possible marine incursion into the Vistrenque Basin from the Mediterranean domain to the south.

Acknowledgements

This work was funded by the France's Ministry of Higher Education and Research and is part of the PhD of the first author (NS). This work also benefited from the financial supports of CEREGE (APIC 2018 RRH) and Carbonate Chair and we thank them warmly for their support. Sampling and analyses on the Canet 1 borehole were carried out thanks to the financial support of the ANR 'PYRAMID', to which this paper is a contribution. This work benefited from internal documents provided by Total E&P (Contract of cooperation and data exchange TOTAL E&P-Aix-Marseille University FR00040451). The authors would also thank Gilles Graffin (STC core library, Boussens) for giving access to samples on the Camargue wells cores. Alain Tonetto (head of PRATIM, Aix-Marseille University) is also thanked for his help to carry out confocal microscope analyses. Scanning electronic microscope observations benefited from the assistance of Omar Boudouma (Sorbonne University). Christian Gorini, Michel Séranne, an anonymous reviewer and the Editor are greatly thanked for their very constructive contribution to improve this manuscript.

941 ## References

942

943 Albarède, F. Michard, A. 1987. Evidence for Slowly Changing Sr-87/Sr-86 in Runoff from
944 Fresh-Water Limestones of Southern France. *Chemical Geology* 64: 55-65.

945 Alonso-Azcárate, J. Bottrell, S.H. and Mas, J.R., 2006. Synsedimentary versus metamorphic
946 control of S, O and Sr isotopic compositions in gypsum evaporites from the Cameros Basin,
947 Spain. *Chemical Geology* 234: 46-57.

948 Andersson, P.S., Wasserburg, G.J., Ingri, J. 1992. The sources and transport of Sr and Nd
949 isotopes in the Baltic Sea. *Earth and Planetary Science Letters* 113: 459-472.

950 Anthonissen D.E., Ogg J.G, 2012. Cenozoic and Cretaceous biochronology of planktonic
951 foraminifera and calcareous nannofossils. In "The geologic time scale 2012", Gradstein, F.M.,
952 Ogg, J.G., Schmitz, M.D., Ogg, G.M. (eds.), Elsevier, Amsterdam, Appendix 3, 1083–1127.

953 Arnaud-Fassetta, G., Suc, J.-P., 2015. Dynamique hydrogéomorphologique et diversité
954 végétale dans le delta du Rhône (France) de -10.000 ans à demain. *In* " Le Rhône, entre nature
955 et société ", Reynard, E., Evéquoz-Dayen, M., Borel, G. (eds.), *Cahiers de Vallesia*, 29, 63–98.

956 Arthaud, F., Séguret, M., 1981. Les structures pyrénéennes du Languedoc et du Golfe du
957 Lion (Sud de la France). Bulletin de la Société géologique de France, 38, 51–63.

958 Arthaud, F., Laurent, P., 1995. Contraintes, déformation et déplacemen dans l'avant-pays
959 Nord-pyrénéen du Languedoc méditerranéen. Geodynamica Acta, 8, 142–157.

960 Arthaud F, Ogier M, Séguret M. 1981. Géologie et géophysique du Golfe du Lion et de sa
961 bordure nord. *Bulletin du BRGM* 1(3): 175–193.

962 Balansa J, Espurt N, Hippolyte J-C, Philip J, Séverine Caritg. 2022. Structural evolution of
963 the superimposed Provençal and Subalpine fold-thrust belts (SE France). *Earth-Science*
964 *Reviews* 227, April 2022, 103972. Doi : https://doi.org/10.1016/j.earscirev.2022.103972

965 Beaudouin, C., Suc, J.-P., Cambon, G., Touzani, A., Giresse, P., Pont, D., Aloïsi, J.-C.,
966 Marsset, T., Cochonat, P., Duzer, D., Ferrier, J., 2005a. Present-day rhythmic deposition in the
967 Grand Rhône prodelta (NW Mediterranean) according to high-resolution pollen analyses.
968 *Journal of Coastal Research*, 21, 2, 292–306.

969 Beaudouin, C., Suc, J.-P., Acherki, N., Courtois, L., Rabineau, M., Aloïsi, J.-C., Sierro, F.J.,
970 Oberlain, C., 2005b. Palynology of the northwestern Mediterranean shelf (Gulf of Lions): First
971 vegetational record for the last climatic cycle. *Marine and Petroleum Geology*, 22, 6–7, 845–
972 863.

973 Beaufort L, Bruneau J, Crepin A, Julian Y. 1954. Ampleur de l'érosion pontienne et du
974 comblement Pliocène en Camargue. *Bulletin de la Société Géologique de France* 6(4), 157-
975 184.

976 Benedicto A, Labaume P, Séguret M, Séranne M. 1996. Low-angle crustal ramp and basin
977 geometry in the Gulf of Lion passive margin: the Oligocene-Aquitanian Vistrenque graben, SE
978 France. *Tectonics* 15(6): 1192–1212.

979 Bessedik M. 1984. The early Aquitanian and upper Langhian-lower Serravallian
980 environments in the Northwestern Mediterranean region. *Paléobiologie continentale*, 14, 2,
981 153–179.

982 Bestani, L., N. Espurt, J. Lamarche, M. Floquet, J. Philip, O. Bellier, and F. Hollender 2015.
983 Structural style and evolution of the Pyrenean–Provence thrust belt, SE France. *Bulletin de la*
984 *Société Géologique de France*, 186, 223-241.

985 Bois C. 1993. Initiation and evolution of the Oligo-Miocene rift basins of southwestern
986 Europe: contribution of deep seismic profiling. *Tectonophysics* 226 : 227-252.

987 Boschetti, T., Cortecci, G., Toscani, L., Iacumin, P. 2011. Sulfur and oxygen isotope
988 compositions of Upper Triassic sulfates from northern Apennines (Italy): paleogeographic and
989 hydrogeochemical implications. *Geologica Acta* 9(2): 129-147.

990 Bodergat A-M, Briot D, Hugueney M, Poidevin J-L, Picot L, Giraud F, Berger J.P, Levy A,
991 Poignant A. 1999. Incursions marines dans l'environnement lacustre du rift oligocène de
992 Limagne (Massif Central, France) : apport des organisms halophiles et des isotopes du
993 strontium, datation par les mammifères. *Bulletin de la Société Géologique de France* 170: 499–
994 511.

995 Briot D, 2008. Sr isotopes of the shells of the euryhaline gastropod *Potamides lamarcki* from
996 the Oligocene of the French Massif Central and Paris Basin – A cule to its habitats.
997 Palaeogeography, Palaeoclimatology, Palaeoecology 268 : 116-122.

998 Cambon, G., Suc, J.-P., Aloïsi, J.-C., Giresse, P., Monaco, A., Touzani, A., Duzer, D.,
999 Ferrier, J., 1997. Modern pollen deposition in the Rhône delta area (lagoonal and marine
1000 sediments), France. *Grana*, 36, 105–113.

1001 Calvet M., Gunnell Y., Laumonier B. 2021. Denudation history and palaeogeography of the
1002 Pyrenees and their peripheral basins: an 84-million-year geomorphological perspective. *Earth*
1003 *Science Review*, 103436.

1004 Casula, G., Cherchi, A., Montadert, L., Murru, M., Sarria, E., 2001. The Cenozoic graben of
1005 Sardinia (Italy): geodynamic evolution from new seismic and field data. *Marine and Petroleum*
1006 *Geology* 18, 863–888.

Cavelier C, Alabouvette G, Amberger J.P, Cautru J.-P, Charollais J, Châteauneuf J.-J, et al. 1984. Paléogène. In : Debrand-Passard ed., *Synthèse géologique du Sud-Est de la France*. *Mémoire du BRGM* 125 : pp. 389-468.

Châteauneuf, J.-J. 1980. Paléostratigraphie et paléoclimatologie de l'Eocène supérieur et de l'Oligocène du bassin de Paris. *Mémoires du Bureau de Recherches géologiques et Minières* 116: 357 pp.

Châteauneuf, J.-J., Nury, D., 1995. La flore de l'Oligocène de Provence méridionale : implications stratigraphiques environnementales et climatiques. *Géologie de la France* 2 : 43-55.

Châteauneuf, J.-J., Villeneuve, M., Nury, D. 2019. La transgression rupélienne (stampienne) dans les « Sables bleutés » du Haut-Var, démontrée par l'étude palynologique à Saint-Maime (Fossé de Montmeyan, Sud-Est France). *Géologie de la France* 1: 1–17.

Chaussidon, M., Albarède, F., Sheppard, S.M.F. 1989. Sulphur isotope variations in the mantle from ion microprobe analyses of micro-sulphide inclusions. *Earth and Planetary Science Letters* 92: 144-156.

Clauzon, G. 1990. Restitution de l'évolution géodynamique néogène du bassin du Roussillon et de l'unité adjacente des Corbières d'après les données écostratigraphiques et paléogéographiques. *Paléobiologie continentale* 17: 125–155.

Coste, H., 1937. Flore descriptive et illustrée de la France, de la Corse et des contrées limitrophes. Librairie des Sciences et des Arts, Paris, 3, 728 pp.

Cravatte, J., Dufaure, P., Prim, M., Rouaix, S. 1974. Les forages du Golfe du Lion – Stratigraphie, Sédimentologie. *Compagnie Françaises du Pétroles, Notes & Mémoires* 11, 209-274.

1030 Denison, R.E., Kirkland, D.W., Evans, R., 1998. Using Strontium Isotopes to Determine the
1031 Age and Origin of Gypsum and Anhydrite Beds. *Journal of Geology*, 106, 1-17.

1032 Depéret C. 1917. Monographie de la faune de mammifères fossiles du Ludien inférieur
1033 d'Euzet-les-Bains (Gard). *Annales de l'Université de Lyon, Sciences, Médecine*, Lyon (N° 40-
1034 288pp).

1035 Dèzes P, Schmid S.M, Ziegler P.A. 2004. Evolution of the European Cenozoic Rift System:
1036 interaction of the Alpine and Pyrenean orogens with their foreland lithosphere. *Tectonophysics*
1037 389: 1–33.

1038 Dinelli, E., Testa, G., Cortecci, G., Barbieri, M. 1999. Stratigraphic and petrographic
1039 constraints to trace element and isotope geochemistry of Messinian sulfates of Tuscany.
1040 *Memoria della Società Geologica Italiana* 54: 61-74.

1041 Fauquette, S., Guiot, J., Suc, J.-P. 1998. A method for climatic reconstruction of the
1042 Mediterranean Pliocene using pollen data. *Palaeogeography, Palaeoclimatology,*
1043 *Palaeoecology* 144: 183–201.

1044 Fauquette S, Bernet M, Suc J.-P, Grosjean A.-S, Guillot S, van der Beek P, Jourdan S,
1045 Popescu S.M, Jiménez-Moreno G, Bertini A, Pittet B, Tricart P, Dumont T, Schwartz S, Zheng
1046 Z, Roche E, Pavia G, Gardien V. 2015. Quantifying the Eocene to Pleistocene topographic
1047 evolution of the southwestern Alps, France and Italy. *Earth and Planetary Science Letters* 412:
1048 220-234.

1049 Faure, G., 1986. Principles of Isotope Geology, 2nd edition, New York, Chichester,
1050 Brisbane, 589 pp.

1051 Feist-Castel M. 1971. Sur les Charophytes fossiles du bassin tertiaire d'Alès (Gard). Geobios,
1052 4, 157-172.

Fontes J.-C, Gaudant J, Mélières F, Filly A, Schlund J.-M. 1996. Origine continentale des évaporites paléogènes du fossé de Valence (Drôme): données minéralogiques, isotopiques et paléoécologiques. *Bulletin de la Société Géologique de France* 167(4): 475–481.

Giraud J. 1902. Études géologiques sur la Limagne. *Bulletin du Service de la Carte Géologique de France*, 13, 87, 410 p.

Gely, J.-P., Sztrákos, K., 2000. L'évolution paléogéographique et géodynamique du Bassin aquitain au Paléogène : enregistrement et datation de la tectonique pyrénéenne. *Géologie de la France* 2 : 31-57.

Giacometti, F., Evans, K. A., Rebay, G., Cliff, J., Tomkins, A. G., Rossetti, P., Vaggelli, G. and Adams, D. T., 2014. Sulfur isotope evolution in sulfide ores from Western Alps: Assessing the influence of subduction-related metamorphism, Geochemistry, Geophysics, Geosystems, 15, 3808–3829.

Godeau, N., Deschamps, P., Guihou, A., Léonide, P., Tendil, A., Gerdes, A., Hamelin, B., Girard, J.-P., 2018. U-Pb dating of calcite cement and diagenetic history in microporous carbonate reservoirs: case of the Urgonian Limestone, France. Geology 46, 3, 247-250.

González-Juárez, D., Escobedo-Moratilla, A., Flores, J., Hidalgo-Figueroa, S., Martínez-Tagüeña, N., Morales-Jiménez, J., Muñiz-Ramírez, A., Pastor-Palacios, G., Pérez-Miranda, S., Ramírez-Hernández, A., Trujillo, J., Bautista, E., 2020. A review of the *Ephedra* genus: distribution, ecology, ethnobotany, phytochemistry and pharmacological properties. Molecules, 25, 3283.

Gorini C, Le Marrec A, Mauffret A. 1993. Contribution to the structural and sedimentary history of the Gulf of Lions (western Mediterranean), from the ECORS profiles, industrial seismic profiles and well data. *Bulletin de la Société géologique de France* 164(3): 353–363.

1076 Gorini, C., A. Mauffret, P. Guennoc, and A. Le Marrec, 1994. Structure of the Gulf of Lion
1077 (northwestern Mediterranean Sea): A review, in Hydrocarbon andPetroleum Geology of
1078 France, Spec. Publ. Eur. Assoc. Pet. Geosci., vol.4, A. Mascle (Ed.), pp. 223–243.

1079 Gottis, M. 1958. L'apport des travaux de la Compagnie d'exploration pétrolière (C.E.P.)
1080 dans la connaissance du basin tertiaire du Roussilon. *Bulletin de la Société géologique de*
1081 *France* série 6, 8, 8, 881–883.

1082 Gradstein, F.M., Ogg, J.G., Schmitz, M.D., Ogg, G.M. (eds.), 2012. The geologic time scale
1083 2012, Elsevier, Amsterdam, 1144 pp.

1084 Guennoc P., Gorini C., Mauffret A. 2000. Histoire géologique du golfe du Lion et
1085 cartographie du rift oligo-aquitanien et de la surface messinienne. *Géologie de la France*, 3, 67-
1086 97.

1087 Halophytes Database (eHALOPH), https://www.sussex.ac.uk

1088 Hou H.-Y. 1983. Vegetation of China with reference to its geographical distribution. *Annals*
1089 *of Missouri Botanical Garden* 70: 509-548.

1090 Joseph P, and Lomas S. 2004. Deep-water sedimentation in the Alpine Foreland Basin of SE
1091 France: new perspectives on the grès d'Annot and related systems - An introduction. Dans P.
1092 Joseph, & S. Lomas (Éds.), Deep-water sedimentation in the Alpine Foreland Basin of SE
1093 France: new perspectives on the grès d'Annot and related systems (Vol. 1, pp. 1-16). *The*
1094 *Geological Society of London, Special Publications*.

1095 Lacombe O., Jolivet L. 2005. Structural and kinematic relationships between Corsica and
1096 the Pyrenees-Provence domain at the time of the Pyrenean orogeny. Tectonics, 24, TC1003.

1097 Leroux, E., Rabineau, M., Aslanian, D., Gorini, C., Molliex, S., Bache, F., Robin, C., Droz,
1098 L., Moulin, M., Poort, J., Rubino, J.-L., Suc, J.-P. 2017. High-resolution evolution of

terrigenous sediment yields in the Provence Basin during the last 6 Ma: relation with climate and tectonics. *Basin Research*, 29 (3): 305–339.

Lesueur J.-L. 1991. Etude sédimentologique et stratigraphique du Bassin Paléogène d'Apt–Manosque–Forcalquier (Alpes de Haute Provence). Modalités de la transition Burdigalienne. Ph.D. thesis, University M. de Montaigne, Bordeaux III, France : 407 pp.

Lettéron, A., Fournier, F., Hamon, Y., Villier, L., Margerel, J.-P., Bouche, A., Feist, M., Joseph, P. 2017. Multi-proxy paleoenvironmental reconstruction of saline lake carbonates: paleoclimatic and paleogeographic implications (Priabonian-Rupelian, Issirac Basin, SE France). *Sedimentary Geology* 358: 97–120.`

Lettéron, A. 2018. Caractérisation sédimentologique, stratigraphique et paléoenvironnementale du système carbonaté lacustre à salinité variable du bassin d'Alès et des régions limitrophes (Priabonien, SE France) : implications paléoclimatiques et paléogéographiques. PhD thesis, Aix-Marseille University: 344 pp.

Lettéron A, Hamoun Y, Fournier F, Demory F, Séranne M, Joseph P. 2022. Stratigraphic architecture of a saline lake system: From lake depocenter (Alès Basin) to margins (Saint-Chaptes and Issirac basins), Eocene-Oligocene transition, south-east France. *Sedimentology* 69, 2, 651-695.

Lindtke, J., S.B. Ziegenbald, B. Brunner, J.M. Rouchy, C. Pierre, and J. Peckmann. 2011. Authigenesis of native Sulphur and dolomite in a lacustrine evaporitic setting (Hellín basin, Late Miocene, SE Spain). *Geological Magazine*: 148 (4) 655-669.

Martini, E., 1971. Standard Tertiary and Quaternary calcareous nannoplankton zonation. In: Farinacci, A. (Ed.), Proceedings of the Second International Conference on Planktonic Microfossils Roma, Ed. Tecnoscienza, Rome, 2, pp. 739–785.

1122 Mascle, A., Vially, R., 1999. The petroleum systems of the South-East Basin and Gulf of
1123 Lions (France). In: Durand B, Jolivet L, Horváth F, Séranne M, eds. The Mediterranean Basins:
1124 tertiary extension within the Alpine Orogen. Volume Special Publication 156. London: The
1125 Geological Society, pp. 121–140.

1126 Mauffret A, Gorini C. 1996. Structural style and geodynamic evolution of Camargue and
1127 Western Provencal basin, southeastern France. *Tectonophysics* 15(2): 356-375.

1128 Mauffret, A., Durand de Grossouvre, B., Dos Reis, A.T., Gorini, C., Nercessian, A., 2001.
1129 Structural geometry in the eastern Pyrenees and western Gulf of Lion (Western Mediterranean).
1130 Journal of Structural Geology, 23, 1701-1726.

1131 Mc Arthur, J.M., Howarth, R.J. and Shields, G.A. 2012. Strontium Isotope Stratigraphy. In:
1132 Gredstein, F.M., Ogg, J.G., Schmotz, M.D. and Ogg, G.M. Eds., A Geologic Time Scale,
1133 Elsevier, Amsterdam, pp. 127-144.

1134 Nix H. 1982. Environmental determinants of biogeography and evolution in Terra Australis.
1135 In W.R. Barker and P.J.M. Grennslade (eds), Evolution of the Flora and Fauna of arid Australia.
1136 Peacock Publication, Frewville: 47-66.

1137 Nury D. 1990. L'Oligocène de Provence méridionale: stratigraphie, dynamique
1138 sédimentaire, reconstitutions paléogéographiques. Document du BRGM n°163. Editions du
1139 BRGM, 412pp.

1140 Nury D, Thomassin B.A, 1994. Paléoenvironnements tropicaux, marins et lagunaires d'un
1141 littoral abrité (fonds meubles à bancs coralliens, lagune évaporitique) à l'Oligocène terminal,
1142 en Basse-Provence (région d'Aix-en-Provence, Marseille, France). *Géologie Méditerranéenne*
1143 21(1-2): 95-108.

1144 Ortí, F., Pérez-López, A., García-Veigas, J., Rosell, L., Cendón, D.I., Pérez-Valera, F. 2014.
1145 Sulfate isotope compositions (δ34S, δ18O) and strontium isotopic ratios (87Sr/86Sr) of Triassic

1146 evaporites in the Betic Cordillera (SE Spain). *Revista de la Sociedad Geológica de España* 27:
1147 79-89.

1148 Oudet, J. 2008. Etude terre-mer de la transition syn-rift/post-rift sur les marges de l'océan
1149 Liguro-Provençal: apports de la modélisation géologique 3D et de la chronostratigraphie
1150 intégrée (Ph.D thesis). Marseille, France: Université de Provence.

1151 Oudet J, Münch Ph, Borgomano J, Quillévéré F, Melinte M, Demory F, Viseur S, Cornée J.-
1152 J. 2010a. Land and sea study of the northeastern golfe du Lion rifted margin. In: X. Le Pichon
1153 and C. Rangin, Eds, Geodynamics of the France Southeast Basin. *Bulletin de la Société*
1154 *géologique de France* 181 (6) 591-607.

1155 Oudet J., Münch P., Verati C., Ferrandini M., Melinte-Dobrinescu M., Gattacecca J., Cornée
1156 J.-J., Oggiano G., Quillévéré F., Borgomano J. & Ferrandini J. 2010b. –Integrated
1157 chronostratigraphy of an intra-arc basin: 40 Ar/ 39 Ar datings, micropalaeontology and
1158 magnetostratigraphy of the early Miocene Castelsardo basin (northern Sardinia, Italy).
1159 *Palaeogeography, Palaeoclimatology, Palaeoecology*., 295, 293-306

1160 Palmer, M.R., C. Helvaci, and A.E. Fallick. 2004. Sulphur, sulphate oxygen and strontium
1161 isotope composition of Cenozoic Turkish evaporites. *Chemical Geology* (209) 341-356.

1162 Perch-Nielsen, K. 1985. Cenozoic calcareous nannofossils. *In*: Bolli, H.M., Saunders, J.B.
1163 and Perch-Nielsen, K. (eds) *Plankton Stratigraphy*. Cambridge University Press, 427–554.

1164 Petelet-Giraud, E., Desprats, J.F., Izac, J.L., Foucher, J.C., 2006. Caractérisation
1165 géochimique du bassin versant du Gardon d'Anduze. Approche des isotopes du strontium du
1166 phénomène de « crue éclair ». Final Report. BRGM/RP-54662-FR public report, 50 pp.

1167 Philip J, Vianey-Liaud M, Martin-Clausas C, Tabuce R, Leonide P, Margerel J.-P, Noël J.
1168 2017 - Stratigraphy of the Haut Var Paleogene continental series (Northeastern Provence,

France) : New insight on the age of the « Sables bleutés du Haut Var » Formation. *Géobios* 50 : 319-339.

Plaziat J.-C, Younis W.R. 2005. The modern environments of Molluscs in southern Mesopotamia, Iraq: A guide to paleogeographical reconstructions of Quaternary fluvial, palustrine and marine deposits. *Carnets de Géologie* 2005/01, (18pp).

Popescu S.-M, Biltekin, D, Winter H, Suc J.-P, Melinte-Dobrinescu M.C, Klotz S, Combourieu-Nebout N, Rabineau, M, Clauzon, G, Deaconu F. 2010. Pliocene and Lower Pleistocene vegetation and climate changes at the European scale: Long pollen records and climatostratigraphy. *Quaternary International* 219: 152–167.

Popescu S.-M, Suc J.-P, Fauquette S, Bessedik M, Jiménez-Moreno G, Robin C, Labrousse L. 2021. Mangrove distribution and diversity during three Cenozoic thermal maxima in the Northern Hemisphere (pollen records from the Arctic – North Atlantic – Mediterranean regions). *Journal of Biogeography* 48: 2771-2784.

Powell A.J, Brinkhuis H, Bujak J.P. 1996. Upper Paleocene-Lower Eocene dinoflagellate cyst sequence biostratigraphy of southeast England. In: Knox R.W.O'B, Corfield R.M, Dunnay R.E. (eds), 1996, Correlation of the Early Paleogene in Northwest Europe, *Geological Society Special Publication*, n° 101.

Raab, M. and Spiro, B., 1991. Sulfur isotopic variations during seawater evaporation with fractional crystallization. *Chemical Geology* 86: 323-333.

Raffi, I., Backman, J., Fornaciari, E., Pälike, H., Rio, D., Lourens, L. and Hilgen, F. 2006. A review of calcareous nannofossil astrobiochronology en compassing the past 25 million years. *Quaternary Science Reviews*, 25 : 3113–3137.

Rémy J.A. 1985. Nouveaux gisements de mammifères et reptiles dans les grès de Célas (Eocène sup. du Gard). Etude des paléothériidés (Perissodactyla, Mammalia). *Palaeontographica, Abteilung A*, 189, 171-225.

Rémy J.A. 1994. Une faunule de vertébrés sous la base des Grès de Célas (Eocène supérieur) à St-Dézery (Gard). *Palaeovertebrata* 23(1-4) : 211-216.

Rémy J.A., Fournier F. 2003. Mammifères fossiles de Grès de Célas (Eocène supérieur du Gard) : Découvertes récentes. *Bulletin de la Société des Sciences Naturelles de Nîmes et du Gard*, Nîmes, 64 :18-30.

Rémy J.A., Lesage J.-L. 2005. Un nouveau gisement de vertébrés d'âge Priabonien et son contexte géologique (Tranchée de Nozières, Gard). *Bulletin de la Société Géologique d'étude des Sciences Naturelles de Nîmes et du Gard* 65 : 7-14.

Romagny, A., Jolivet, L., Menant, A., Bessière, E., Maillard, A., Canva, A., Gorini, C., Augier, R., 2020. Detailed tectonic reconstructions of the Western Mediterranean region for the last 35 Ma, insights on driving mechanisms. Earth Science Bulletin, 191, 37.

Rouchy J.-M. 1997. Paleogene continental rift system ofWestern Europe: locations of basins, paleogeographic and structural framework, and the distribution of evaporites. In: Busson, G., Schreiber, B.C. eds., Sedimentary Deposition in Rift and Foreland Basins in France and Spain. Columbia Univ. Press, New York: pp. 45–94.

Salpin, M., Schnyder, J., Baudin, F., Suan, G., Suc, J.-P., Popescu, M.-S., Fauquette, S., Reinhardt, L., Schmitz, M., Labrousse, L. 2019. Evidence for subtropical warmth in Canadian Arctic (Beaufort-Mackenzie, Northwest Territories, Canada) during the early Eocene. In 'Circum-Arctic Structural Events: Tectonic Evolution of the Arctic Margins and Trans-Arctic Links with Adjacent Orogens', *Geological Society of America Special Paper* 541 (27) : 637–664.

Sanchis E, Séranne M. 2000. Structural style and tectonic evolution of a polyphase extensional basin of the Gulf of Lion passive margin: the Tertiary Alès Basin, southern France. *Tectonophysics* 322: 243–264.

Semmani N. 2022. Analysis of the paleoclimatic and paleogeographic archives in the Paleogene sedimentary system of the Vistrenque continental basin (Camargue, South-east France). PhD thesis, Aix-Marseille University, 288 pp.

Semmani N., Fournier F., Léonide P., Feist, M., Boularand S, Borgomano J. 2022. Transgressive-regressive cycles in saline lake margin oolites: paleogeographic implications (Priabonian, Vistrenque basin, SE France). *BSGF - Earth Sciences Bulletin* 193, 8.

Séranne M, Benedicto A, Truffert C, Pascal G, Labaume P. 1995. Structural style and evolution of the Gulf of Lion Oligo-Miocene rifting: Role of the Pyrenean orogeny. *Marine and Petroleum Geology* 12: 809–820.

Séranne, M. 1999. The Gulf of Lion continental margin (NW Mediterranean) revisited by IBS: an overview. In: Durand, B, Jolivet, L, Horváth, F, Séranne, M, eds. The Mediterranean basins: Tertiary extension within the Alpine Orogen. Volume Special Publication, 156. London: *The Geological Society* 15–36.

Séranne M, Couëffé R, Husson E, Baral C, Villard J. 2021. The transition from Pyrenean shortening to Gulf of Lion rifting in Languedoc (South France) –A tectonic-sedimentation analysis. *BSGF - Earth Sciences Bulletin* 192, 27.

Sissingh W. 2001. Tectonostratigraphy of the West Alpine Foreland: correlation of Tertiary sedimentary sequences, changes in eustatic sea-level and stress regimes. *Tectonophysics*: 333, 361–400.

1237 Sissingh W. 2006. Synkinematic paleogeographic evolution of the West European Platform:
1238 correlation with Alpine plate collision and foreland deformation. *Géologie en Mijnbouw,*
1239 *Nehterlands Journal of Geosciences* 85(2):131-180.

1240 Sittler C, Schuler M, Caratini C, Chateauneuf J.-J, Gruas-Cavagnetto C., Jardine S., Ollivier
1241 M.-F, Roche E, Tissot C. 1975. Extension stratigraphique, répartition géographique et écologie
1242 de deux genres polliniques paléogènes observés en Europe occidentale: Aglaoreidia et
1243 Boehlensipollis, *Bulletin de la Société Botanique de France* 122, 231-245.

1244 Suan, G., Popescu, S.-M., Suc, J.-P., Schnyder, J., Fauquette, S., Baudin, F., Yoon, D.,
1245 Piepjohn, K., Sobolev, N., Labrousse, L. 2017. Subtropical climate conditions and mangrove
1246 growth in Arctic Siberia during the early Eocene. *Geology* 45: 539–542.

1247 Suc, J.-P. 1984. Origin and evolution of the Mediterranean vegetation and climate in Europe.
1248 *Nature* 307: 429–432.

1249 Suc, J.-P., Diniz, F., Leroy, S., Poumot, C., Bertini, A., Dupont, L., Clet, M., Bessais, E.,
1250 Zheng, Z., Fauquette, S., Ferrier, J. 1995. Zanclean (~ Brunssumian) to early Piacenzian (~
1251 early-middle Reuverian) climate from 4° to 54° north latitude (West Africa, West Europe and
1252 West Mediterranean areas). *Mededelingen Rijks Geologische Dienst* 52: 43–56.

1253 Suc, J.-P., Fauquette, S., 2012. The use of pollen floras as a tool to estimate palaeoaltitude
1254 of mountains: the eastern Pyrenees in the Late Neogene, a case study. *Palaeogeography,*
1255 *Palaeoclimatology, Palaeoecology*, 321–322, 41–54.

1256 Suc, J.-P., Fauquette, S., Popescu, S.-M., Robin, C. 2020. Subtropical mangrove and
1257 evergreen forest reveal Paleogene terrestrial climate and physiography at the North Pole.
1258 *Palaeogeography, Palaeoclimatology, Palaeoecology* 551, 109755.

1259 Suc, J.-P., Popescu, S.-M., Fauquette, S., Bessedik, M., Jiménez-Moreno, G., Bachiri
1260 Taoufiq, N., Zheng, Z., Médail, F. 2018. Reconstruction of Mediterranean flora, vegetation and

climate for the last 23 million years based on an extensive pollen dataset. *Ecologia mediterranea* 44 (2): 53–85.

Sztrákos K. & Steurbaut E. 2017. — Révision lithostratigraphique et biostratigraphique de l'Oligocène d'Aquitaine occidentale (France). *Geodiversitas* 39(4) : 741-781.

Tesson, M., Labaune, C., Gensous, B., Suc, J.-P., Melinte-Dobrinescu, M.C., Parize, O., Imbert, P., Delhaye-Prat, V., 2011. Quaternary "compound" incised valley in a microtidal environment, Roussillon continental shelf, Western Gulf of Lions, France. *Journal of Sedimentary Research*, 81, 708–729.

Triat J.M, Truc G. 1974. Evaporites paléogènes du domaine rhodanien. *Revue de Géographie Physique et de Géologie Dynamique* 16: 235–262.

Utrilla, R., Pierre, C., Orti, F., Pueyo, J.J., 1992. Oxygen and sulphur isotope composition as indicators of the origin of Mesozoic and Cenozoic evaporites from Spain. *Chem. Geol.* 102: 229– 244.

Valette M, Benedicto A. 1995. Chevauchements gravitaires halotectoniques dans le bassin distensif de Camargue (marge du golfe du Lion, SE de la France). Bulletin de la Société Géologique de France 166(2): 137-147.

Vollstaedt, H., Eisenhauer, A., Wallmann, K., Böhm, F., Fietzke, J., Liebetrau, V., Krabbenhöft, A., Farkaš, J., Tomašových, A., Raddatz, J., Veizer, J., 2014. The Phanerozoic δ88/86Sr record of seawater: New constraints on past changes in oceanic carbonate fluxes. *Geochimica and Cosmochimica Acta*, 128, 249–265.

Westerhold, T., Marwan, N., Drury, A.J., Liebrand, D., Agnini, C., Anagnostou, E., Barnet, J.S.K., Bohaty, S.M., De Vleeschouwer, D., Florin, D., Lauretano, V., Littler, K., Lourens, L.J., Lyle, M., Pälike, H., Röhl, U., Tian, J., Wilkens, R.H., Wilson, P.A., Zachos, J.C. 2020. An

astronomically dated record of Earth's climate and its predictability over the last 66 million years. *Science* 369: 1383–1387.

Zachos J, Pagani M, Sloan L, Thomas E, Billups K, 2001. Trends, rythms and aberrations in global climate 65 Ma to present. *Science* 292, 686-693.

Zheng Z. 1990. Végétation et climats néogènes des Alpes maritimes franco-italiennes d'après les données des analyses palynologiques. *Paléobiol. cont.* 17: 217-244.

Ziegler, P.A. 1992. European Cenozoic srift system. In: Ziegler, P.A. (Ed.), Geodynamics of Rifting, Volume I, Case History Studies on Rifts: Europe and Asia. *Tectonophysics* 208: 91–

Ziegler, P.A. and Dèzes P., 2007. Cenozoic Uplift of Variscan Massifs in the Alpine Foreland: Timing and Controlling Mechanisms. *Global Planetary Change*, 58, 237-269.

Figure and table caption

Figure 1: A) Paleotectonic map of Western Europe during the Oligocene-Aquitanian times showing the location of Western European rift basins (ECRIS) and the subduction area to the south and southeast of Corsica-Sardinia, from Bois (1993). B) Structural map of Southeast France and location of the Vistrenque Basin among the various Cenozoic continental basins, modified after Benedicto (1996). Sampling loci for pollen analyses, U/Pb dating, and Sulfur/Strontium isotopes purposes are located in the Alès, Issirac and Saint-Chaptes basins (AB, IB, SCB), Vistrenque Graben (VG) and Roussillon Basin (RB), geographic coordinates are given in **Supplementary data** (**Table S1**). C) Geological section across the Gulf of Lion margin (modified after Benedicto, 1996).

Figure 2: A) Map of the Bouguer gravity anomaly, modified after Chauvin and Follin-Arbelet (1985). B) interpreted seismic profile SG3 in the Northern Vauvert compartment, after Benedicto (1996), (see location in Fig. 3 hereinafter). C) NW-SE geological cross-section through the Vistrenque Basin on the northern Vauvert compartment (modified after Benedicto et al., 1996). D) Stratigraphic synthesis of the Vistrenque Basin compiled from the boreholes data by Gorini (1993), modified after Bache (2008).

Figure 3: Vistrenque Basin: A) Lithological columns and correlations of Gallician 9 and Pierrefeu 1 wells (after Semmani, 2022); B) Structural map of the Vistrenque Basin and well location (after Benedicto et al., 1996); C) Location map of wells and seismic profiles from the Gallician and Pierrefeu area (location: black rectangle on Fig. 3B).

Figure 4: A) Geological map of the Alès-Saint-Chaptes-Issirac (ASCI) basins and location of the pollen sampling. B) Chronostratigraphic chart of the ASCI lake system (after Lettéron et al., 2022) and location of palynological and sulfate samples analyzed in this study.

Figure 5: Correlation panel of wells Gallician 1, Gallician 4, Gallician 9, Vauvert 1 and Pierrefeu 1 from the Vistrenque Basin (after Semmani, 2022) showing the sedimentary units, lithologies and lithostratigraphic correlations. Lithostratigraphic correlations are carried out using lithological similarities and gamma ray (GR) signal. Drill core locations and the positions of samples used for U/Pb dating (squares) and pollen analyses (circles), and $^{87}Sr/^{86}Sr$ & $\delta^{34}S$ measurements (triangles) are also plotted.

Figure 6: A) Microphotograph of the cavity in thin section of the sample G9 13D from Gallician 9 well (depth ~ 1960 m) displaying the growth of successive cement stages: microstalactitic cements A1 & A2, and coarse bladed calcite I1 with further bitumen infill. B) elemental mapping of the red box in A) showing the concentrations of ^{238}U and ^{206}P. C) Confocal microscopy photograph of the cavity in (A) where the fluorescence allows to observe the different generations of cement. The cementation stages A2 and I1 are non-luminescent and therefore indistinguishable under cathodoluminescence. D) Tera-Wasserburg plots displaying $^{238}U/^{206}Pb$ versus $^{207}Pb/^{206}Pb$ from the A1 cement (early diagenetic anisopachous cement).

Figure 7: A) Thick geological section scan (sample G9 7; Gallician 9 well, depth ~ 1894 m) showing the yellowish beige pendant anisopachous cement around clasts in a fluvial conglomerate. B) close-up view of the rectangular box in A) displaying the position of the laser ablation spots alongside the cement. C) Tera-Wasserburg plots displaying $^{238}U/^{206}Pb$ versus $^{207}Pb/^{206}Pb$ from the anisopachous cement of the G9 7 sample (number of spots = 74). D) and E) Microphotographs of the vein calcite infill within the G9 K35 sample (Gallician 9, depth ~ 2487 m) under plane polarized light and cathodoluminescence respectively. Note the dull

luminescence of the calcite fill (right hand picture). F) Tera-Wasserburg plots displaying $^{238}U/^{206}Pb$ versus $^{207}Pb/^{206}Pb$ from the calcite vein infill of the G9 K35 sample (number of spots = 45).

Figure 8: Synthetic pollen diagrams (*Pinus* excluded) illustrating (1) to the left the local to regional paleovegetation (including altitudinal trees) and (2) to the right the local paaeovegetation (the latter trees excluded) – their proposed climatostratigraphic correlations with the reference oxygen isotope curve (smoothed curve over 20 ka in blue, smoothed curve over 1 Ma in red; Westerhold et al., 2020). Pollen diagrams are vertically arranged according to the basin stratigraphy and available chronostratigraphic information (mammal faunas, calcareous nannofossils). Time-intervals corresponding to the Priabonian and Chattian stages are shaded in light grey to make easier the chronostratigraphic correlations. Pollen group composition is specified in the text and more in **Supplementary data Table S3**.

Figure 9: $\delta^{34}S$ vs $^{87}Sr/^{86}Sr$ crossplot for Paleogene anhydrites from SE France: A) Vistrenque Basin (Pierrefeu 1 well); the solid line represents the water-mixing model for a mixture of a Late Oligocene seawater with a riverine water whose composition is influenced by recycling of Triassic evaporites (see **Table 3** for Sr and S isotope compositions and concentrations of each end-member); the dashed area represents possible isotope compositions of sulfates having precipitated from the modelled water mixture by considering the fractional crystallization effect; B) Alès Basin (Les Fumades: SC-1 and SC-2 wells). The arrow indicates how bacterial sulfate reduction results into higher $\delta^{34}S$. The Triassic (Keuper) evaporite domain is compiled from Albarède and Michard (1987), Dinelli et al. (1999), Alonso-Azcarate *et al.* (2006), Ortí *et al.* (2014), Utrilla *et al.* (1992) and Boschetti *et al.* (2011). The granite and metamorphic rock domain derives from Petelet-Giraud *et al.* (2006), Chaussidon *et al.* (1989), Giacometti et al. (2014).

Figure 10: Chronostratigraphic framework of the Paleogene succession of the Vistrenque Basin. Stratigraphic attributions for the main lithological units are obtained using U/Pb absolute dating (blue squares), pollen analyses and geochemical modelling on sulfates, see text for details about the dating results. Reference oxygen isotope curve (smoothed curve over 20 ka in blue, smoothed curve over 1 Ma in red; Westerhold et al., 2020). Climatic events and Antarctic ice-sheets coverages are derived from Zachos et al. (2001).

Figure 11: Paleogeographic map of Southeast France during the late Priabonian. Location of continental basins are compiled from Lettéron et al. (2017, 2022) and Semmani et al. (2022). Paleogeography of marine domain is modified from Joseph and Lomas (2004). The structural framework is compiled from Séranne et al. (2021) and Semmani et al. (2022) west of the Diois-Barronies High and from Balansa et al. (2022) for Northern and Eastern Provence.

Figure 12: Paleogeographic map of Southeast France during the early-middle Rupelian. Location of continental basins are compiled from Nury (1990), Lettéron et al. (2017, 2022), Semmani et al. (2022). Paleogeography of marine domain is modified from Joseph and Lomas (2004). The structural framework is compiled from Séranne et al. (2021) and Semmani et al. (2022) west of the Diois-Barronies High and from Balansa et al. (2022) for Northern and Eastern Provence.

Figure 13: Paleogeographic map of South-East France during the Chattian. Location of continental basins are compiled from Cavelier et al. (1984), Nury (1990), Séranne et al. (2021). Paleogeography of marine domain is modified from Oudet (2008).

Table 1: Ages obtained in the Vistrenque Basin using U/Pb dating on calcite, pollen-based climatostratigraphy, Sr and S isotope signatures of sulfates.

Table 2: Climatic reconstruction based on pollen data. The succession of pollen sites is that shown in Figure 8. Mean annual temperatures (MAT), mean temperature of the coldest (MTC) and of the warmest (MTW) months and mean annual precipitation (MAP) are reconstructed using the Climatic Amplitude Method (Fauquette et al., 1998). The results are given as an interval and a Most Likely Value (in bold) for each site.

Table 3: $^{87}Sr/^{86}Sr$ and $\delta^{34}S$ measurements on anhydrite/gypsum samples and native sulfur from Pierrefeu-1 well (Vistrenque Basin), SC-1 and SC-2 well (Alès Basin). The stratigraphic sequences of the Alès Basin are defined in Lettéron et al. (2022).

1400

1401

1402

1403

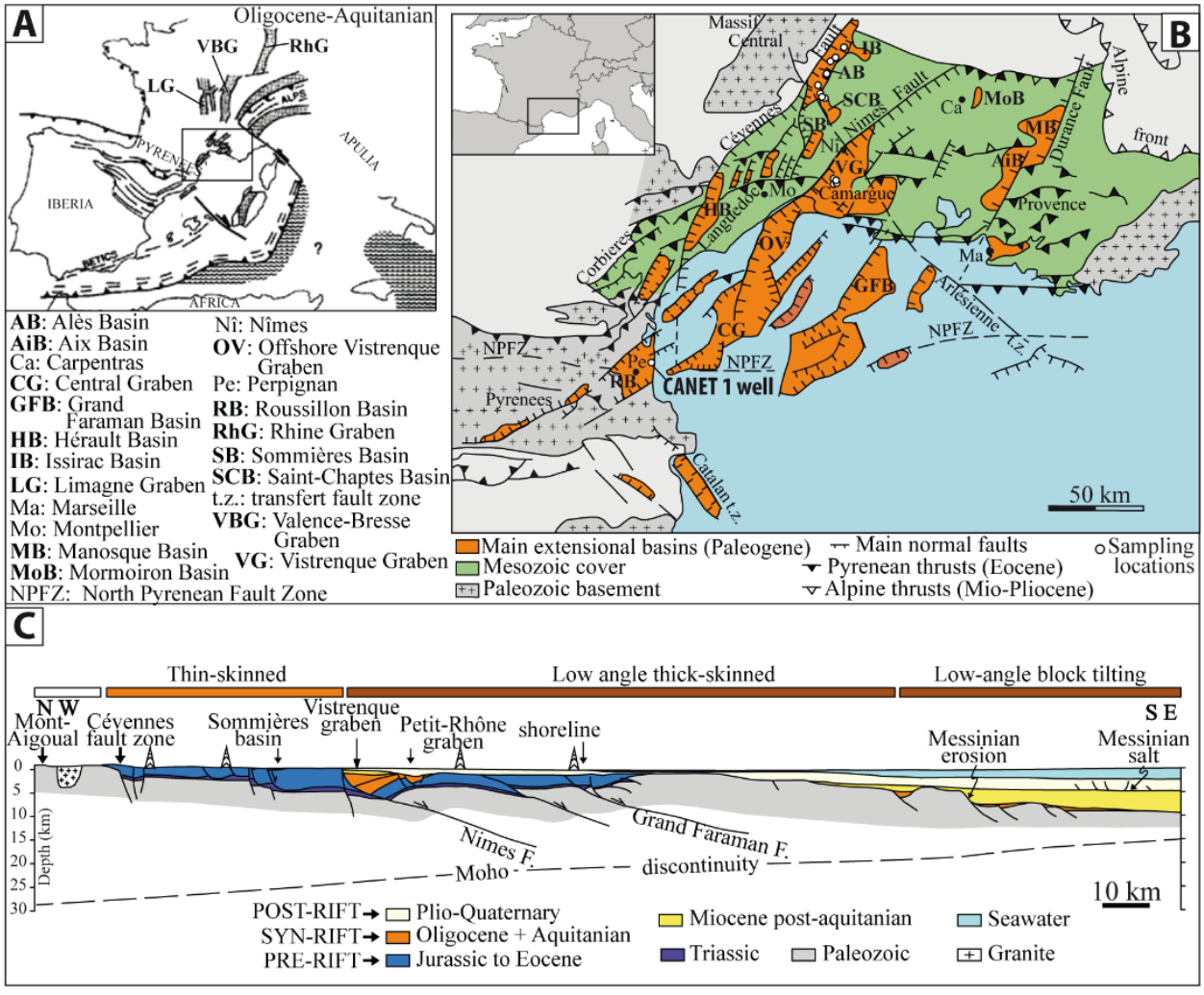
A
Oligocene-Aquitanian
VBG
RhG
LG
ALPS
PYRENEES
IBERIA
APULIA
AFRICA
METIC
?
AB: Alès Basin
AiB: Aix Basin
Ca: Carpentras
CG: Central Graben
GFB: Grand Faraman Basin
HB: Hérault Basin
IB: Issirac Basin
LG: Limagne Graben
Ma: Marseille
Mo: Montpellier
MB: Manosque Basin
MoB: Mormoiron Basin
NPFZ: North Pyrenean Fault Zone
Nî: Nîmes
OV: Offshore Vistrenque Graben
Pe: Perpignan
RB: Roussillon Basin
RhG: Rhine Graben
SB: Sommières Basin
SCB: Saint-Chaptes Basin
t.z.: transfert fault zone
VBG: Valence-Bresse Graben
VG: Vistrenque Graben
B
Massif Central
Cévennes Fault
HB
AB
SCB
Nîmes Fault
Ca
MoB
MB
AiB
Durance Fault
Alpine front
SB
Nî
VG
Camargue
Mo
Provence
HB
Languedoc
OV
Corbières
Ma
GFB
Arlesienne t.z.
NPFZ
CG
NPFZ
Pe
RB
CANET 1 well
Pyrenees
Catalan t.z.
50 km
Main extensional basins (Paleogene)
Mesozoic cover
Paleozoic basement
Main normal faults
Pyrenean thrusts (Eocene)
Alpine thrusts (Mio-Pliocene)
Sampling locations
C
Thin-skinned
Low angle thick-skinned
Low-angle block tilting
NW
SE
Mont-Aigoual
Cévennes fault zone
Sommières basin
Vistrenque graben
Petit-Rhône graben
shoreline
Messinian erosion
Messinian salt
Depth (km)
0
5
10
15
20
25
30
Nimes F.
Grand Faraman F.
Moho
discontinuity
10 km
POST-RIFT
SYN-RIFT
PRE-RIFT
Plio-Quaternary
Oligocene + Aquitanian
Jurassic to Eocene
Miocene post-aquitanian
Triassic
Paleozoic
Seawater
Granite

Figure 1

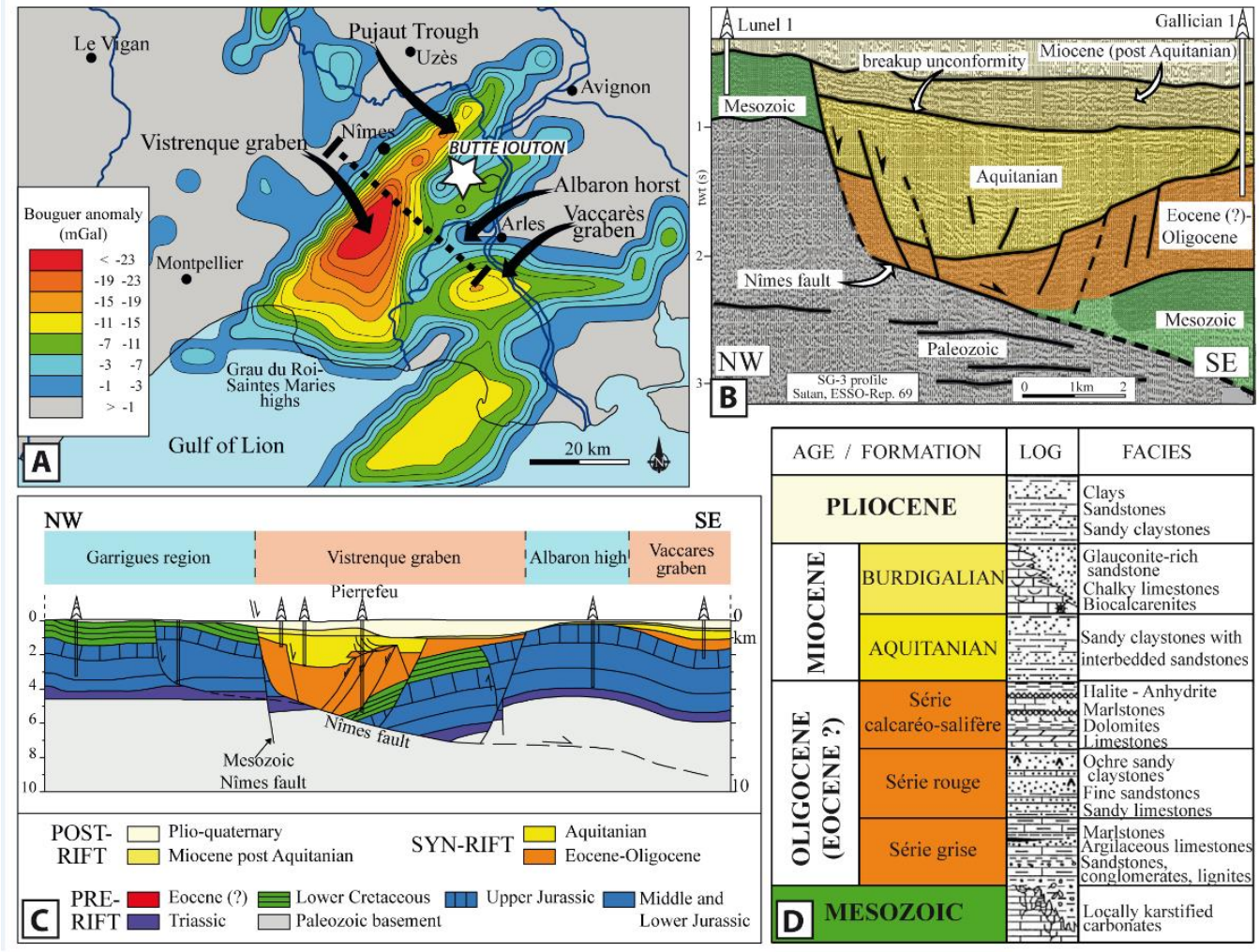
A
Le Vigan
Pujaut Trough
Uzès
Avignon
Vistrenque graben
Nîmes
BUTTE IOUTON
Albaron horst
Arles
Vaccarès graben
Montpellier
Bouguer anomaly (mGal)
< -23
-19 -23
-15 -19
-11 -15
-7 -11
-3 -7
-1 -3
> -1
Grau du Roi-Saintes Maries highs
Gulf of Lion
20 km
B
Lunel 1
Gallician 1
breakup unconformity
Miocene (post Aquitanian)
Mesozoic
Aquitanian
Eocene (?)-Oligocene
Nîmes fault
Mesozoic
Paleozoic
NW
SE
SG-3 profile
Satan, ESSO-Rep. 69
0 1km 2
twt (s)
C
NW
SE
Garrigues region
Vistrenque graben
Albaron high
Vaccares graben
Pierrefeu
Nîmes fault
Mesozoic
Nîmes fault
km
POST-RIFT
Plio-quaternary
Miocene post Aquitanian
SYN-RIFT
Aquitanian
Eocene-Oligocene
PRE-RIFT
Eocene (?)
Triassic
Lower Cretaceous
Paleozoic basement
Upper Jurassic
Middle and Lower Jurassic
D
AGE / FORMATION
LOG
FACIES
PLIOCENE
Clays
Sandstones
Sandy claystones
MIOCENE
BURDIGALIAN
Glauconite-rich sandstone
Chalky limestones
Biocalcarenites
AQUITANIAN
Sandy claystones with interbedded sandstones
OLIGOCENE (EOCENE ?)
Série calcaréo-salifère
Halite - Anhydrite
Marlstones
Dolomites
Limestones
Série rouge
Ochre sandy claystones
Fine sandstones
Sandy limestones
Série grise
Marlstones
Argilaceous limestones
Sandstones, conglomerates, lignites
MESOZOIC
Locally karstified carbonates

Figure 2

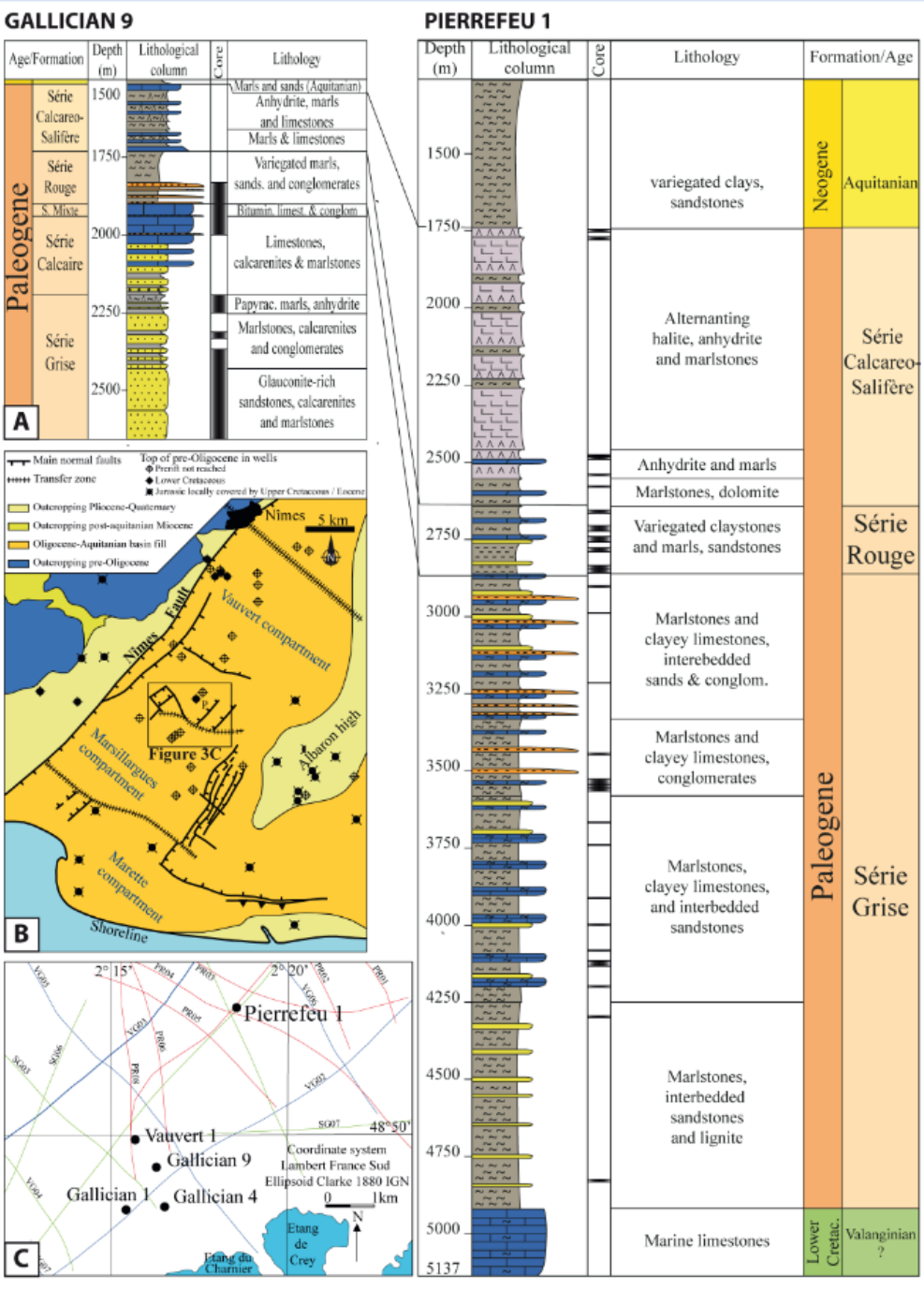
GALLICIAN 9
Age/Formation
Depth (m)
Lithological column
Core
Lithology
Paleogene
Série Calcareo-Salifère
Série Rouge
S. Mixte
Série Calcaire
Série Grise
1500
1750
2000
2250
2500
Marls and sands (Aquitanian)
Anhydrite, marls and limestones
Marls & limestones
Variegated marls, sands. and conglomerates
Bitumin. limest. & conglom.
Limestones, calcarenites & marlstones
Papyrac. marls, anhydrite
Marlstones, calcarenites and conglomerates
Glauconite-rich sandstones, calcarenites and marlstones
A
Main normal faults
Transfer zone
Top of pre-Oligocene in wells
Permit not reached
Lower Cretaceous
Jurassic locally covered by Upper Cretaceous / Eocene
Outcropping Pliocene-Quaternary
Outcropping post-aquitanian Miocene
Oligocene-Aquitanian basin fill
Outcropping pre-Oligocene
Nîmes
5 km
Nîmes Fault
Vauvert compartment
Figure 3C
Marsillargues compartment
Albaron high
Marette compartment
Shoreline
B
2°15'
2°20'
Pierrefeu 1
Vauvert 1
Gallician 9
Gallician 1
Gallician 4
48°50'
Coordinate system
Lambert France Sud
Ellipsoid Clarke 1880 IGN
0
1km
N
Etang de Crey
Etang du Charnier
C
PIERREFEU 1
Depth (m)
Lithological column
Core
Lithology
Formation/Age
1500
1750
2000
2250
2500
2750
3000
3250
3500
3750
4000
4250
4500
4750
5000
5137
variegated clays, sandstones
Alternanting halite, anhydrite and marlstones
Anhydrite and marls
Marlstones, dolomite
Variegated claystones and marls, sandstones
Marlstones and clayey limestones, interebedded sands & conglom.
Marlstones and clayey limestones, conglomerates
Marlstones, clayey limestones, and interbedded sandstones
Marlstones, interbedded sandstones and lignite
Marine limestones
Neogene
Aquitanian
Paleogene
Série Calcareo-Salifère
Série Rouge
Série Grise
Lower Cretac.
Valanginian ?

Figure 3

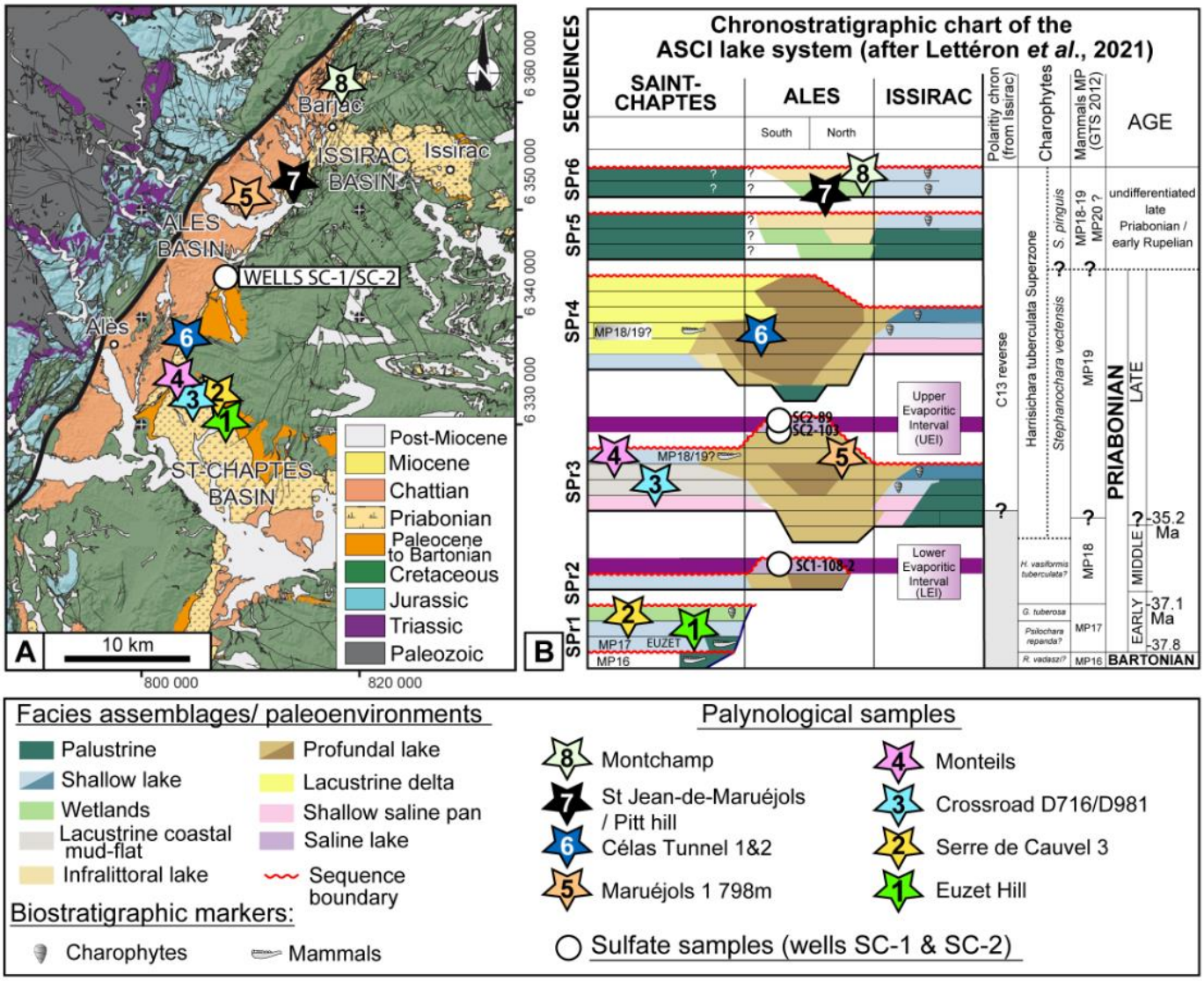
A
10 km
800 000
820 000
6 360 000
6 350 000
6 340 000
6 330 000
Barjac
ISSIRAC BASIN
Issirac
ALES BASIN
WELLS SC-1/SC-2
Alès
ST-CHAPTES BASIN
Post-Miocene
Miocene
Chattian
Priabonian
Paleocene to Bartonian
Cretaceous
Jurassic
Triassic
Paleozoic
B
Chronostratigraphic chart of the ASCI lake system (after Lettéron et al., 2021)
SEQUENCES
SAINT-CHAPTES
ALES
South
North
ISSIRAC
Polarity chron (from Issirac)
Charophytes
Mammals MP (GTS 2012)
AGE
SPr6
SPr5
SPr4
SPr3
SPr2
SPr1
MP18/19?
Upper Evaporitic Interval (UEI)
Lower Evaporitic Interval (LEI)
SC2-89
SC2-103
SC1-108
C13 reverse
Harrisichara tuberculata Superzone
S. pinguis
Stephanochara vectensis
H. vasiformis tuberculata?
G. tuberosa
Psilochara reparida?
R. vadaszi?
MP18-19
MP20 ?
MP19
MP18
MP17
MP16
undifferentiated late Priabonian / early Rupelian
PRIABONIAN
LATE
MIDDLE
EARLY
BARTONIAN
-35.2 Ma
-37.1 Ma
-37.8
MP17
EUZET
MP16
Facies assemblages/ paleoenvironments
Palustrine
Shallow lake
Wetlands
Lacustrine coastal mud-flat
Infralittoral lake
Profundal lake
Lacustrine delta
Shallow saline pan
Saline lake
Sequence boundary
Biostratigraphic markers:
Charophytes
Mammals
Palynological samples
8 Montchamp
7 St Jean-de-Maruéjols / Pitt hill
6 Célas Tunnel 1&2
5 Maruéjols 1 798m
4 Monteils
3 Crossroad D716/D981
2 Serre de Cauvel 3
1 Euzet Hill
Sulfate samples (wells SC-1 & SC-2)

Figure 4

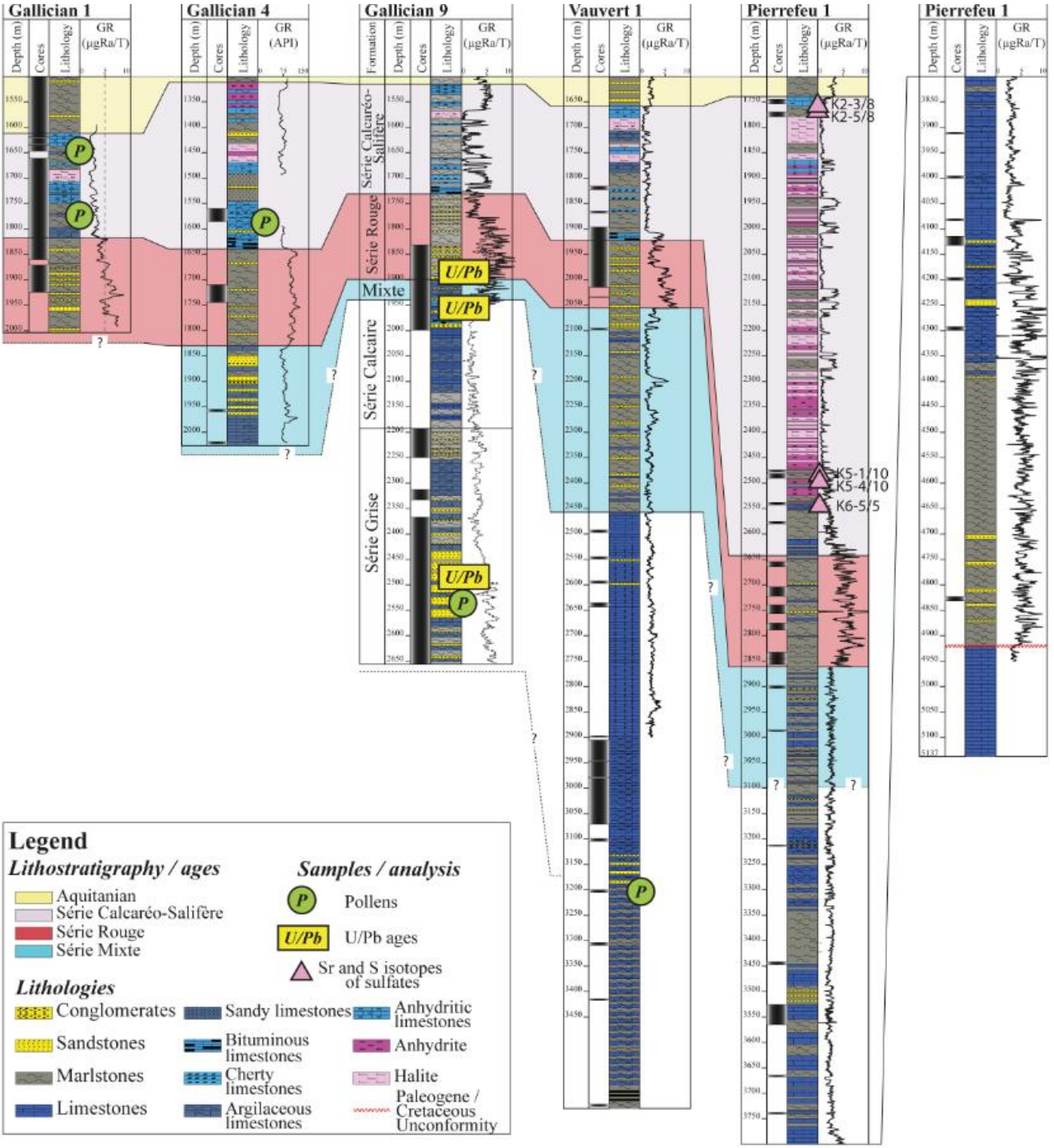
Gallician 1
Gallician 4
Gallician 9
Vauvert 1
Pierrefeu 1
Pierrefeu 1
Depth (m)
Cores
Lithology
GR (µgRa/T)
GR (API)
Formation
Série Calcaréo-Salifère
Série Rouge
Mixte
Série Calcaire
Série Grise
U/Pb
P
K2-3/8
K2-5/8
K5-1/10
K5-4/10
K6-5/5
Legend
Lithostratigraphy / ages
Aquitanian
Série Calcaréo-Salifère
Série Rouge
Série Mixte
Samples / analysis
Pollens
U/Pb ages
Sr and S isotopes of sulfates
Lithologies
Conglomerates
Sandstones
Marlstones
Limestones
Sandy limestones
Bituminous limestones
Cherty limestones
Argilaceous limestones
Anhydritic limestones
Anhydrite
Halite
Paleogene / Cretaceous Unconformity

Figure 5

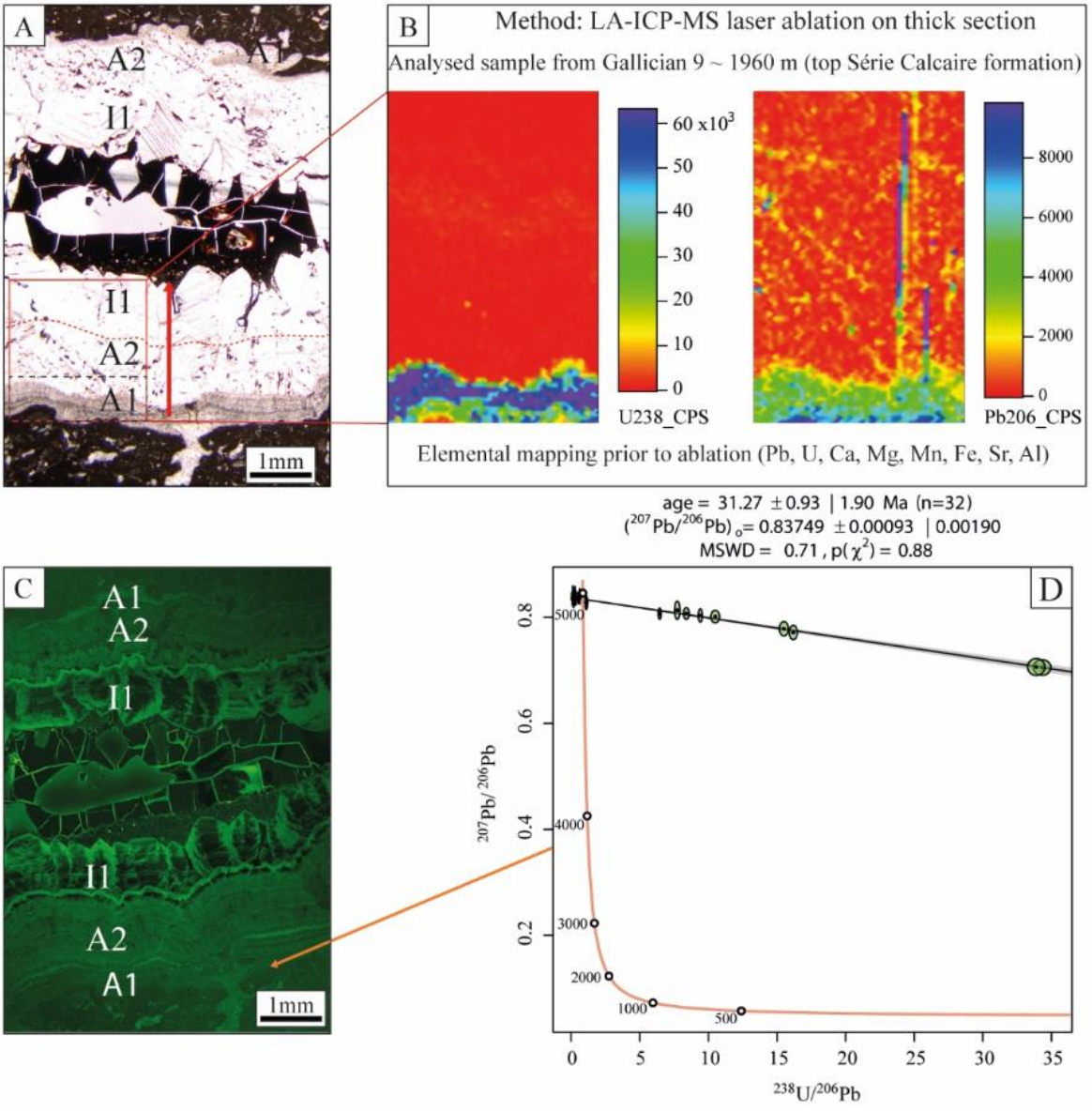
A
A2
A1
I1
I1
A2
A1
1mm
B
Method: LA-ICP-MS laser ablation on thick section
Analysed sample from Gallician 9 ~ 1960 m (top Série Calcaire formation)
60 x10³
50
40
30
20
10
0
U238_CPS
8000
6000
4000
2000
0
Pb206_CPS
Elemental mapping prior to ablation (Pb, U, Ca, Mg, Mn, Fe, Sr, Al)
C
A1
A2
I1
I1
A2
A1
1mm
age = 31.27 ±0.93 | 1.90 Ma (n=32)
(207Pb/206Pb)o= 0.83749 ±0.00093 | 0.00190
MSWD = 0.71 , p(χ²) = 0.88
D
5000
4000
3000
2000
1000
500
0.8
0.6
0.4
0.2
207Pb/206Pb
0
5
10
15
20
25
30
35
238U/206Pb

Figure 6

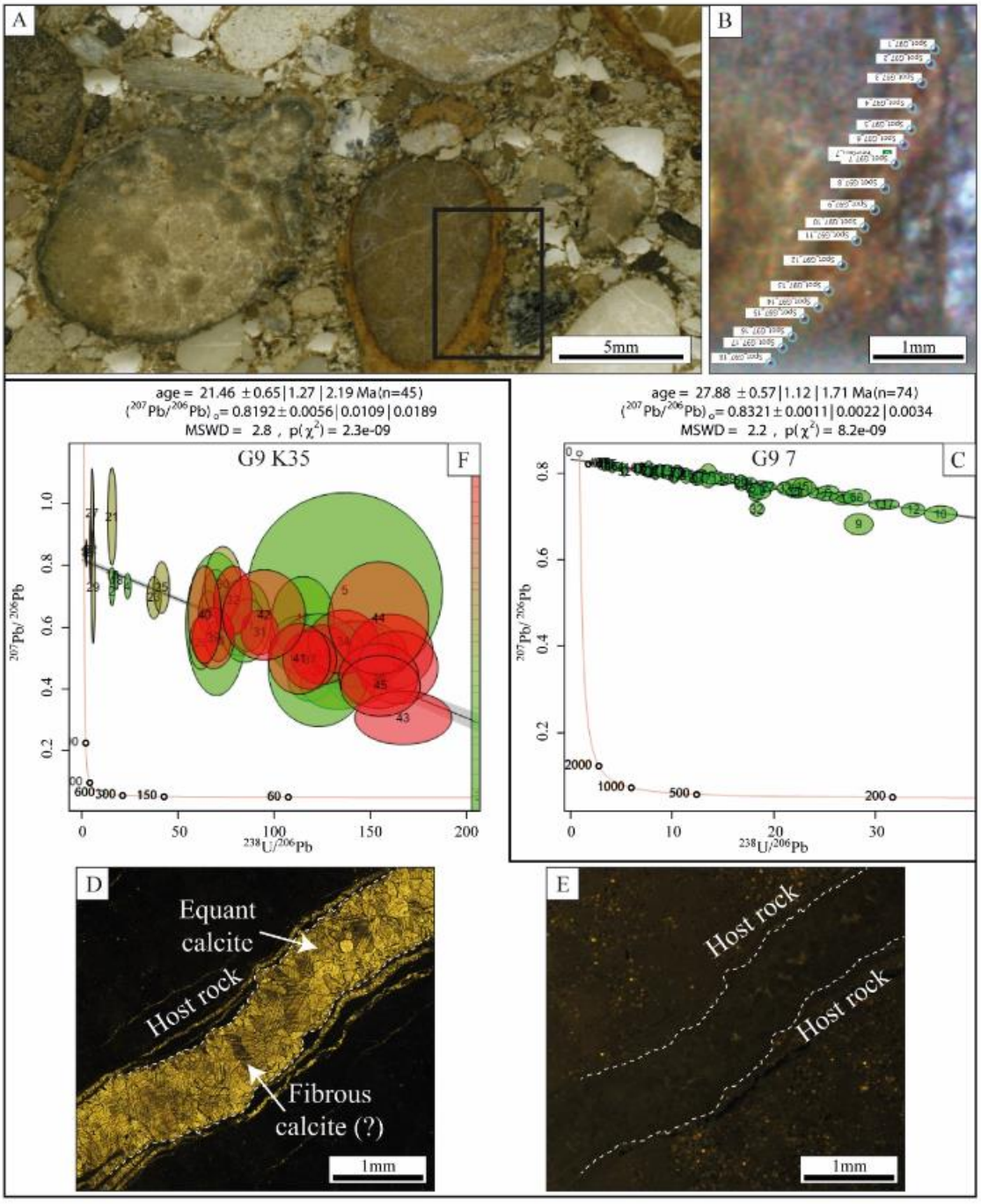
A
5mm
B
1mm
age = 21.46 ±0.65|1.27|2.19 Ma⟨n=45⟩
(207Pb/206Pb)o= 0.8192±0.0056|0.0109|0.0189
MSWD = 2.8 , p(χ2) = 2.3e-09
G9 K35
F
207Pb/206Pb
238U/206Pb
age = 27.88 ±0.57|1.12|1.71 Ma⟨n=74⟩
(207Pb/206Pb)o= 0.8321±0.0011|0.0022|0.0034
MSWD = 2.2 , p(χ2) = 8.2e-09
G9 7
C
2000
1000
500
200
D
Equant calcite
Host rock
Fibrous calcite (?)
1mm
E
Host rock
Host rock
1mm

Figure 7

Figure 8

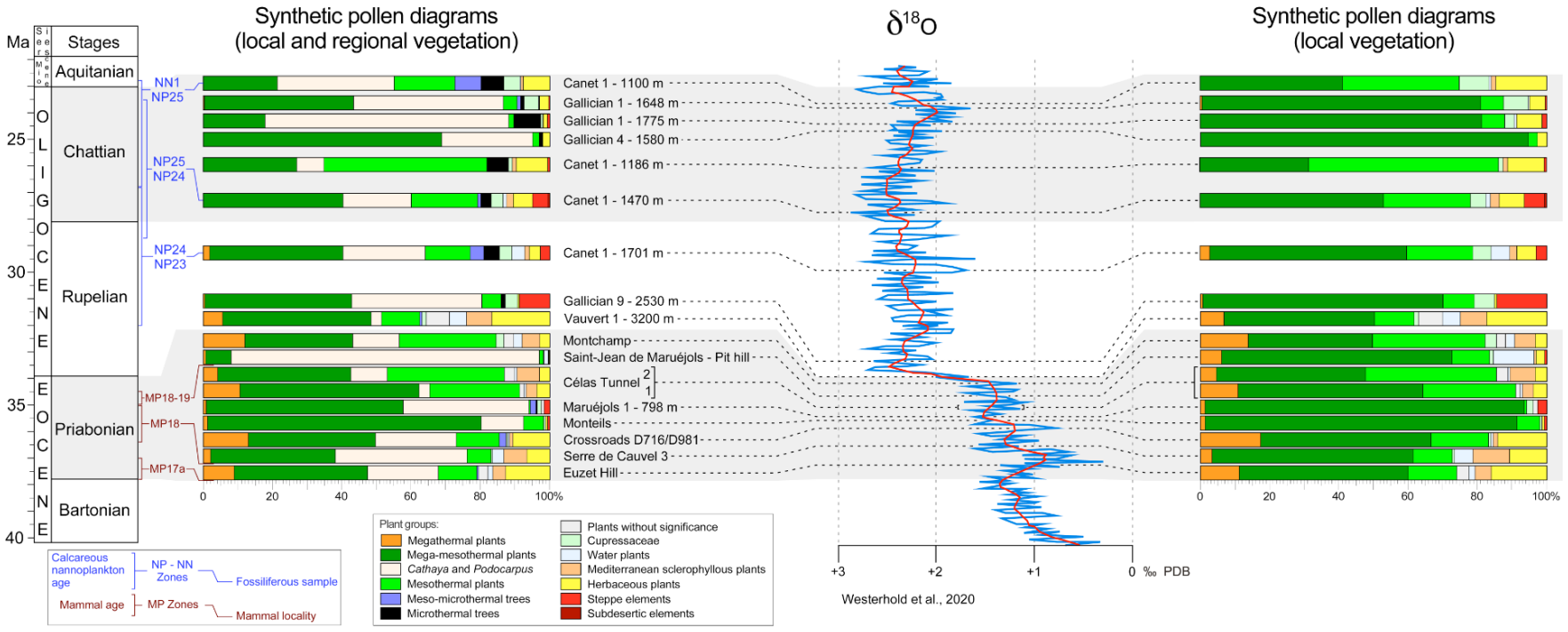
Synthetic pollen diagrams
(local and regional vegetation)
δ18O
Synthetic pollen diagrams
(local vegetation)
Ma
Stages
Aquitanian
Chattian
Rupelian
Priabonian
Bartonian
OLIGOCENE
EOCENE
25
30
35
40
NN1
NP25
NP25
NP24
NP24
NP23
MP18-19
MP18
MP17a
Canet 1 - 1100 m
Gallician 1 - 1648 m
Gallician 1 - 1775 m
Gallician 4 - 1580 m
Canet 1 - 1186 m
Canet 1 - 1470 m
Canet 1 - 1701 m
Gallician 9 - 2530 m
Vauvert 1 - 3200 m
Montchamp
Saint-Jean de Maruéjols - Pit hill
Célas Tunnel 2
Célas Tunnel 1
Maruéjols 1 - 798 m
Monteils
Crossroads D716/D981
Serre de Cauvel 3
Euzet Hill
0
20
40
60
80
100%
+3
+2
+1
0 ‰ PDB
Westerhold et al., 2020
Calcareous nannoplankton age
NP - NN Zones
Fossiliferous sample
Mammal age
MP Zones
Mammal locality
Plant groups:
Megathermal plants
Mega-mesothermal plants
Cathaya and Podocarpus
Mesothermal plants
Meso-microthermal trees
Microthermal trees
Plants without significance
Cupressaceae
Water plants
Mediterranean sclerophyllous plants
Herbaceous plants
Steppe elements
Subdesertic elements

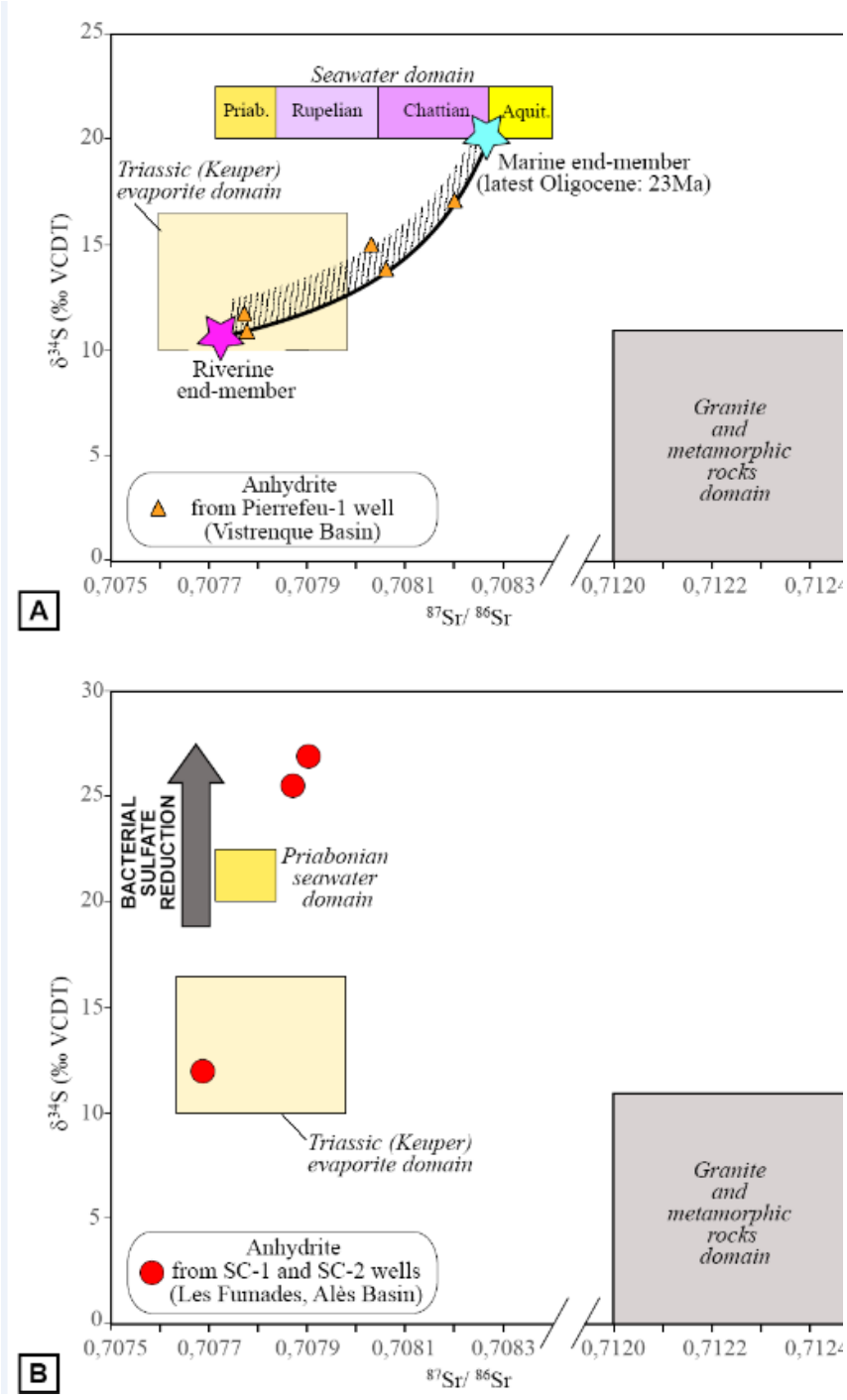
Seawater domain
Priab.
Rupelian
Chattian
Aquit.
Marine end-member
(latest Oligocene: 23Ma)
Triassic (Keuper)
evaporite domain
Riverine
end-member
Granite
and
metamorphic
rocks
domain
Anhydrite
from Pierrefeu-1 well
(Vistrenque Basin)
A
δ34S (‰ VCDT)
87Sr/ 86Sr
0,7075
0,7077
0,7079
0,7081
0,7083
0,7120
0,7122
BACTERIAL
SULFATE
REDUCTION
Priabonian
seawater
domain
Triassic (Keuper)
evaporite domain
Granite
and
metamorphic
rocks
domain
Anhydrite
from SC-1 and SC-2 wells
(Les Fumades, Alès Basin)
B

Figure 9

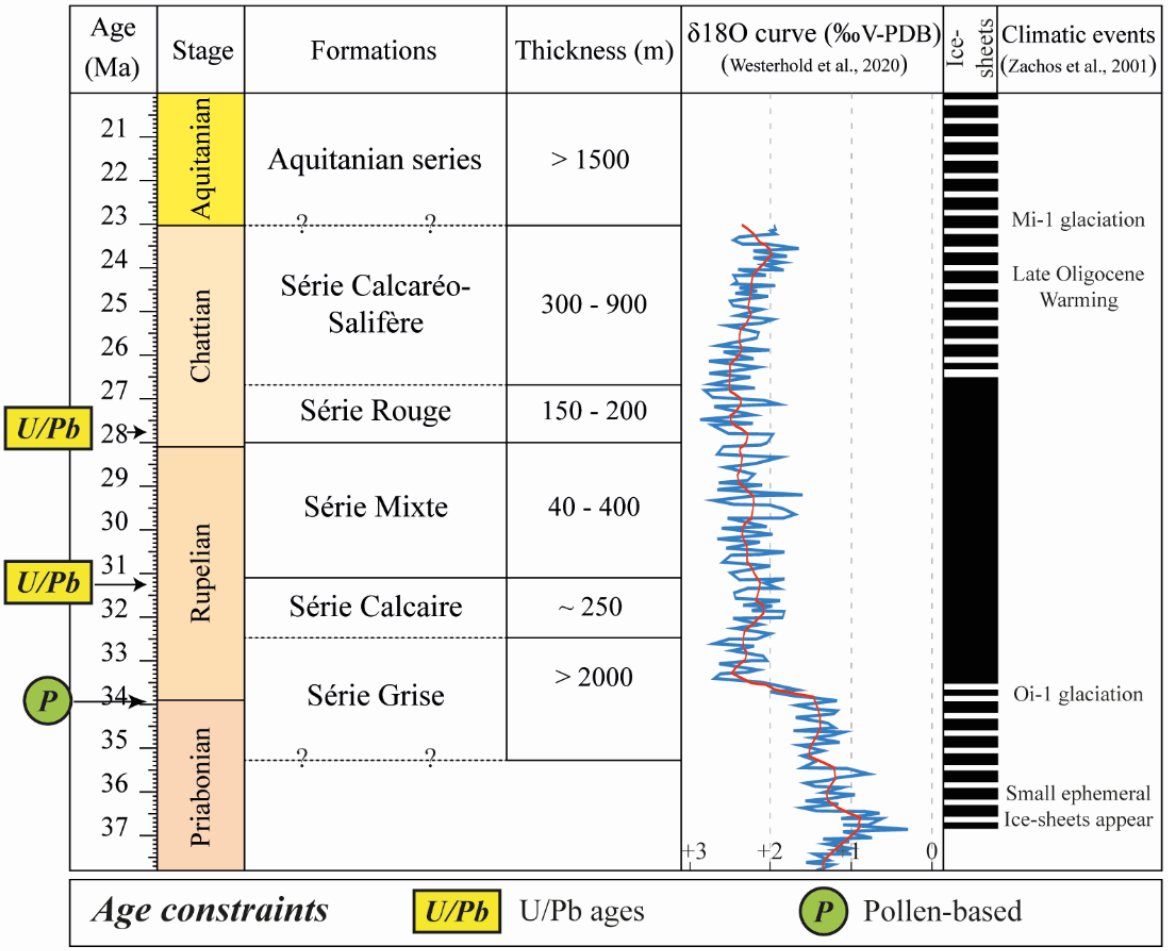
Age (Ma)
Stage
Formations
Thickness (m)
δ18O curve (‰V-PDB) (Westerhold et al., 2020)
Ice-sheets
Climatic events (Zachos et al., 2001)
21
22
23
24
25
26
27
28
29
30
31
32
33
34
35
36
37
Aquitanian
Chattian
Rupelian
Priabonian
Aquitanian series
> 1500
Série Calcaréo-Salifère
300 - 900
Série Rouge
150 - 200
Série Mixte
40 - 400
Série Calcaire
~ 250
Série Grise
> 2000
U/Pb
U/Pb
P
+3
+2
+1
0
Mi-1 glaciation
Late Oligocene Warming
Oi-1 glaciation
Small ephemeral Ice-sheets appear
Age constraints
U/Pb
U/Pb ages
P
Pollen-based

Figure 10

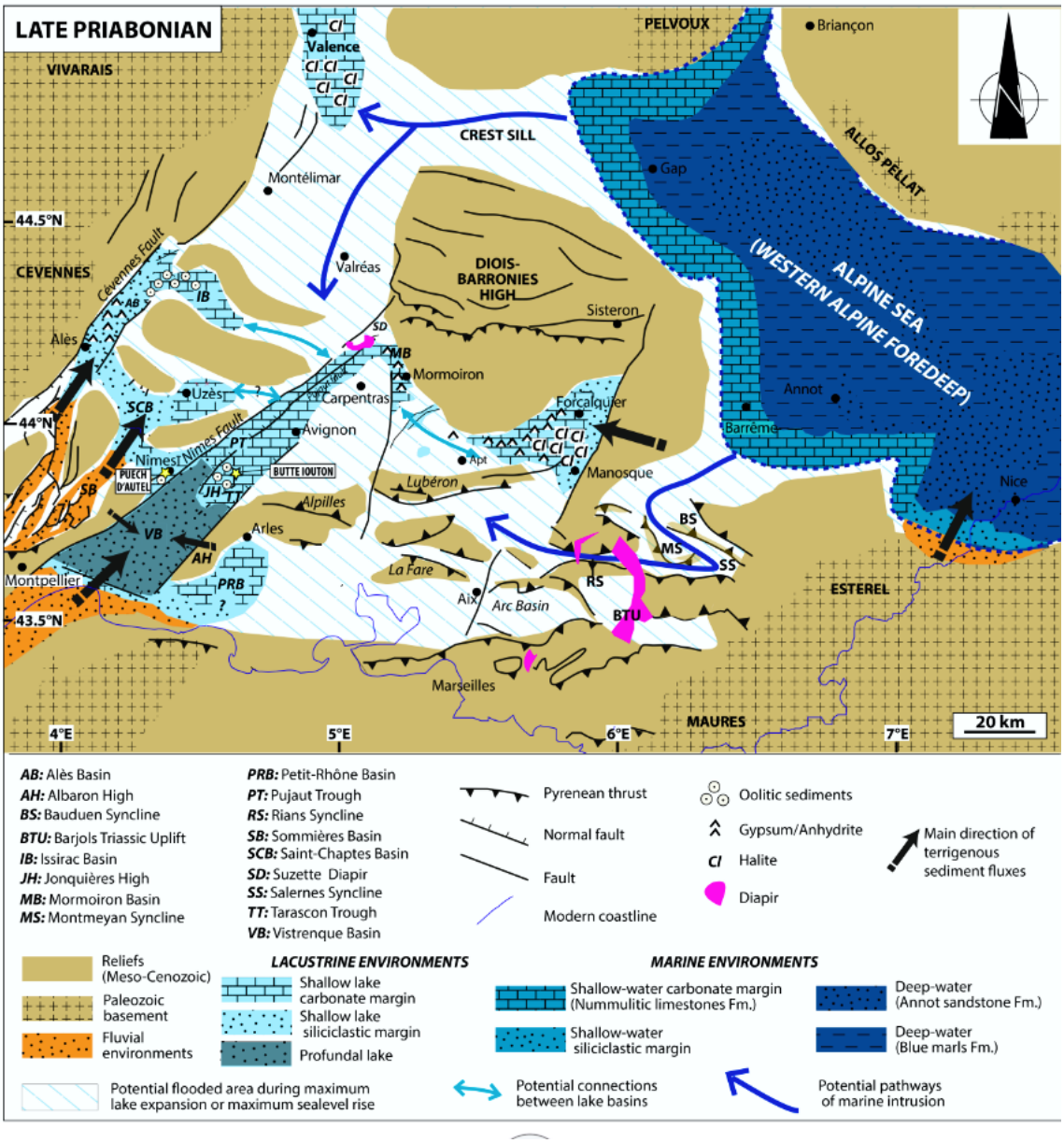
LATE PRIABONIAN
VIVARAIS
CEVENNES
PELVOUX
Briançon
Valence
CREST SILL
Montélimar
Gap
ALLOS PELLAT
ALPINE SEA
(WESTERN ALPINE FOREDEEP)
44.5°N
Cevennes Fault
DIOIS-
BARRONIES
HIGH
Valréas
Sisteron
Alès
Mormoiron
Carpentras
Uzès
Forcalquier
Annot
44°N
Avignon
Barrême
Nimes
Nimes Fault
Apt
Manosque
Nice
PUECH
D'AUTEL
BUTTE IOUTON
Lubéron
Alpilles
Arles
Montpellier
La Fare
Aix
Arc Basin
ESTEREL
43.5°N
Marseilles
MAURES
4°E
5°E
6°E
7°E
20 km
AB: Alès Basin
AH: Albaron High
BS: Bauduen Syncline
BTU: Barjols Triassic Uplift
IB: Issirac Basin
JH: Jonquières High
MB: Mormoiron Basin
MS: Montmeyan Syncline
PRB: Petit-Rhône Basin
PT: Pujaut Trough
RS: Rians Syncline
SB: Sommières Basin
SCB: Saint-Chaptes Basin
SD: Suzette Diapir
SS: Salernes Syncline
TT: Tarascon Trough
VB: Vistrenque Basin
Pyrenean thrust
Normal fault
Fault
Modern coastline
Oolitic sediments
Gypsum/Anhydrite
Cl Halite
Diapir
Main direction of terrigenous sediment fluxes
Reliefs (Meso-Cenozoic)
Paleozoic basement
Fluvial environments
LACUSTRINE ENVIRONMENTS
Shallow lake carbonate margin
Shallow lake siliciclastic margin
Profundal lake
MARINE ENVIRONMENTS
Shallow-water carbonate margin (Nummulitic limestones Fm.)
Shallow-water siliciclastic margin
Deep-water (Annot sandstone Fm.)
Deep-water (Blue marls Fm.)
Potential flooded area during maximum lake expansion or maximum sealevel rise
Potential connections between lake basins
Potential pathways of marine intrusion

Figure 11

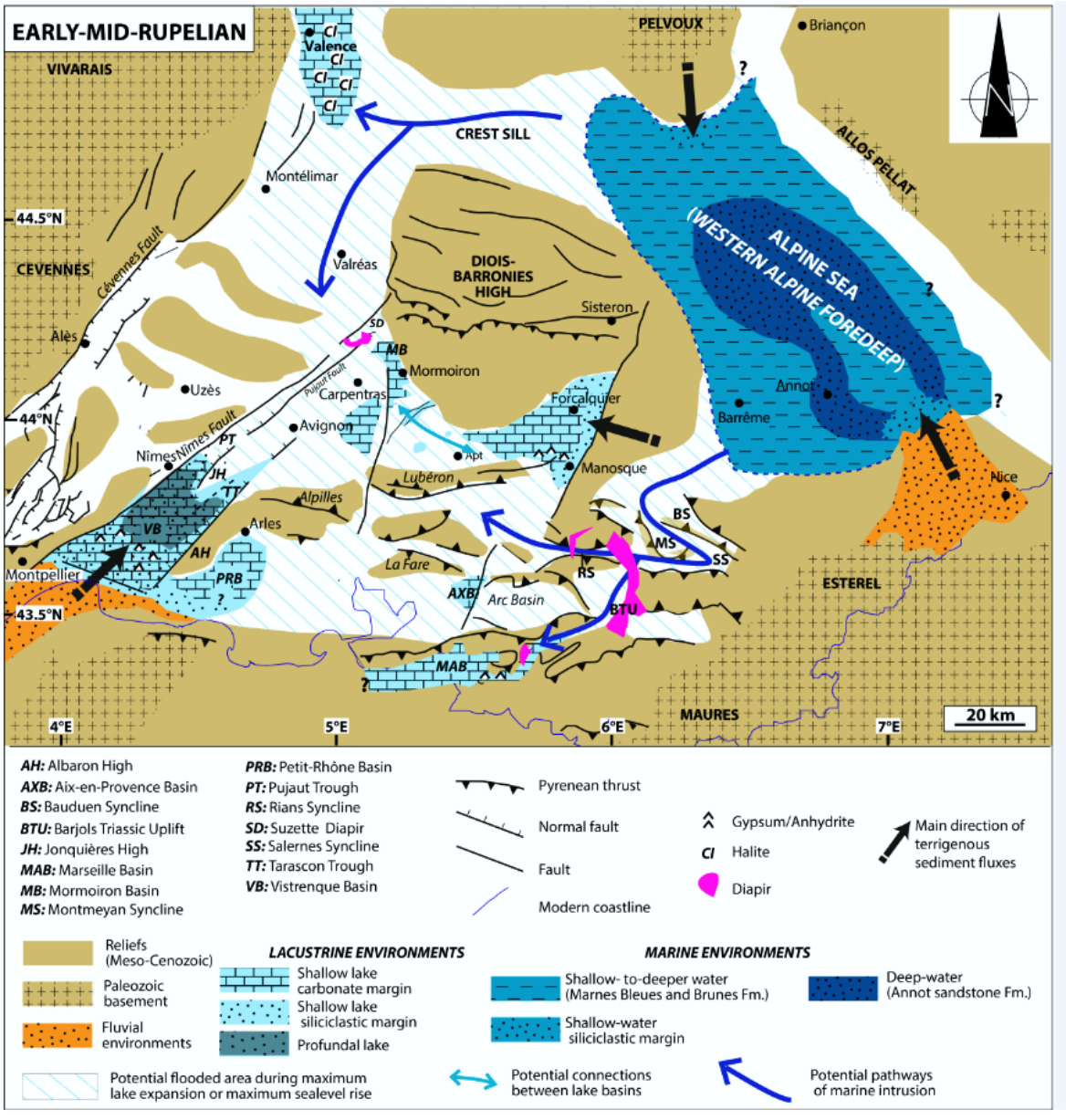
EARLY-MID-RUPELIAN
VIVARAIS
CEVENNES
Cévennes Fault
Valence
Montélimar
Valréas
CREST SILL
PELVOUX
Briançon
ALLOS PELLAT
ALPINE SEA
(WESTERN ALPINE FOREDEEP)
DIOIS-
BARRONIES
HIGH
Sisteron
Alès
Uzès
Carpentras
Mormoiron
Pujaut Fault
Nîmes Fault
Nîmes
Avignon
Apt
Forcalquier
Barrême
Annot
Manosque
Lubéron
Alpilles
Arles
Montpellier
La Fare
Arc Basin
ESTEREL
Nice
MAURES
44.5°N
44°N
43.5°N
4°E
5°E
6°E
7°E
20 km
AH: Albaron High
AXB: Aix-en-Provence Basin
BS: Bauduen Syncline
BTU: Barjols Triassic Uplift
JH: Jonquières High
MAB: Marseille Basin
MB: Mormoiron Basin
MS: Montmeyan Syncline
PRB: Petit-Rhône Basin
PT: Pujaut Trough
RS: Rians Syncline
SD: Suzette Diapir
SS: Salernes Syncline
TT: Tarascon Trough
VB: Vistrenque Basin
Pyrenean thrust
Normal fault
Fault
Modern coastline
Gypsum/Anhydrite
Cl Halite
Diapir
Main direction of terrigenous sediment fluxes
Reliefs (Meso-Cenozoic)
Paleozoic basement
Fluvial environments
LACUSTRINE ENVIRONMENTS
Shallow lake carbonate margin
Shallow lake siliciclastic margin
Profundal lake
MARINE ENVIRONMENTS
Shallow- to-deeper water (Marnes Bleues and Brunes Fm.)
Shallow-water siliciclastic margin
Deep-water (Annot sandstone Fm.)
Potential flooded area during maximum lake expansion or maximum sealevel rise
Potential connections between lake basins
Potential pathways of marine intrusion

Figure 12

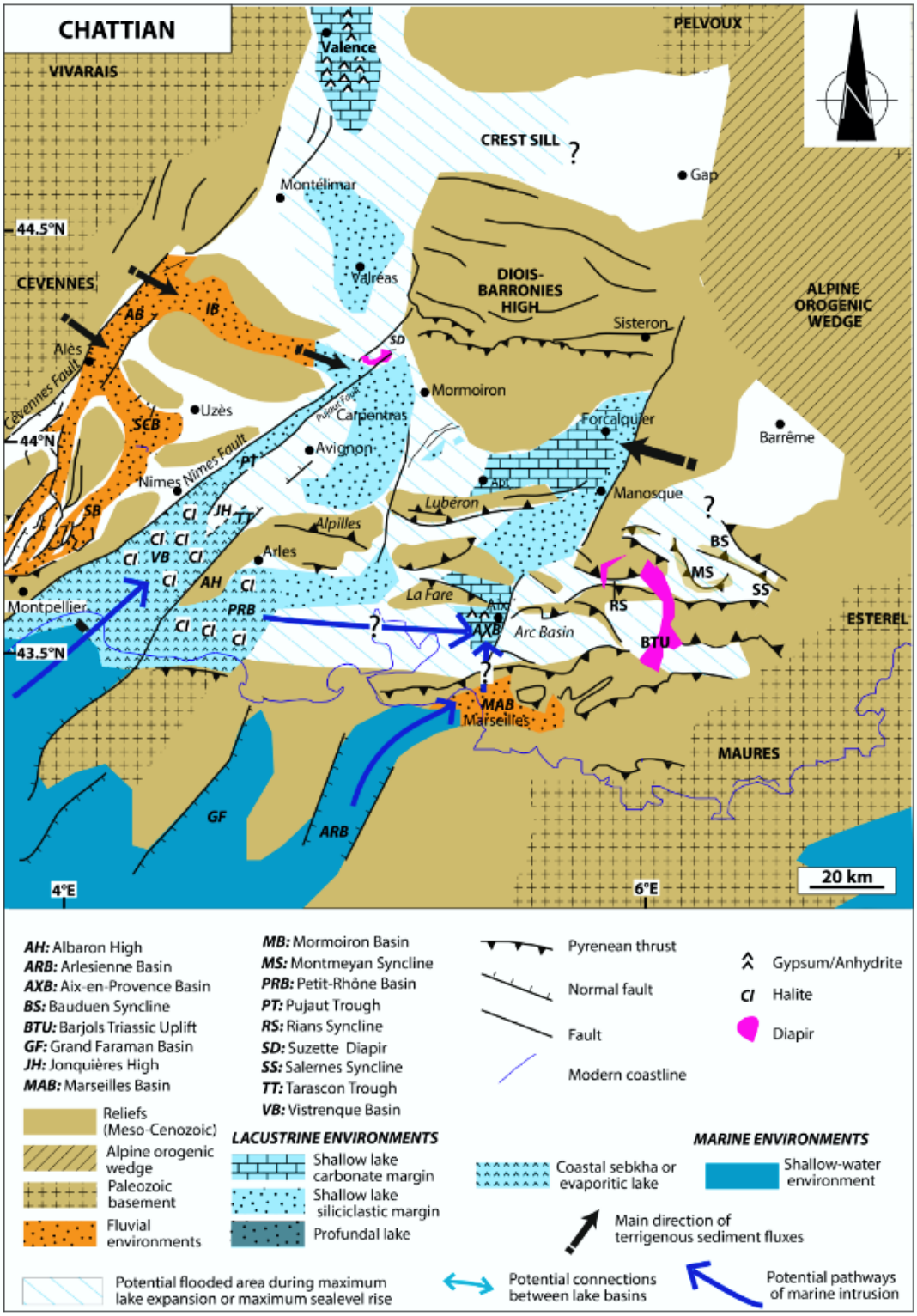
CHATTIAN
VIVARAIS
Valence
PELVOUX
CREST SILL
?
Gap
Montélimar
44.5°N
CEVENNES
Valréas
DIOIS-
BARRONIES
HIGH
ALPINE
OROGENIC
WEDGE
Sisteron
AB
IB
SD
Alès
Cévennes Fault
Mormoiron
Uzès
Pujaut Fault
Carpentras
SCB
44°N
Forcalquier
Barrême
Avignon
Nimes Nimes Fault
PT
Nimes
Aix
Manosque
Lubéron
SB
JH
TT
Alpilles
BS
CI
VB
Arles
MS
SS
AH
La Fare
RS
Montpellier
PRB
Aix
ESTEREL
AXB
Arc Basin
BTU
43.5°N
MAB
Marseilles
MAURES
GF
ARB
4°E
6°E
20 km
AH: Albaron High
ARB: Arlesienne Basin
AXB: Aix-en-Provence Basin
BS: Bauduen Syncline
BTU: Barjols Triassic Uplift
GF: Grand Faraman Basin
JH: Jonquières High
MAB: Marseilles Basin
MB: Mormoiron Basin
MS: Montmeyan Syncline
PRB: Petit-Rhône Basin
PT: Pujaut Trough
RS: Rians Syncline
SD: Suzette Diapir
SS: Salernes Syncline
TT: Tarascon Trough
VB: Vistrenque Basin
Pyrenean thrust
Normal fault
Fault
Modern coastline
Gypsum/Anhydrite
CI Halite
Diapir
Reliefs (Meso-Cenozoic)
Alpine orogenic wedge
Paleozoic basement
Fluvial environments
LACUSTRINE ENVIRONMENTS
Shallow lake carbonate margin
Shallow lake siliciclastic margin
Profundal lake
MARINE ENVIRONMENTS
Coastal sebkha or evaporitic lake
Shallow-water environment
Main direction of terrigenous sediment fluxes
Potential flooded area during maximum lake expansion or maximum sealevel rise
Potential connections between lake basins
Potential pathways of marine intrusion

Figure 13

Lithostratigraphic units	Age	Dating approach	Analysed sample	Well – depth (m)
Série Calcaréo-salifère	Late Chattian to earliest Aquitanian?	Geochemical modelling on sulphates	Anhydrite	Pierrefeu 1 – 1750 1775 – 2485 – 2545
	Early to middle Chattian	Pollen climatostratigrpahy	Pollen assemblage	Gallician 1 – 1648 Gallician 1 – 1775 Gallician 4 – 1580
Série Rouge	Early Chattian [a]	U/Pb dating * Absolute age: 27.88 +/1.71 Ma [b]	Vadose cement	Gallician 9 – 1894
Série Mixte	Middle Rupelian to early Chattian	Bounding	/	/
Série Calcaire	Early to middle Rupelian [a]	U/Pb dating * Absolute age: 31.27 +/1.90 Ma [b]	Vadose cement	Gallician 9 – 1960
Série Grise	Priabonian (?) to early Rupelian	Pollen climatostratigraphy	Pollen assemblage	Gallician 9 – 2530 Vauvert 1 – 3200

[b] Ages are calibrated with the Geological time Scale after Gradstein et al. (2012).

[a] Errors include measurements errors and errors associated with statistic calculations, considering 95% confidence interval

Table 1

Site	Basin	MAT (°C)	MTC (°C)	MTW (°C)	MAP (mm)
Canet 1 - 1100 m	Roussillon	16-**19**-25	10-**11.6**-14	25-**26.2**-29	1100-**1640**-2200
Gallician 1 - 1648 m	Vistrenque	16-**18.9**-25	5-**9**-14	25-**26.2**-29	1100-**1560**-1960
Canet 1 - 1186 m	Roussillon	15-**18.4**-25	2.5-**10.4**-14	25-**26.2**-29	1000-**1260**-1400
Canet 1 - 1470 m	Roussillon	16-**19**.1-24	10-**11.7**-14	25-**26.1**-28	1100-**1230**-1300
Canet 1 - 1701 m	Roussillon	19-**20.7**-25	10-**12.7**-16.5	26-**26.7**-28	1200-**1530**-1960
Gallician 9 - 2530 m	Vistrenque	12-**15.8**-20	2.5-**7.3**-14	20-**23.3**-27	800-**870**-2200
Vauvert 1 - 3200 m	Vistrenque	17-**19.7**-25	12-**13.2**-15	25-**26.2**-28	1200-**1325**-1400
Montchamp	Alès	20-**21.4**-25	12-**14.4**-15	26-**26.4**-28	1100-**1530**-1800
Celas Tunnel 2	Alès	19-**20.9**-25	12-**14.5**-17	25-**26.7**-29	1500-**1670**-1800
Celas Tunnel 1	Alès	19-**20.9**-25	10-**12.5**-15	26-**26.9**-28	1500-**1760**-2000
Maruéjols 1 - 798 m	Alès	19-**20.9**-25	12-14-17	26-**27.1**-29	1100-**1630**-2000
Monteils	Saint-Chaptes	15-**18.7**-25	10-**11.7**-14	25-**26.1**-28	1500-**1650**-1800
Crossroads D716/D981	Saint-Chaptes	19-**21.1**-25	12-**13**-14	26-**27**-29	1000-**1400**-1560
Serre de Cauvel 3	Saint-Chaptes	18-**20.2**-25	12-**12.8**-14	25-**26.2**-28	1100-**1540**-1800
Euzet Hill	Saint-Chaptes	17-**20.1**-24	12-**13.9**-16	25-**26.3**-28	1200-**1530**-1600

Table 2

Well	Formation/ Sequence	Sample ID	Lithology	Age	$^{87}Sr/^{86}Sr$	$\delta^{34}S$ ‰VCDT
Pierrefeu 1 (Vistrenque Basin)	Calcaréo-salifère	K2-3/8	anhydrite	Oligocene	0,707777	+10,92
	Calcaréo-salifère	K2-5/8	anhydrite	Oligocene	0,707772	+11,75
	Calcaréo-salifère	K5-1/10	anhydrite	Oligocene	0,708061	+13,87
	Calcaréo-salifère	K5-4/10	anhydrite	Oligocene	0,708031	+15,02
	Calcaréo-salifère	K6-5/5	anhydrite	Oligocene	0,708201	+17,11
SC-1 well (Alès Basin) SC-2 well (Alès Basin)	Sequence SPr2	SC1-108-2	anhydrite/gypsum	Priabonian	0,707685	+12,11
	Sequence SPr3	SC2-103	anhydrite/gypsum	Priabonian	0,707903	+26,98
	Sequence SPr3	SC2-89	anhydrite/gypsum	Priabonian	0,707870	+25,59
	Sequence SPr3	SC2-89	native sulphur	Priabonian		-6.42
	Sequence SPr3	SC2-89	native sulphur	Priabonian		-5.99

Table 3

SUPPLEMENTARY DATA

MICROPALEONTOLOGY: CALCAREOUS NANNOFOSSILS AND PALYNOLOGY

The micropalaeontological content (pollen grains and spores, dinoflagellate cysts, calcareous nannofossils) of thirteen locations (boreholes and exposed sections) has been searched. They belong to the Vistrenque Basin (Gallician 1 – 4 – 9, Vauvert 1), the Alès Basin (Maruéjols 1, Euzet Hill, Serre de Cauvel, Crossroad D716/D981, Monteils, Célas Tunnel, Saint-Jean de Maruéjols Pit hill, Montchamp) and the Roussillon Basin (Canet 1) (Fig. Y; Table S1). Occurrences of calcareous nannofossils are presented in Table S2, palynological results are detailed in Table S3.

Location	North Latitude	East Longitude	Elevation (m)	Basin
Canet 1	42°41'23.41"	3°04'66.00"	-1099 -1700	Roussillon
Gallician 9	43°38'35.64"	4°16'58.49"	-2515	Vistrenque
Gallician 4	43°38'13.86"	4°17'06.36"	-1581	
Gallician 1	43°38'14.98"	4°16'58.22"	-1647 -1775	
Vauvert 1	43°38'58.04"	4°16'39.43"	-3177	
Euzet Hill	44°04'35.71"	4°12'41.02"	127	Alès
Serre de Cauvel	44°04'36.90"	4°12'28.10"	120	
Crossroad D716/D981	44°04'50.50"	4°11'57.50"	132	
Monteils	44°05'08.00"	4°11'39.00"	168	
Célas Tunnel	44°07'37.70"	4°10'34.80"	201	
Saint-Jean de Maruejols Pit hill	44°15'59.05"	4°17'48.36"	128	
Maruéjols 1	44°15'35.76"	4°15'20.78"	-633	
Montchamp	44°19'56.20"	4°21'29.30"	220	

Table S1. Latitude, longitude, elevation and reference basin of the studied locations.
For boreholes, elevation refers to depth of samples with respect to elevation of the hole top.

Canet 1 borehole.

Six samples were chosen within clay layers from the lithostratigraphic interval ascribed to Aquitanian–late Oligocene by Gottis (1958) in order to obtain pollen grains, four of them revealed a rich pollen flora (Fig. S1) and three of them contained abundant dinoflagellate cysts. As a consequence, calcareous nannofossils were successfully searched in these last samples (Table S2).

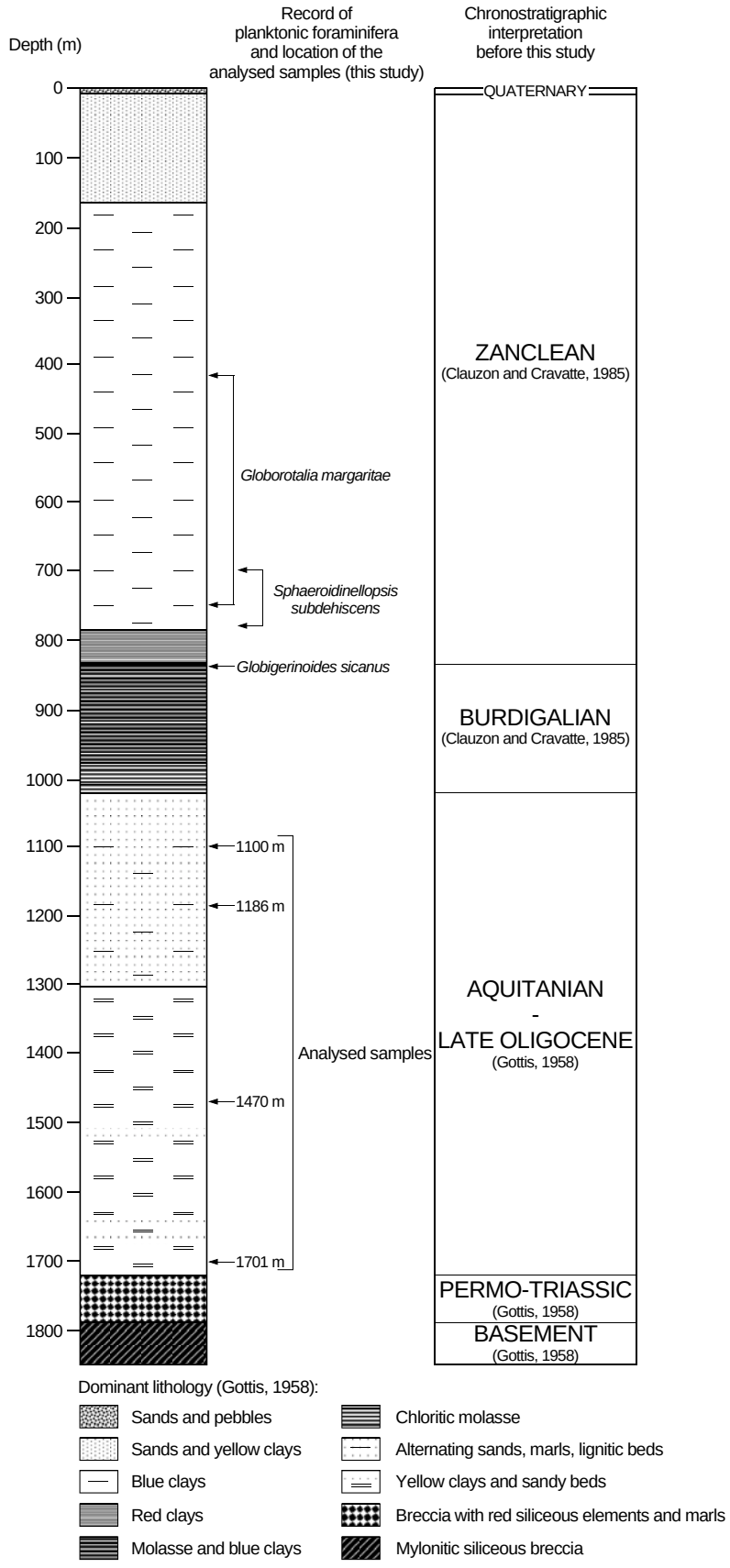

Figure S1. Canet 1 borehole: lithostratigraphic log, biostratigraphic markers, location of the analysed samples in this study, chronostratigraphic interpretation previous to this study.

Samples	Calcareous nannofossils
Gallician 1 – 1594 m	*Coccolithus pelagicus*, *Cyclicargolithus floridanus*, *Pontosphaera multipora*, *Reticulofenestra bisecta*, *R. lockeri*, *Sphenolithus moriformis*, *Zygrablithus bijugatus*
Gallician 1 – 1810 m	*Coccolithus pelagicus*, *Sphenolithus moriformis*, *Zygrablithus bijugatus*, *Reticulofenestra* cf. *lockeri*
Canet 1 – 1100 m	*Calcidiscus pataecus, Coccolithus pelagicus, Cyclicargolithus abisectus, C. floridanus, Discoaster deflandrei, Helicosphaera carteri, Pontosphaera discopora, P. multipora, Reticulofenestra bisecta,* small reticulofenestrids*, Sphenolithus* cf. *delphix, S. moriformis, Zygrhablithus bijugatus*
Canet 1 – 1470 m	*Calcidiscus pataecus, Chiasmolithus altus, Coccolithus pelagicus, Cyclicargolithus abisectus, C. floridanus, Discoaster deflandrei, Helicosphaera mediterranea, Pontosphaera enormis, P. multipora, Reticulofenestra bisecta,* small reticulofenestrids, *Sphenolithus moriformis, Zygrhablithus bijugatus*
Canet 1 – 1701 m	*Chiasmolithus altus, Coccolithus pelagicus, Cyclicargolithus abisectus, C. floridanus, Helicosphaera etholoa, Pontosphaera enormis, P. multipora, Zygrhablithus bijugatus, Reticulofenestra bisecta, Sphenolithus moriformis,*
Maruéjols 1 – 433 m	*Coccolithus pelagicus*, *Cyclicargolithus floridanus*, *Pontosphaera multipora*, *Reticulofenestra bisecta*, *R. lockeri*, *Sphenolithus moriformis*, *Zygrablithus bijugatus*
Crossroad D716/D981	*Coccolithus pelagicus*, *Sphenolithus moriformis*, *Helicosphaera* sp.

Table S2. Records of calcareous nannofossils.

Pollen and spore floras

Site	Canet 1				Gallician 1		Gallician 4	Gallician 9	Vauvert 1	Montchamp	Saint-Jean de Maruéjols	Célas Tunnel		Maruéjols 1	Monteils	Crossroads D716/D981	Serre de Cauvel	Euzet Hill
Taxa / Depth (m) or sample name or sample number	1100 m	1186 m	1470 m	1701 m	1648 m	1775 m	1580 m	2530 m	3200 m		Pit hill	1	2	798 m			3	
MEGATHERMS (MAT>24°C)*																		
Amanoa (Euphorbiaceae)									1				1			3	2	
Bambusa (Poaceae)																1		
Avicennia (Acanthaceae)				1	1					1	3	1	1	1		3		
Bombax-type (Malvaceae)																1		1
Buxus bahamensis-type (Buxaceae)											1		1					
Afzelia-Peltophorum-type (Leguminosae)				1				1								5		2
Canthium-type (Rubiaceae)										9	2	11				1		
Peltogyne-type (Leguminosae)																		1
Croton-Jatropha (Euphorbiaceae)				1						4	2	1				6		1
Euphorbiaceae										1		4						
Leguminosae Caesalpinioideae										1						1		
Malpighiaceae																		1
Mappianthus (Icacinaceae)				1														3
Mussaenda-type (Rubiaceae)									1				2	1		2	3	2
Phyllanthus (Phyllanthaceae)																		2
Rhizophoraceae										3							2	
Rubiaceae																	1	
Sapindaceae									1	2			1		2			1
Theaceae																2		1
Thunbergia (Acanthaceae)																		1
Uncaria-type (Rubiaceae)									6		1		1			1		3
MEGA-MESOTHERMS (20 °C<MAT<24 °C)*																		
cf. *Alfaroa* (Juglandaceae)									2				1				2	
Alangium (Cornaceae)									1		1	4	1		1			
Arecaceae				4				1	1		1		2					1
Castanopsis-Lithocarpus (Fagaceae)			3									2	5	1	1			1
Cissus (Vitaceae)																1		
Cyrillacese-Clethracae														1				
Distylium (Hamamelidaceae)			1	1		1	1	1	2	9	13	2	2	1	6	6	3	10
Dodonaea (Sapindaceae)													1			1		
Embolanthera (Hamamelidaceae)									4	4	1	2		2	2			1
Engelhardia (Juglandaceae)	3	19	22	18	2	3	1	7	48	9	14	24	13	2	33	8	49	54
Fothergilla (Hamamelidaceae)																		2
Hamamelis (Hamamelidaceae)																		1
Ilex floribunda-type (Aquifoliaceae)												1				1		1
Leea (Vitaceae)											3						1	
Menispermaceae			1							25	2	35	23		11	6	1	6
Microtropis (Celastraceae)									1									
Myrica (Myricaceae)		2	2			1				1			3		1			
Nyssa aquatica-type (Cornaceae)																		1
Nyssa cf. *sinensis* (Cornaceae)	2												1					
cf. *Phyllostylon* (Ulmaceae)													1			1		
Platycarya (Juglandaceae)			1	2					1	1	2	1					1	
Rhodoleia (Hamamelidaceae)									5		16				1			1
Rhoiptelea (Juglandaceae)			1															
Ricinus-type (Euphorbiaceae)													1					
Sapotaceae	1	4	5		2	1			2	1	6	4	7	2	3	11		1
Sciadopitys (Sciadopityaceae)	9		1	1														
Symplocos (Symplocaceae)									2	2		5	4			5		2
Taxodium-type (Cupressaceae)	3		2	11	7			1	2	1				46			16	
Cupressaceae papillate pollen grains (former 'Taxodiaceae')	44	23	43	49	185	116	140	97		2	51	4	1	88	78	39	13	
Cathaya (Pinaceae)	74	11	10	24	55	352	26	22		6	1127		1	27	3	3	4	5
Podocarpus (Podocarpaceae)	24	3	30	29	101	134	28	73	5	17	214	5	17	64	18	46	89	39
MESOTHERMS (14 °C<MAT<20 °C)*																		
Acer (Sapindaceae)											16					1	1	1
Alnus (Betulaceae)	4	3	1	2														
Anacardiaceae	1																	
Araliaceae	1				1	1			1	27		33	37			5	1	
Betula (Betulaceae)	1																	
Buxus sempervirens-type (Buxaceae)		1								3	1	2	5					
Carpinus (Betulaceae)	3	1						3	1									
Carya Juglandaceae)	10	38	12	6	4	2		6				1				2	2	3
Celtis (Cannabaceae)													2					
Ericaceae	7	1	1	1	1	1					2		1					
Eucommia (Eucommiaceae)																	1	
Hedera (Araliaceae)											1							2
Ilex (Aquifoliaceae)																		
Juglans (Juglandaceae)				1														
Liquidambar (Altingiaceae)			1	3			1	1		3	1	1	3				1	
Lonicera (Caprifoliaceae)																2	1	
Parrotia (Hamamelidaceae)					1				4		6							8
Populus (Salicaceae)			1	1	1					1			1			1	1	
Pterocarya (Juglandaceae)	1	4	1	1	2					1	1							3
Quercus (Fagaceae)	23	11	22	13	3	2	3	1	6	4	4	3	2	1	2	18	6	1
Salix (Salicaceae)																1		
Sambucus (Adoxaceae)																		1
Taxaceae																		3
Ulmus (Ulmaceae)		6		1	2	1		2	4	11	1	2	4		8	1	6	2
Zelkova (Ulmaceae)		19			1	3		1	2		1		1				1	
MESO-MICROTHERMS (12 °C<MAT<14 °C)*																		
Cedrus (Pinaceae)	12		1						1					1		4		
Fagus (Fagaceae)	4		1	2														1
Tsuga (Pinaceae)	6			7	4									3				
MICROTHERMS (MAT<12 °C)*																		
Abies (Pinaceae)	7	4	5	4	2	19	1	1						1				
Picea (Pinaceae)	12	7	1	6	2	34	1	2										
TAXA WITHOUT ECOLOGICAL SIGNIFICANCE														4				
Pinus diplostellate-type (Pinaceae)	172	9	2	19	11		39	18	3	5	161	1	2	111	2	79		11
Indeterminable pollen grains of Pinaceae	259	109	81	135	187	9427	264	310	3	4	3864	5	3		37	166	93	15
***Cupressus-Juniperus*-type** (Cupressaceae)	13	2	7	8	17	4		9	2	5	2			3	1	1	1	
Aristolochia (Aristolochiaceae)													1					
cf. Cucurbitaceae																		
Ranunculaceae									4				1					4
Rosaceae									2				1					
WATER PLANTS																		
Aglaoreidia (fossil taxon)											13						3	
Lemna (Lemnaceae)									4									
Lythraceae										1								
Myriophyllum (Haloragaceae)				1					1	1								
Nymphеaceae				*4*								*1*						
Oenotheraceae				*2*									1					
Potamogeton (Potamogetonaceae)	1									1								
Restio (Restionaceae)				1													2	
Restionaceae			2		1				3	1						1	3	3
SCLEROPHYLLOUS MEDITERRANEAN PLANTS																		
Jasminum (Oleaceae)													1					
Olea (Oleaceae)	1	1							10	5	1	5	9			2	16	6
Phillyrea (Oleaceae)	1								2	4			1				2	2
Quercus ilex-type (Fagaceae)		1	4	3														
HERBACEOUS PLANTS																		
Amaranthaceae	4		1	3					1	1	1	1				1	1	
Brassicaceae																	1	1
Campanulaceae									3							1		7
Caryophyllaceae	1																	
Compositae Asteroideae	1		4									1			1	1		4
Compositae Cichorioideae	1		2													1		
Convolvulus (Convolvulaceae)	1											1				13	1	1
Cyperaceae	2		3	1					2	1	1						12	4
Lamiaceae																		1
Leguminosae Papilionideae										3								
Liliaceae							1											
Plantago (Plantaginaceae)	3								2			1				1		3
Plumbaginaceae	2	1				2		1										
Poaceae	7	15	1	3	11	9	2		19		2	1				2		2
Resedaceae																		1
Rumex (Polygonaceae)												1					1	2
Sanguisorba-type (Rosaceae)																		1
Thymeleaceae																1		
STEPPE PLANTS																		
Artemisia (Compositae)			1															
Ephedra (Ephedraceae)		1	8	6	1	2		22			1			4	1			
SUBDESERTIC PLANTS																		
Calligonum (Polygonaceae)			1															
Number of identified pollen grains	**721**	**296**	**286**	**377**	**605**	**10115**	**508**	**580**	**165**	**181**	**5541**	**166**	**167**	**364**	**212**	**459**	**344**	**238**
Unidentified pollen grains										4	1	2	2					
Indeterminable pollen grains	10	39	116	37	54	229	303	8	20	36	14	43	40	2	15	60	17	19
PTERIDOPHYTE SPORES													334					
Osmunda (Osmundaceae)														3			5	
Polypodiaceae	1																	
Pteris (Pteridaceae)																		1
Unidentified monolete spores	21	4	4	5			1	3	4	2	1	1	5	2	3	128	5	
Unidentified trilete spores	12	4	1	5			3	7	9		12	2	8		21	199	4	
Unidentified spores	4		4	1	5		3	3	1	8	1	2	2	6	3		2	12
ALGAE																		
Botryococcus										Present	Present	Present	Present		Abundant	Present		Present
REWORKED POLLEN GRAINS AND SPORES																		
Pollen grains	35	4	16	102	65	1		205		2	1	18	2	21	1	7	24	
Fern spores	16	2	5	3				3	1					1				

* MAT (mean annual temperature) with respect to the Nix (1982)'s temperature gradient

Table S3. Detailed content in pollen grains and spores of the analysed samples.

1. Advances with respect to previous palynological records.

Several palynological records were previously performed in the studied region. Most of them are characterised by a listing of the most usually identified plants with a limited or missing counting of pollen grains (Provence: Sittler, 1965; Schuler and Sittler, 1976; Marseilles Basin: Châteauneuf, 1977; Alès Basin: Michoux, 1983). Such studies are particularly damaged by the non-recognition of most of the triporate, tricolpate and tricolporate pollen grains, which often belong to subtropical and tropical plants, i.e. meaningful elements for palaeoenvironmental reconstructions. The use of these poor pollen records is thus very limited for understanding palaeovegetation and palaeoclimate. Even lesser elaborated palynological analyses have been performed on few Camargue wells and do not provide significant information (Jan du Chêne, 1989; Buisson, 1993).

Because of improvements in botanical identification of pollen grains achieved in the seventies on the Neogene pollen floras thanks to the use of the rich ISEM pollen collection in Montpellier (Suc, 1976; Bessedik, 1980, 1981; Suc and Bessedik, 1981), supported by pollen photographs, some progress was introduced in Paleogene microfloras (Célas: Gruas-Cavagnetto, 1973; Provence: Châteauneuf and Nury, 1995), unfortunately still devoid of countings. Accordingly, these pollen records have a limited interest.

Our pollen study confirms the same differences and similarities between the Célas macroflora and microflora than previously indicated by Gruas-Cavagnetto (1973) but emphasizes the important role in the local vegetation made by Hamamelidaceae (*Distylium*, *Embolanthera*, *Rhodoleia*), Sapotaceae, Euphorbiaceae (*Croton*, *Amanoa*, *Canthium*-type) in addition to Araliaceae and Menispermaceae listed in the macroflora. One matter persists due to abundant cones of the fossil genus *Doliostrobus* Marion in the macroflora that Kvacek (2002) ascribed to an extinct family, Doliostrobaceae, expected close of both Araucariaceae and Cupressaceae. Cupressaceae pollen grains (including those of the former Taxodiaceae) are very scarce in the Célas microflora while those of Araucariaceae have not been observed.

2. Dinoflagellate cysts.

Dinoflagellate cysts have been recorded in some samples (Plate 4): Canet 1 (1100 m, 1470 m, 1701 m), Gallician 4 (1580 m), Gallician 9 (2530 m), Crossroads D716/D981, and Serre de Cauvel (samples 1 and particularly 2, the sample in which dinoflagellate cysts are the most abundant). On the whole, dinoflagellate cysts are not well preserved, often broken and thus identifiable with great difficulty. Many reworked dinoflagellate cysts occur. All the individuals have been observed both in transmitted light microscopy (TLM) and under fluorescent UV light microscopy (FLM) in order to detect the reworking (Doláková and Burešová, 2007 ; Hoyle et al., 2018): the reworked dinoflagellate cysts show a dull brown colour at the difference of the non reworked specimens which show a bright yellow colour as illustrated in Plate 4.

3. Morphological description of some pollen grains.

These descriptions are based on observations at transmitted light microscope (TLM) according to LO-analysis (*Lux* = light vs. *Obscuritas* = darkness) technique and/or scanning electronic microscope (SEM).

Afzelia-Peltophorum-type (Leguminosae) (Plate 1, Figs. 2a-e, 3a-d, 4).

Oblate to equiaxal tricolporate and reticulate pollen grains show large and short non-linear ectoapertures (colpi), endoapertures (pori) being often indistinct. The supratectal reticulum is made of large lumina. Muri are densely micro-echinate. Columellae with large head structurate the tectum, also supported by smaller other ones. This pollen has been recorded in several locations (Canet 1, Gallician 9, Crossroads D716/D981, Euzet Hill; Table S3).

Similar pollen types are found in the tribes Detarioideae (*Afzelia*, *Intsia*) and Caesalpinioideae (*Peltophorum*, *Delonix*) (Plate 1, Figs. 1a-e; Banks and Lewis, 2018) but none of the observed species from the ISEM Collection shows small spines.

Peltogyne-type (Leguminosae; Plate 3, Figs.6a-d, 7).

Oblate tricolporate and clavate pollen with thick costae along the ectoapertures (colpi) and a distinct thin annulus bordering the endoapertures (pori). Large and smaller clavae constitute the ornamentation of the pollen. This pollen has been recorded in the Euzet Hill location.

This pollen morphology is similar to that of the modern species *Peltogyne confertiflora* (Hayne) Benth. (Detarioideae) (Graham and Barker, 1981: plate 12, fig. E).

Croton-Jatropha (Euphorbiaceae; Plate 2, Figs. 3, 5a-b).

Inaperturate spheroidal pollen grain with a coarsely reticulate ornamentation constituted by more or less dense clavae, which have an almost triangular shape that provides the so-called *Croton*-pattern. This pollen has been recorded in several locations (Canet 1, Montchamp, Saint-Jean de Maruéjols Pit hill, Célas Tunnel, Crossroads D716/D981, Euzet Hill; Table S3).

Such very peculiar pollen types are characteristic of *Croton* (Plate 2, Figs. 4a-c) and *Jatropha* genera (Carreira et al., 1996; Ribes de Lima, 2007; Ribeiro de Souza et al., 2020).

Amanoa (Phyllanthaceae; Plate 1, Figs. 6a-c).

Tricolporate oblate pollen showing a large semi-tectate curvilinear reticulum (a thin membrane covers the lumina), with long colpi (ectoapertures) resulting in a small apocolpium, bordered by costae. Endoapertures are rectangular. This pollen has been recorded in several locations (Vauvert 1, Célas Tunnel, Crossroads D716/D981, Serre de Cauvel; Table S3).

This pollen morphology is characteristic of the genus *Amanoa* (Plate 1, Figs. 5a-b; Punt, 1962; Köhler, 1965).

Dodonaea (Sapindaceae; Plate 2; Figs. 6a-b).

Equiaxal tricolporate pollen, subtriangular in polar view, with prominent apertural areas characterized by thickening endexine, especially around the rectangular endoapertures. The ornamentation can be psilate, rugulate or slightly reticulate. This pollen has been recorded at Célas Tunnel and Crossroads D716/D981 locations (Table S3).

Because of its distinctive shape, this pollen corresponds in part to the fossil ‘genus’ *Pentapollenites* conceived by Krutzsch (1962), manifestly illustrated at the scanning electronic microscope by Châteauneuf (1980: plate 17, fig. 7), which now receives a robust botanical ascription as *Dodonaea* (Plate 2, Figs. 7a-c; Merville, 1965), a primitive genus within the Sapindaceae (Muller and Leenhouts, 1976). Henceforth, the name *Pentapollenites* must be rejected as it probably also includes other botanical genera.

Alangium (Cornaceae; Plate 1, Figs. 7, 8).

Prolate tricolporate and reticulate pollen, elliptic in equatorial view, with long ectoapertures (colpi) edged by thick costae. Lalongate endoapertures (pori) are surrounded by a thin annulus. The supratectate reticulum is somewhat lengthened along the pole axis. The tectum is thick and clearly separated from the endexine. This pollen has been recorded at Vauvert 1, Célas Tunnel, Saint-Jean de Maruéjols Pit hill and Monteils locations (Table S3).

Such a pollen is characteristic of several species of the *Alangium* genus (Plate 1, Fig. 9; Reitsma, 1970).

Plate 1. Photographs at TLM and SEM of some fossil and modern pollen grains (shots by J.-P. Suc). Modern pollen grains originate from the ISEM - Montpellier Collection.
Scale bar = 10 µm.
Figs 1a-e. *Afzelia cochinchinensis* (Pierre)J.Léonard = *A. xylocarpa* (Kurz)Craib (Leguminosae) – ISEM Collection number: 9427 (plant specimen collected in Vietnam); equatorial view aperture facing at TLM.
LO-analysis: a, reticulate ornamentation; b, focus on the head of columellae; c, focus on the foot of columellae; d, optical section.
Figs. 2a-e. *Afzelia-Peltophorum*-type (Leguminosae) – Euzet Hill; equatorial view (intercolpium) at TLM.
LO-analysis: a, reticulate ornamentation; b, focus on the head of columellae; c, focus on the foot of columellae; d, aperture; e, optical section.
Figs. 3a-d. *Afzelia-Peltophorum*-type (Leguminosae) – Crossroad D716/D981; equatorial view (intercolpium) at TLM.
LO-analysis: a, reticulate ornamentation; b, focus on the head of columellae; c, focus on the foot of columellae; d, optical section.
Fig. 4. *Afzelia-Peltophorum*-type (Leguminosae) – Euzet Hill; equatorial view aperture facing at SEM.
Figs. 5a-b. *Amanoa caribaea* Krug & Urb. (Phyllanthaceae) – ISEM Collection number: 41784 (plant specimen collected in Cameroon); equatorial views aperture facing (a) and polar view (b) at TLM.
LO-analysis: a, reticulate ornamentation and apertures; b, optical section.
Figs. 6a-c. *Amanoa* (Phyllanthaceae) – Crossroad D716/D981; equatorial view aperture facing (a-b) and polar view (c) at TLM.
LO-analysis: a, reticulate ornamentation and aperture; b, optical section.
Fig. 7. *Alangium* (Cornaceae) – Célas Tunnel 1; equatorial view (intercolpium) at TLM.
Fig. 8. *Alangium* (Cornaceae) – Saint-Jean de Maruéjols Pit hill; equatorial view aperture facing at TLM.
Fig. 9. *Alangium barbatum* (R.Br. ex C.B.Clarke) Baill. ex Kuntze (Cornaceae) – ISEM Collection number: 17360 (plant specimen collected in Burma); equatorial views aperture facing and optical section at TLM.
Figs. 10a-b. *Bombax*-type (Malvaceae) – Crossroad D716/D981; polar view at TLM.
LO-analysis: a, reticulate ornamentation; b, optical section.
Figs. 11a-b. *Avicennia* (Acanthaceae) – Montchamp; equatorial view aperture facing at TLM.
LO-analysis: a, reticulate ornamentation; b, optical section.
Figs. 12a-c. *Avicennia* (Acanthaceae) – Saint-Jean de Maruéjols Pit hill; equatorial view (intercolpium) at TLM.
LO-analysis: a, reticulate ornamentation; b, focus at base of columellar, colpi; c, optical section.

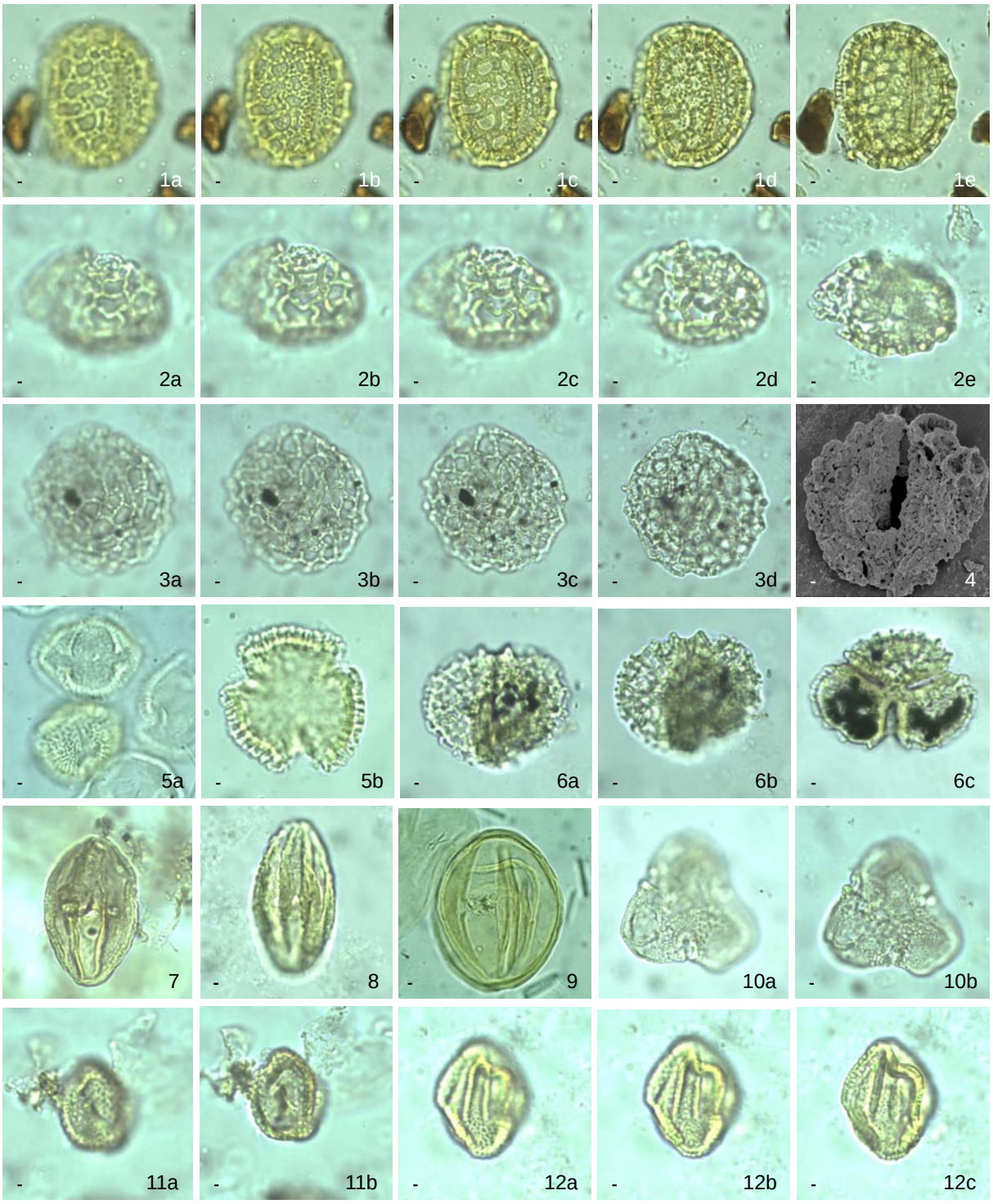
- 1a
- 1b
- 1c
- 1d
- 1e
- 2a
2b
- 2c
- 2d
- 2e
- 3a
- 3b
- 3c
- 3d
- 4
- 5a
- 5b
- 6a
- 6b
- 6c
7
- 8
- 9
10a
- 10b
- 11a
- 11b
- 12a
- 12b
- 12c

Plate 2. Photographs at TLM and SEM of some fossil and modern pollen grains (shots by J.-P. Suc). Modern pollen grains originate from the ISEM - Montpellier Collection or from the GeoBioStratData – Rillieux la Pape Collection.
Scale bar = 10 µm.
Figs 1a-b. Araliaceae – Célas Tunnel 2.; equatorial view (intercolpium) at TLM.
LO-analysis: a, reticulate ornamentation and apertures; b, optical section.
Figs. 2a-b. Araliaceae – Montchamp; equatorial view aperture facing at TLM.
LO-analysis: a, reticulate ornamentation and apertures; b, apertures and optical section.
Fig. 3. *Croton* (Euphorbiaceae) – Euzet Hill; view at SEM.
Figs. 4a-c. *Croton scabiosus* Bedd. (Euphorbiaceae) – ISEM Collection number: 15339 (plant specimen collected in India); view at TLM.
LO-analysis: a, reticulate ornamentation; b, focus on the foot of columellae; c, optical section.
Figs. 5a-b. Croton (Euphorbiaceae) – Saint-Jean de Maruéjols Pit hill; view at TLM.
LO-analysis: a, reticulate ornamentation; b, focus on the foot of columellae and optical section.
Figs. 6a-b. *Dodonaea* (Sapindaceae) – Crossroad D716/D981; equatorial view aperture facing at TLM.
LO-analysis: a, aperture; b, aperture and optical section.
Figs. 7a-c. *Dodonaea triquetra* J.C.We,dl. (Sapindaceae) – ISEM Collection number: 36963 (plant specimen collected in Australia); equatorial view aperture facing at TLM.
LO-analysis: a, psilate ornamentation and apertures; b, aperture; c, aperture and optical section.
Figs. 8-c. *Embolanthera glabrescens* H.L.Li (Hamamelidaceae) – ISEM Collection number: 14245 (plant specimen collected in Vietnam); polar view at TLM.
LO-analysis: a, reticulate ornamentation; b, focus on the foot of columellae; c, optical section.
Figs. 9a-c. *Embolanthera* (Hamamelidaceae) – Vauvert 1 3200 m; polar view at TLM.
LO-analysis: a, reticulate ornamentation; b, focus on the foot of columellae; c, optical section.
Figs. 10a-c. *Fothergilla gardenii* L. (Hamamelidaceae) – GeoBioStratData Collection number: 839 (plant specimen collected in North America); polar view at TLM.
LO-analysis: a, reticulate ornamentation; b, focus on the foot of columellae; c, optical section.
Figs. 11a-c. *Fothergilla* (Hamamelidaceae) – Euzet Hill; polar view at TLM.
LO-analysis: a, reticulate ornamentation; b, focus on the foot of columellae; c, optical section.
Figs. 12a-b. Mappianthus (Icacinaceae) – Euzet Hill; equatorial view at TLM.
LO-analysis: a, echinulate ornamentation and aperture; b, optical section.
Fig. 13. *Leea* (Vitaceae) – Saint-Jean de Maruéjols Pit hill; equatorial view at TLM.
LO-analysis: reticulate ornamentation and aperture.

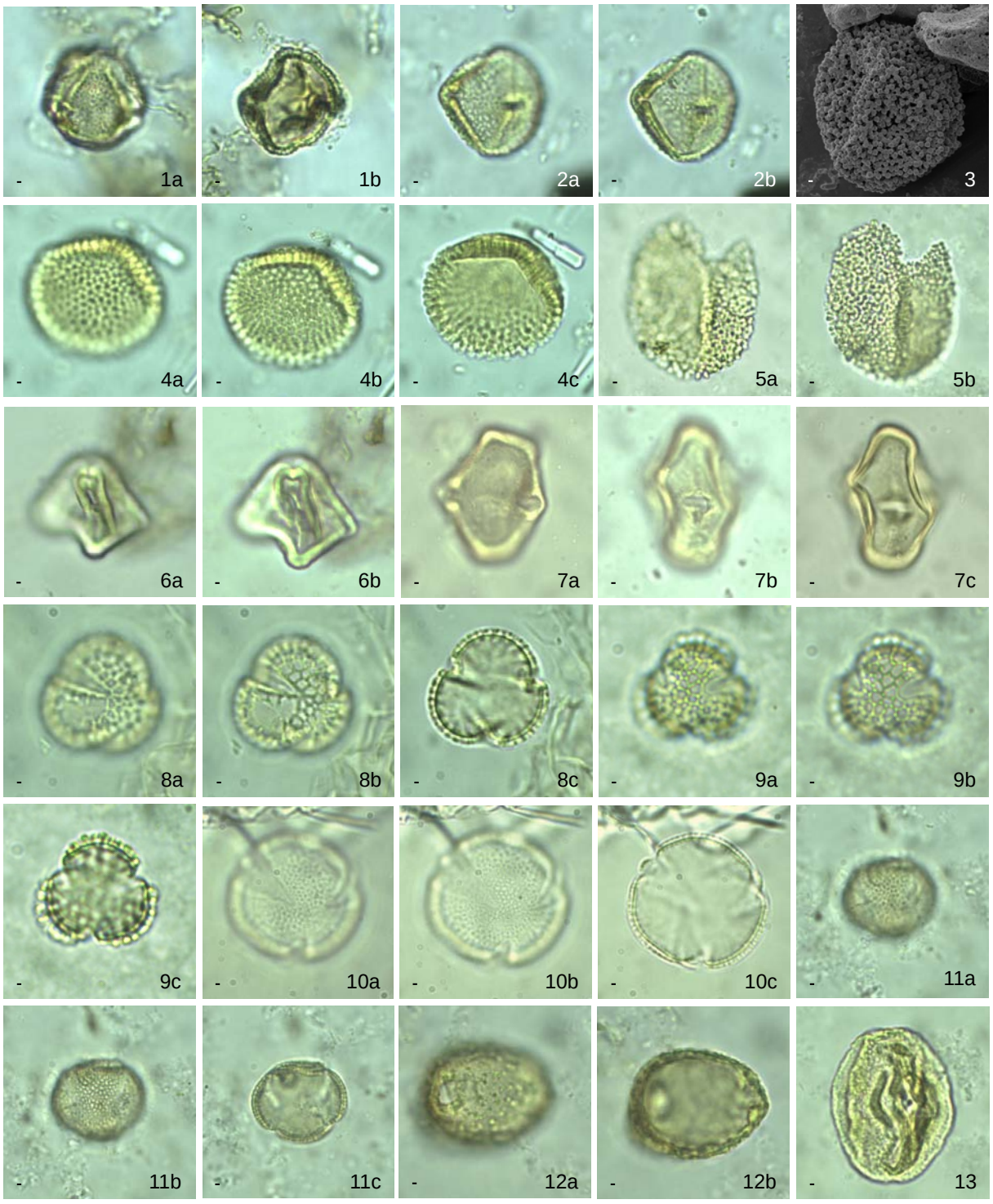
- 1a
- 1b
- 2a
- 2b
- 3
- 4a
- 4b
- 4c
- 5a
- 5b
- 6a
- 6b
- 7a
- 7b
- 7c
- 8a
- 8b
- 8c
- 9a
- 9b
- 9c
- 10a
- 10b
- 10c
- 11a
- 11b
- 11c
- 12a
- 12b
- 13

Plate 3. Photographs at TLM and SEM of some fossil and modern pollen grains (shots by J.-P. Suc). Modern pollen grains originate from the ISEM - Montpellier Collection.
Scale bar = 10 µm.
Figs. 1a-e. *Distylium* (Hamamelidaceae) – Euzet Hill; polar view at TLM.
LO-analysis: a, reticulate ornamentation; b, apertures and optical section.
Figs. 2a-c. Menispermaceae – Euzet Hill; equatorial view aperture facing at TLM.
LO-analysis: a, reticulate ornamentation and aperture; b, focus on the base of columellae; c, optical section.
Figs; 3a-c. *Olea* (Oleaceae) – Euzet Hill; equatorial view (intercolpium) at TLM.
LO-analysis: a, reticulate ornamentation; b, focus on the base of columellae; c, optical section.
Fig. 4. *Mussaenda laxa* (Hook.f.)Hutch. ex Gamble (Rubiaceae) – ISEM Collection number: 9954 (plant specimen collected in India); polar view, optical section at TLM.
Fig. 5. *Mussaenda*-type (Rubiaceae) – Serre de cauvel 3; polar view, optical section at TLM.
Figs. 6a-d. *Peltogyne*-type (Leguminosae) – Euzet Hill; polar view at TLM.
LO-analysis: a, clavate ornamentation; b, focus on the base of clavae; c, apertures; d, optical section.
Fig. 7. *Peltogyne*-type (Leguminosae) – Euzet Hill; view with aperture at SEM.
Figs. 8a-c. *Phyllanthus simplex* Retz. = *P. virgatus* G.Forst. (Phyllanthaceae) – ISEM Collection number: 10100 (plant specimen collected in India); polar view at TLM.
LO-analysis: a, reticulate ornamentation and apertures; b, focus on the base of columellae and apertures; c, optical section.
Figs. 9a-c. *Phyllanthus* (Phyllanthaceae) – Euzet Hill; polar view at TLM.
LO-analysis: a, reticulate ornamentation and apertures; b, focus on the base of columellae and apertures; c, optical section.
Fig. 10. *Phyllanthus* (Phyllanthaceae) – Euzet Hill; view at SEM showing the reticulum and apertures.
Fig. 11. Rhizophoraceae – Montchamp; equatorial view at TLM showing the apertures.
Fig. 12. *Rhoiptelea* (Juglandaceae) – Canet 1 1470 m; polar view, optical section at TLM.
Fig. 13. *Symplocos* (Symplocaceae) – Euzet Hill; polae view showing apertures at TLM.
Fig. 14. *Cedrus* (Pinaceae) – Crossroad D716/D981; profile view at TLM.
Fig. 15. *Podocarpus* (Podocarpaceae) – Célas Tunnel 2; proximal view at TLM.
Fig. 16. *Podocarpus* (Podocarpaceae) - Crossroad D716/D981; distal view at TLM.

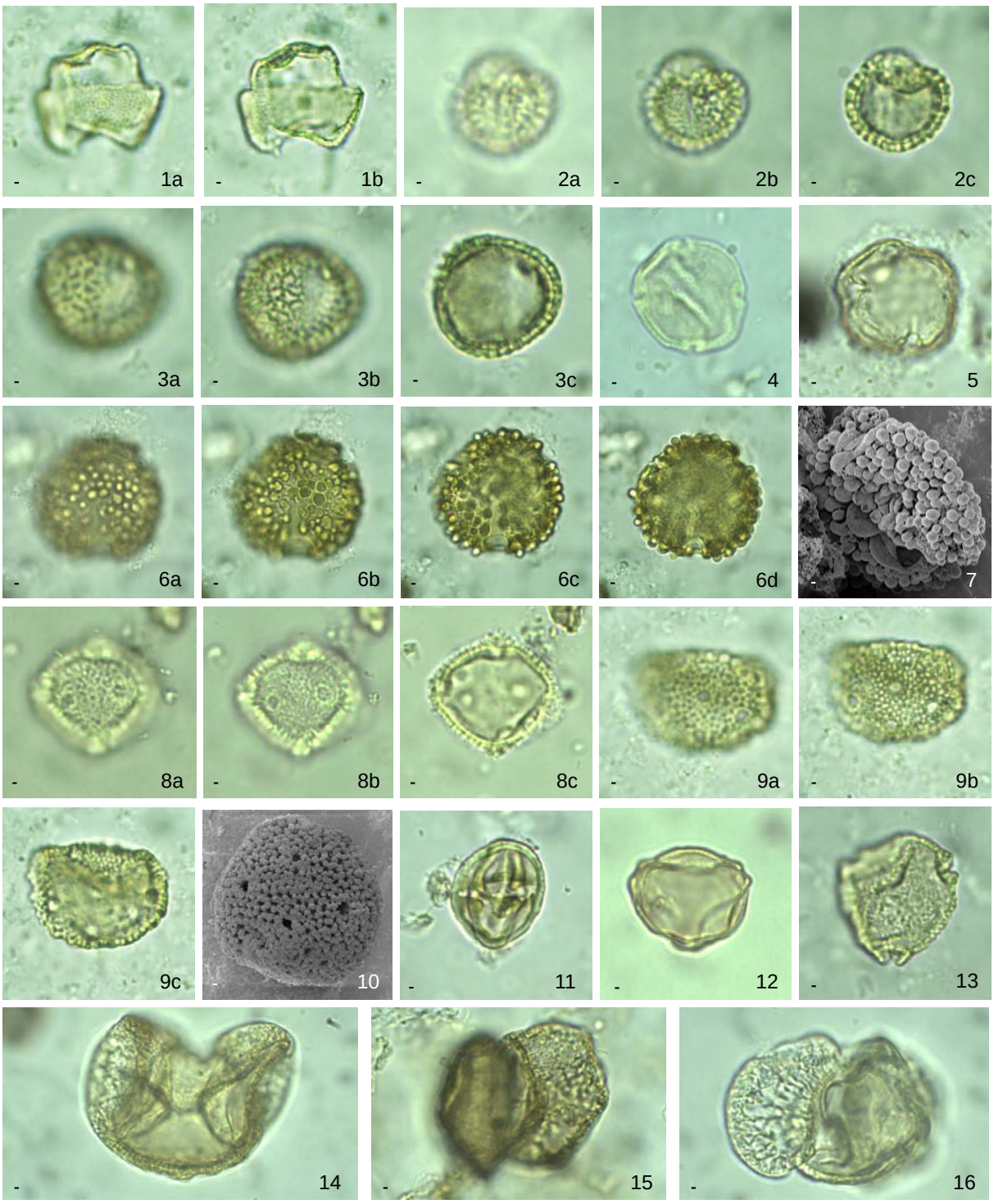
- 1a
- 1b
- 2a
- 2b
- 2c
- 3a
- 3b
- 3c
- 4
- 5
- 6a
- 6b
- 6c
- 6d
- 7
- 8a
- 8b
- 8c
- 9a
- 9b
- 9c
- 10
- 11
- 12
- 13
- 14
- 15
- 16

Plate 4. Photographs at TLM and FLM of some fossil dinoflagellate cysts (shots by S.-M. Popescu).
Scale bar = 10 µm.
Figs. 1a-c. *Deflandrea phosphoritica* – Gallician 9 (2530 m): a-b, TLM; c, FLM.
Figs. 2a-c. *Spiniferites* sp. – Gallician 9 (2530 m): a-b, TLM; c, FLM.
Figs. 3a-c. *Nematosphaeropsis* sp. – Crossroad D716/D981: a-b, TLM; c, FLM.
Figs. 4a-c. *Cleitosphaeridium* sp. – Serre de Cauvel (sample 2): a-b, TLM; c, FLM.
Figs. 5a-c. *Impagidinium* sp. – Serre de Cauvel (sample 2): a-b, TLM; c, FLM.
Figs. 6a-c. *Lingulopdinium machaerophorum* – Serre de Cauvel (sample 2): a-b, TLM; c, FLM.
Figs. 7a-c. *Glaphyrocysta* sp. – Canet 1 (1100 m): a-b, TLM; c, FLM.
Figs. 8a-c. *Impagidinium patulum* – Canet 1 (1100 m): a-b, TLM; c, FLM.

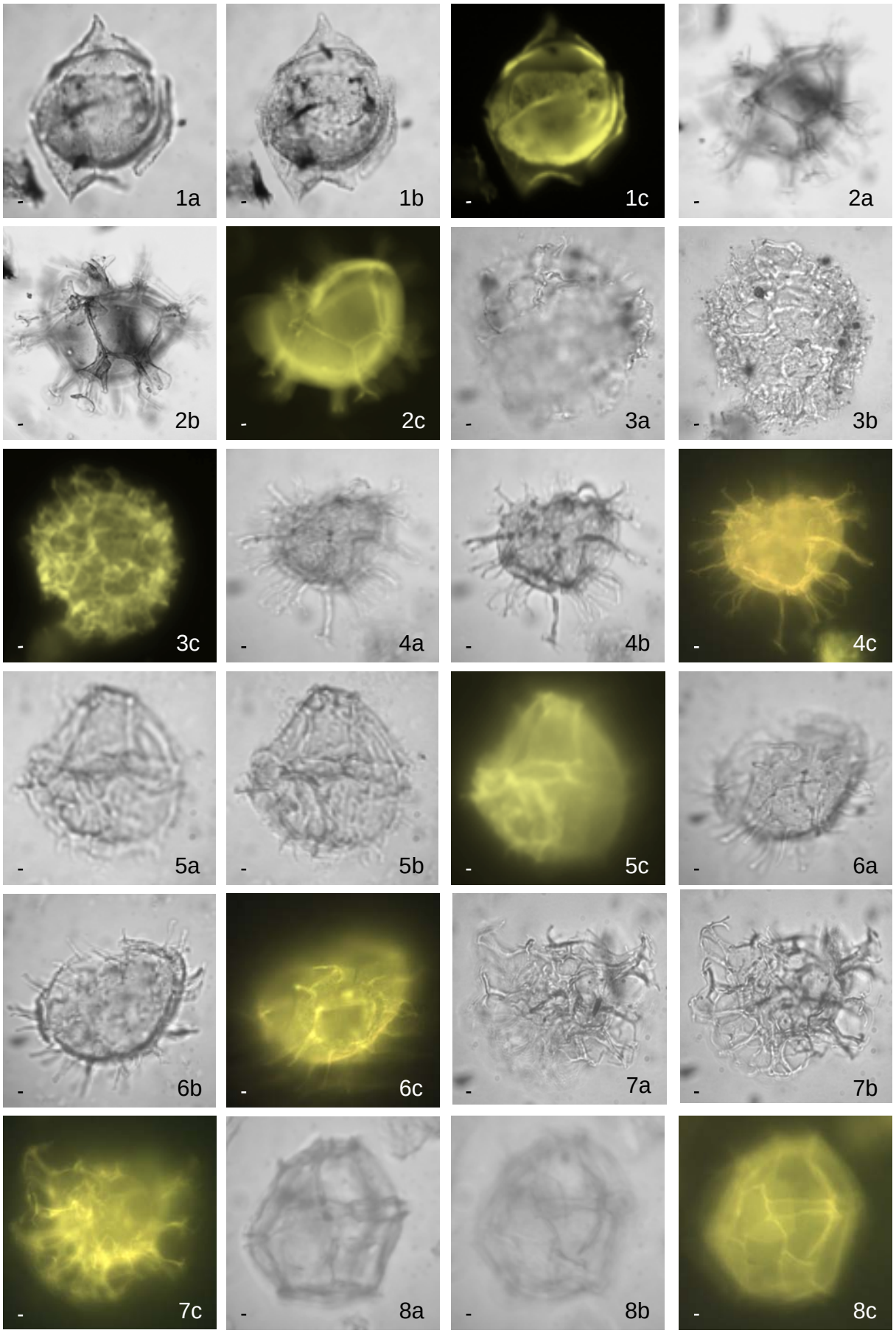
- 1a
- 1b
- 1c
- 2a
- 2b
- 2c
- 3a
- 3b
- 3c
- 4a
- 4b
- 4c
- 5a
- 5b
- 5c
- 6a
- 6b
- 6c
- 7a
- 7b
- 7c
- 8a
- 8b
- 8c

4. Climatostratigraphy vs. palynostratigraphy.

Two obvious items imply to use pollen data as a climatostratigraphic tool (numerical variability) in contrary to a classical biostratigraphic tool (first occurrence and last occurrence datums):

- plants evolve along geological times but evolution only affects the species level during the Cenozoic period, usually unattainable through the pollen morphology;
- plants shift in latitude and altitude along geological times with respect to changes in temperature and precipitation.

As a consequence, palynostratigraphy based on occurrences of supposed species is to be considered as an old-fashioned approach and must be definitely abandoned. One of the most critical examples of such an obsolete use is provided by the use of the pseudo-species *Boelhensipollis hohli*, which has been proposed as a marker of the Oligocene series (Sittler and Schuler, 1976) and hence abundantly indeed excessively exploited (e.g.: Châteauneuf, 1980; Olivier-Pierre, 1980; Schuler, 1988; Châteauneuf and Nury, 1995; Cavagnetto, 2002; Châteauneuf et al., 2019).

The problem resulting from this deficient concept shows multiple aspects:

- quality of the published photographs is often insufficient to convince that an unique taxon corresponds to the so-called *Boelhensipollis hohli* pollen;
- Sittler and Schuler (1976) suppose that two pollen-types are included within their *Boelhensipollis hohli* that makes more inappropriate the use of a species designation;
- these authors describe the *Boelhensipollis hohli* pollen-type as heteropolar, i.e. non-joined colpi (strictly tricolporate pattern) on one side of the polar view and joined colpi (syncolporate pattern) on the other side, and they propose two possible botanical ascriptions: *Elaeagnus* (Elaeagnaceae) and *Serjania* (Sapindaceae); *Elaeagnus* modern species do not show heteropolar pollen while some *Serjania* modern species show heteropolar pollen (Muller and Leenhouts, 1976);
- in addition, it is difficult to conceive the sudden appearance of the temperate genus *Elaeagnus* at the earliest Oligocene, while it has been already recorded in Northern Canada during the Early Eocene Climatic Optimum (Salpin et al., 2019);

it is also unbelievable that *Serjania*, a tropical genus, appeared simultaneously with a significant climate cooling, while several pollen grains belonging to Sapindaceae have been recorded in the Priabonian samples (Table S3) and are present in Eocene sediments from Southwestern France (Fauquette et al., in progress).

References.

Banks, H., Lewis, G., 2018. Phyligenetically informative pollen structures of ‘caesalpinioid’ pollen (Caesalpinioideae, Cercidoideae, Detarioideae, Dialioideae and Duparquetioideae: Fabaceae). *Botanical Journal of the Linnean Society*, 187, 59–86.

Bessedik, M., 1980. La flore pollinique d’un niveau gypseux de la série de Portel (Aude-France): Oligocène terminal. *Mémoires du Muséum national d’histoire naturelle*, ser. 8, Botanique, 27, 196–203.

Bessedik, M., 1981. *Recherches palynologiques sur quelques sites du Burdigalien du midi de la France*. PhD thesis, Univ. Montpellier 2, 43 pp.

Buisson, J.-J., 1993. Permis Vauvert-Gallician – ‘Farm out’ Coparex. Synthèse sur le secteur de Gallician. Document interne n° 93-0345 Elf-Aquitaine Production, 27 pp.

Carreira, L.M.M., de Souza Secco, R., Barth, O.M., 1996. Pollen morphology of the lianescent species of the genus *Croton* (Euphorbiaceae). *Grana*, 35, 74–78.

Cavagnetto, C., 2002. La palynoflore du basin d’As Pontes en Galice dans le nord-ouest de l’Espagne à la limite Rupélien–Chattien (Oligocène). *Palaeontographica*, B, 263, 161–204.

Châteauneuf, J.-J., 1977. Etude palynologique de l'Oligocène du bassin de Marseille. *Géologie méditerranéenne*, 4, 1, 37–46.
Châteauneuf, J.-J., 1980. Palynostratigraphie et paleoclimatology de l'Eocène supérieur et de l'Oligocène du bassin de Paris (France). *Mémoire du B.R.G.M.*, 116, 357 pp.
Châteauneuf, J.-J., Nury, D., 1995. La flore de l'Oligocène de Provence méridionale: implications stratigraphiques, environnementales et climatiques. *Géologie de la France*, 2, 43–55.
Châteauneuf, J.-J., Villeneuve, M., Nury, D., 2019. La transgression rupélienne (stampienne) dans les "Sables bleutés" du Haut-Var, démontrée par l'étude palynologique à Saint-Maime (Fossé de Montmeyan, Sud-Est France). *Géologie de la France*, 1, 1–17.
Clauzon, G., Cravatte, J., 1985. Révision chronostratigraphique de la série marine pliocène traverse par le sondage Canet 1 (Pyrénées-Orientales): apports à la connaissance du néogène du Roussillon. *Comptes-Rendus de l'Académie des Sciences de Paris*, 301, série 2, 19, 1351–1354.
Doláková, N., Burešová, A., 2007. Use of fluorescent microscopy in the study of redeposited palynomorphs in the cave and marine sediments of Moravia (Czech Republic). *Acta Palaeobotanica*, 47, 1, 275–279.
Gottis, M. 1958. L'apport des travaux de la Compagnie d'exploration pétrolière (C.E.P.) dans la connaissance du basin tertiaire du Roussilon. *Bulletin de la Société géologique de France,* série 6, 8, 8, 881–883. :
Graham, A., Barker, G., 1981. Palynology and tribal classification in the Caesalpinioideae. *In* 'Advances in Legume Systematics', Polhill, R.M. and Raven, P.H., eds., Royal Botanic Garden, Kew, 801–834.
Gruas-Cavagnetto, C., 1973. Première contribution à l'étude de la palynoflore de la Formation de Célas (Bassin d'Alès, Gard). *Paléobiologie continentale*, 4, 2, 1–13.
Hoyle, T.M., Leroy, S.A.G., López-Merino, L., Richards, K., 2018. Using fluorescence microscopy to discern *in situ* from reworked palynomorphs in dynamic depositional environments – An example from sediments of the late Miocene to early Pleistocene Caspian Sea. *Review of Palaeobotany and Palynology*, 256, 32–49.
Jan du Chêne, R., 1989. Etude palynologique du sondage EURAFREP (Camargue) : BAM 1. Aanalyse des échantillons 980 m à 1160 m et 1475 à 1950 m. *In* 'Rapport de fin de sondage Baumelles 1 (BAM 1). Permis Vauvert-Gallician', Document interne EURAFREP, p. 29–36.
Köhler, E., 1965. Die pollenmorphologie der biovulaten Euphorbiaceae und ihre bedeutung für die taxonomie. *Grana Palynologica*, 6, 1, 26–120.
Krutzsch, W. 1962.Mikropaläontologische (sporenpaläontologische) untersuchungen in der braunkohle des Geiseltales. II. Die formspezies des pollengattung *Pentapollenites* Krutzsch (1958). *Paläontologie*, 1, H. 2, 73–103.
Kvacek, Z., 2002. Novelties on Doliostrobus (Doliostrobaceae), an extinct conifer genus of the European Palaeogene. *Časopis Národního muzea, Řada přírodovědná*, 171, 1–4, 131–175.
Merville, M., 1965. Le pollen des Sapindacées d'Afrique occidentale. *Pollen et Spores*, 7, 3, 465–489.
Michoux, D., 1983. Etude palynologique des sédiments ludiens du fossé d'Alès (Gard). In "Inventaire des ressources nationales de charbon. Lignites du fosse d'Alès-Barjac", Alabouvette, B., Chedhomme, J., Fredet, J.M., Lartaud, V., Rapport du B.R.G.M., 83 SGN 519 GEO/LRO, Annexe 4, 9 pp.
Muller, J., Leenhouts, P.W., 1976. A general survey of pollen types of Sapindaceae in relation to taxonomy. In "The evolutionary significance of the exine", Ferguson, I.K., Muller, J., eds., Linnean Society Symposium Series, 1, 407–445.

Ollivier-Pierre, M.-F., 1980. Etude palynologique (spores et pollens) de gisements paléogènes du Massif Armoricain. Stratigraphie et paléogéographie. *Mémoires de la Société géologique et minéralogique de Bretagne*, 25, 1–239.

Punt, W., 1962. Pollen morphology of the Euphorbiaceae with special reference to taxonomy. *Wentia*, 7, 1–116.

Reitsma, Tj., 1970. Pollen morphology of the Alangiaceae. *Review of Palaeobotany and Palynology*, 10, 249–332.

Ribes de Lima, L., Vitorino da Cruz-Barros, A., Pirani, J.R., da Silva Corrêa, A.M., 2007. Pollen morphology of *Croton* sect. *Lamprocroton* (Müll. Arg.) Pax (Euphorbiaceae) and its taxonomic implications. *Nordic Journal of Botany*, 25, 206–216.

Ribeiro de Souza, L., Marques da Silva, O.L., de Assis Ribeiro dos Santos, F., Carneiro-Torres, D.S., 2020. Pollen morphology of *Croton* of the New World and pollen evolution of tribe Crotoneae (Euphorbiaceae). *Review of Palaeobotany and Palynology*, 281, 104279.

Salpin, M., Schnyder, J., Baudin, F., Suan, G., Suc, J.-P., Popescu, S.-M., Fauquette, S., Reinhardt, L., Schmitz, M., Labrousse, L., 2019. Evidence for subtropical warmth in Canadian Arctic (Beaufort-Mackenzie, Northwest Territories, Canada) during the early Eocene. *In* 'Circum-Arctic Structural Events: Tectonic Evolution of the Arctic Margins and Trans-Arctic Links with Adjacent Orogens', *Geological Society of America Special Paper*, 541, 27, 637–664.

Schuler, M., 1980. *Environnements et paléoclimats paléogènes. Palynologie et biostratigraphie de l'Eocène et de l'Oligocène inférieur dans les fosses rhénan, thodanien et de Hesse*. PhD thesis, University L. Pasteur Strasbourg, 383 pp.

Schuler, M., Sittler, C., 1976. Données paléoclimatiques à l'aube des temps néogènes en Haute Provence (France). *Géologie méditerranéenne*, 3, 3, 155–160.

Sittler, C., 1965. Le Paléogène des fosses rhénan et rhodanien. Etudes sédimentologiques et paléoclimatiques. *Mémoires du Service de la carte géologique d'Alsace et de Lorraine*, 24, 392 pp.

Sittler, C., Schuler, M., 1975. Extension stratigraphique, répartition géographique et écologie de deux genres polliniques paléogènes observes en Europe occidentale: *Aglaoreidia* et *Boehlensipollis*. Société botanique de France, Colloque Palynologie, 231–245.

Suc, J.-P., 1976. Quelques taxons-guides dans l'étude paléoclimatique du Pliocène et du Pléistocène inférieur du Languedoc (France). *Revue de Micropaléontologie*, 18, 4, 246–255.

Suc, J.-P., Bessedik, M., 1981. A methodology for Neogene palynostratigraphy. International Symposium on Concept and Method in Paleontology, Barcelona, pp. 205–208.

GEOCHEMICAL MODELLING

	Late Oligocene seawater end-member	Riverine end-member
$^{87}Sr/^{86}Sr$	0.70825	0.7077
$\delta^{34}S$ VCDT	20	11
[Sr]	15	0.1
$[SO_4^{2-}]$	2800	70

Table S4. Sulphur and Strontium isotope composition and concentrations for the late Oligocene seawaterand riverine end-members (best-case scenario).